Effect of the ammonium groups on the properties and stability of anion conductive membranes

A Doctoral Thesis

Present to

Interdisciplinary Graduate School of Medicine and Engineering

University of Yamanashi

September 2017

Ahmed Mahmoud

Contents

Chapter 2

Effect of ammonium groups on the properties of anion conductive membranes based on partially fluorinated aromatic polymers

Chapter 3

High Hydroxide Ion Conductivity with Enhanced Alkaline Stability of Partially Fluorinated and Quaternized Aromatic Copolymers as Anion Exchange Membranes

Chapter 1. Background and Introduction

1.1Background

1.1.1 Urgent demand for clean energy resources

Nowadays, economics is completely dependent on fossil fuels including coal, oil and natural gas which are non-renewable resources and will be exhausted in the future.[1] The energy provided by fossil fuels release pollutants and hazardous emissions to animals and plants. These emissions (especially CO_2) are the reason behind the global warming. On the other hand, all stages of fossil fuel production, either mining, extraction, processing or transportation have suspicious risks for humans and ecosystems.[1,2] The solution is to move quickly from fossil fuel to clean alternative energy resources. One of the alternative solutions is to increase the use of nuclear power which has negligible emissions and considered as inexhaustible.[3] However, the latter has the safety risks of handling the radioactive wastes and the possibility of catastrophic accidents such as Fukushima nuclear power Plant, Japan 2011 and that of Chernobyl in the USSR in 1985 besides the high cost that hinder the widespread of nuclear power.[3,4] Renewables (such as wind and solar energy) and biomass are alternatives to clean energy resource with zero-emission greenhouse gases. However solar energy can be used directly through the radiating thermal and light energy, unfortunately, it requires complex technologies besides wide land and rare metal catalysis.[1]

Recently, much efforts have been directed towards the development of polymer electrolyte membrane based technologies for renewable energy storage and transformation; such as redox flow batteries, polymer electrolyte membrane fuel cells (Alkaline and acidic) or water electrolysis for hydrogen production.[5] Among these applications, Fuel cells turned to be a viable clean energy resource for mobile and stationary applications.[6]

Fuel cells are electrochemical system that combine hydrogen and oxygen to produce electricity, heat and water. Fuel cells are considered a flameless or zero-emission process compared to the fossil fuel combustion. Fuel cells can achieve two times and half higher efficiency than that in

internal combustion engines. Moreover, fuel cell is a nearly silent process without moving parts.[7] Different types of fuel cells have been developed including; anion exchange membrane fuel cells (AEMFCs), Proton exchange membrane fuel cells (PEMFCs), solid oxide fuel cells (SOFCs), molten carbonate fuel cell (MCFCs) and phosphoric acid fuel cells (PAFCs). Among them, PEMFCs and AEMFCs have gained more attention due to their low temperature (below 200 ^{o}C) applications in stationary, vehicles and mobile devices.[8,9]

1.2 Introduction

1.2.1 Anion exchange membranes as a viable alternative to protonic counterpart

PEMFCs have been excessively studied for several decades and found their way in different applications. However, in such strong acidic and corrosive medium, platinum group metal catalysis (Pt, Os, Ir, Ru, Rh and Pd) are mainly required due to their resistance under corrosive conditions. Unfortunately, the rarity and high cost of these precious metals, obstacle the wide commercialization of PEMFCs that devoted the scientist's efforts towards the alkaline anion exchange membrane fuel cells (AAEMFCs). The alkaline environment of AAEMFCs permits faster electro-kinetics of the electrodes allowing the use of non-platinum group metals such as (Ag, Ni and Co).[5,8,9] Moreover, the alkaline conditions open the door for multi choices of fuels such as hydrazine, ethylene glycol, alcohols and sodium borohydride besides the availability of H_2 with some impurities (PEMFCs requires high purity of H_2).[10] Due to these advantages, alkaline fuel cells gained much more attention in the recent years as the next generation of fuel cell technology. AAEMFCs are mainly based on anion exchange membrane (AEM) in which the function is a little different than that of proton exchange membranes (PEM, i.e. Nafion). Figure 1-1, Shows a schematic diagram of the function of AEM in comparison to that of PEM.[11] In the acidic fuel cells,

conduction of H^+ take place through the PEM by transferring the protons from anode to cathode according to equations (1,2).

At anode: $2H_2 \rightarrow 4H^+ + 4e^- \; E = 0.00\ V$ (1)

At cathode $O_2 + 4H^+ + 4e^- \rightarrow 2H_2O \; E = 1.23\ V$ (2)

While, in the alkaline fuel cells the solid AEM transfers the hydroxide ions from cathode to anode in which OH^- oxidized to produce water as by product and electrons moving through external wire resulting in electric current. (equations 3,4).

at anode: $2H_2 + 4OH^- \rightarrow 4H_2O + 4e^- \; E = -0.828\ V$ (3)

at cathode: $O_2 + 2H_2O + 4e^- \rightarrow 4OH^- \; E = 0.401\ V$ (4)

In both cases the overall reaction is the same as shown in the following equation (5):

$$2H_2 + O_2 \rightarrow 2H_2O \; E_{cell} = 1.23\ V \text{ (both acid and alkali)} \quad (5)$$

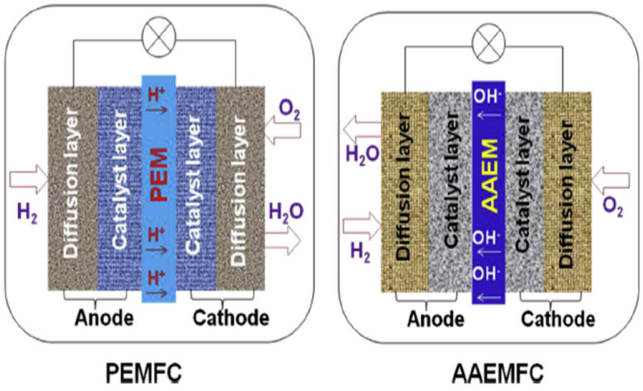

Figure 1-1. Schematic diagram of Anion and proton exchange membrane fuel cells.[11]

Besides their application in fuel cells, AEMs found their way in different membrane-based energy conversion and storage devices such as reverse electro-dialysis, secondary batteries, desalination and water electrolysis (Figure 1-2).[12,13] The membrane should meet essential requirements depending on its application. In the fuel cell applications, AEM is considered the key part of the cell, since it allows and organizes the OH^- transportation from cathode to anode, in addition, it prevent the gas crossover between the two electrodes. So that, AEM should possess high hydroxide

ion conductivity, excellent chemical and mechanical properties under harsh alkaline conditions besides the low gas permeability.[13] A standard AEM that fulfill all the aforementioned requirements has not been reported. Thus, more efforts required to develop an applicable AEM.

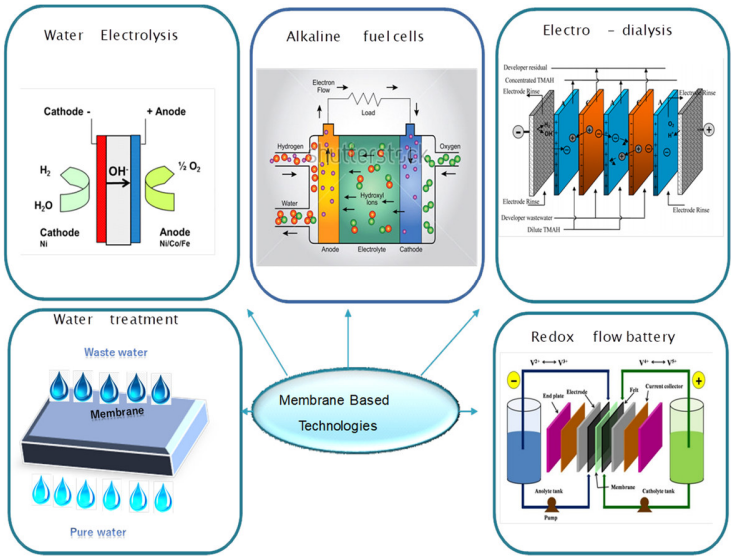

Figure 1-2. Various applications of anion exchange membranes.[14-17]

1.2.2 Challenges of Anion exchange membranes

However the alkaline conditions allows the promising utilization of non-precious metal catalysis, AEMs face many challenges comparing to PEMs that will be summarized in the following lines:-

1.2.2.1 Ionic mobility (Low ionic conductivity)

One of the main challenges for AEMs is the lower ionic conductivity compared to proton conductivity in PEMs. Fundamentally, the mobility of hydroxide ions (20.64×10^{-8} m^2/sV) is much lower than proton (36.23×10^{-8} m^2/s V) in infinite diluted solution at 298 K. The lower mobility of OH^- may end to lower conductivity than that of proton. Moreover, the lower dissociation constant of quaternary ammonium as a weak base ($pK_b = 4$) compared to the strong acidic aryl sulfonium, ($pK_a = -1$) is considered another barrier for efficient ion conduction.[13, 18, 19, 20]

However, recently some AEMs were reported to exhibit same level of conductivity to that of Protonic membranes specially at elevated temperature. Such as poly(phenylene oxide) based AEMs that exhibited 198 mS/cm at 90 ^{o}C which is as similar efficient conduction as that of Nafion membranes.[21] suggesting that at elevated temperature, OH^- conduction can be as fast as H^+ ions.

Another issue related to the exposure of AEM (OH^- form) to CO_2 (air) even for short time, in which the membrane can be exchanged to the lower conductive bicarbonate ion form leading to lower power density in fuel cell.[13] In other words, when we handle the AEMs in air (CO_2), we treat with membranes in bicarbonate ion form not hydroxide ion form.

1.2.2.2 Hydroxide ion transport (Conduction mechanism)

It was reported that proton and hydroxide ions follow Grøtthuss mechanism in aqueous solutions, however the details of two mechanisms are little different. [22-26] Hydronium ion (H_3O^+) is naturally form hydrogen bonding network with water without further activation or solvent rearrangement, while hydroxide ions tend to form stable solvation shells that try to reorganize the solvent molecules and perturb the hydrogen bond network. [18-22] In the literature, according to the transport similarities it aqueous solution, it was hypothesized that hydroxide transport in AEM_S could be similar to that of PEMs that exhibit vehicle mechanism and Grøtthuss type mechanism, however the Grøtthuss mechanism is the dominant transport mechanism.[13, 22]

In the literature, many conduction mechanisms for hydroxide ions in AEMs, were suggested taking in to account the surrounding environment in the membrane and /or fuel cell in a similar way to that of PEMs. The hydroxide transport can be resulted of the combination of different mechanisms including: i) Grøtthuss mechanism via hydrogen and covalent bonds, ii) surface site hopping on membrane quaternary ammonium, iii) diffusion and migration mechanism due to the concentration or potential gradient on the charged particles and iv) convection mechanism due to the pressure gradient and /or electrostatic potential gradient of the mobile species (Figure 1-3).[27-35] So that, the conduction mechanism may differ according to the differences in temperature, concentration

and/or potential gradient in the fuel cell.

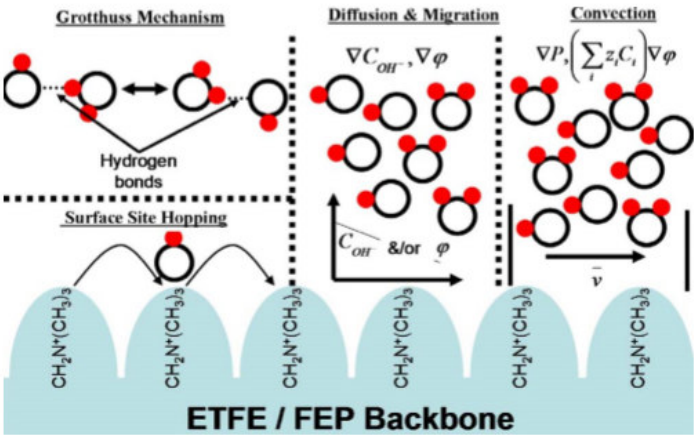

Figure 1-3. Suggested conduction mechanisms in AEMs. [27]

1.2.2.3 How to achieve high anionic conductivity without membrane swelling???

As described above, AEMs possess lower conductivity compared to the protonic membranes. Taking into account that the diffusion of H^+ is four times higher than that of OH^- ions, a fourfold increase in hydroxide ion conductivity required to reach same performance of acidic polymer electrolytes.[36] Demonstrating that AEMs need to carry four times higher IECs, so that many attempts were devoted to increasing the conductivity of AEMs by increasing the ion exchange capacity (IEC). Unfortunately, that increase in IEC values come on to the account of membrane swelling. At high IECs, the membrane exhibit excessive water uptake to the level that permits the mechanical failure when the membrane fabricated in the fuel cell stack.[13]

Some synthetic strategies have been reported to mitigate the membrane swelling at high IECs such as crosslinking[37] or block copolymerization[38] achieving promising success in this regard. It was reported that the good phase separation between hydrophilic and hydrophobic segments in most of these strategies is responsible for the balance between high conductivity (at high IEC) and low water uptake. Because of the water molecules are essential for efficient conduction and based on similarities in conduction mechanisms in both AEM and PEM as described above, It was found that better phase separation in the Nafion membranes permits the overlap between hydrophilic

domains forming good interconnectivity between the ionic channels while in absence of phase separation (such as sulfonated polyetherketone (SPEEK)), a dead-end channels formed leading to tightly bound water molecules and lower conductivity as well (Figure 1-4) .[13, 39, 40]

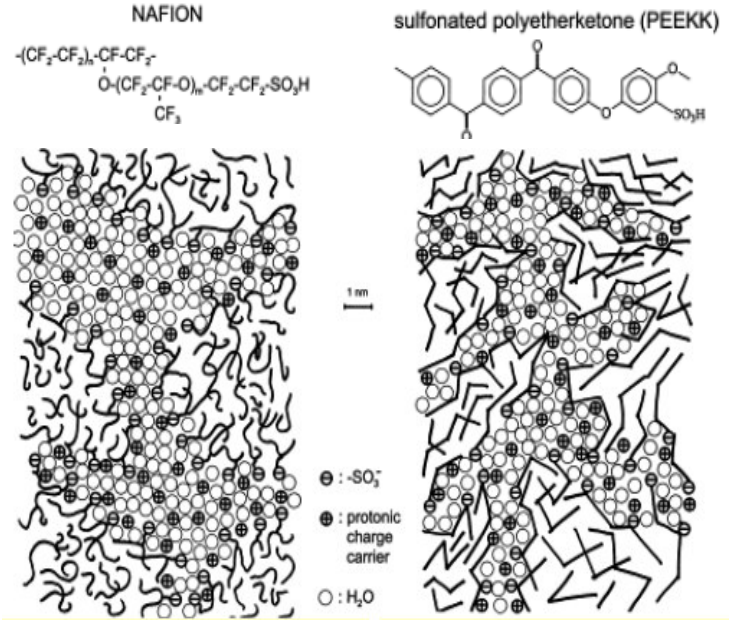

Figure1-4. Shematic diagram of phase separation in NAFION and SPEEK membranes.[40]

1.2.2.4 Alkaline stability

The most critical challenge that face AEMs is the alkaline stability under strong alkaline conditions specifically at elevated temperatures (over 80 ^{o}C). Generally, AEMs are constructed of polymer backbone tethered to quaternary ammonium (QA) *via* benzylic group that provide different locations for alkaline attack by OH^- ions either in polymer main chain, benzylic tether or quaternary ammonium (QA) (Figure 1-5). So that the stability of AEMs is mainly dependent on the chemical stability of polymer backbone and QA as well. [13]

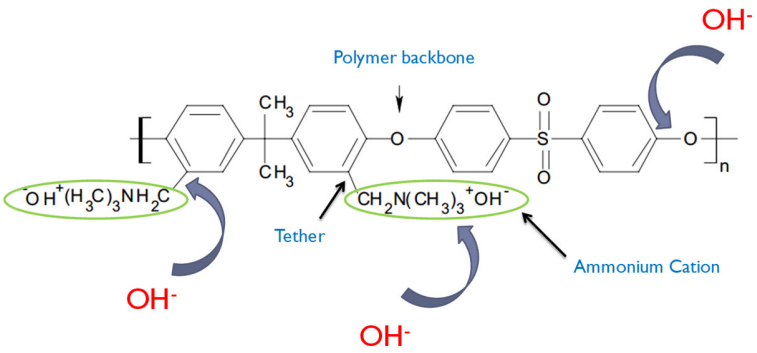

Figure 1-5. Possible degradation pathways of AEMs.

1.2.2.4.1 Stability of the polymer backbone

Fundamentally, the stability of polymer backbone depends on the chemical structure of the polymer main chain. Some polymer backbones are susceptible to alkaline attack more than others. For example, poly(arylene ether) (PAE) that contains C-O bond is prone to degradation more than polyphenylenes or polystyrenes.[41,42] A computational and experimental study by Yoong-Kee *et. al.,* demonstrated that PAE degraded faster than QA since the barrier energy for aryl-ether degradation was 85.8 kJ/mol compared to 90.8 kJ/mol for QA degradation (Figure 1-6).[43] The results suggested 62 % degradation of aryl-ether and 12% of BTMA in 0.5M NaOH at 80 °C for 2h.[43]

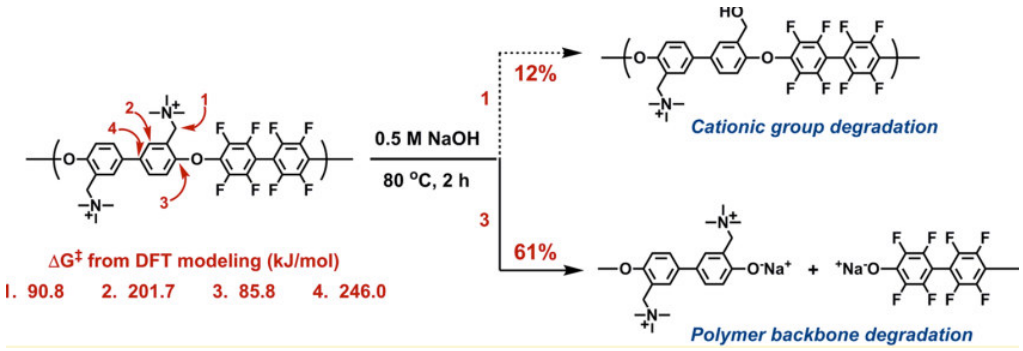

Figure 1-6. The possible degradation of poly(arylene ether) backbones.[43]

Also the ether bond free backbones can undergo degradation or chemical transformation in alkaline medium, such as poly(vinylidene fluoride) (PVDF) that undergo E2 elimination when be attacked by OH^- ions (Figure 1-7a).[44] Moreover, polystyrenes can be oxidized in presence of alkali to form

carboxylic acid (Figure 1-7b).[45] The backbone degradation or transformation almost affect the mechanical properties of the membrane as well as conductivity and cell performance.[13]

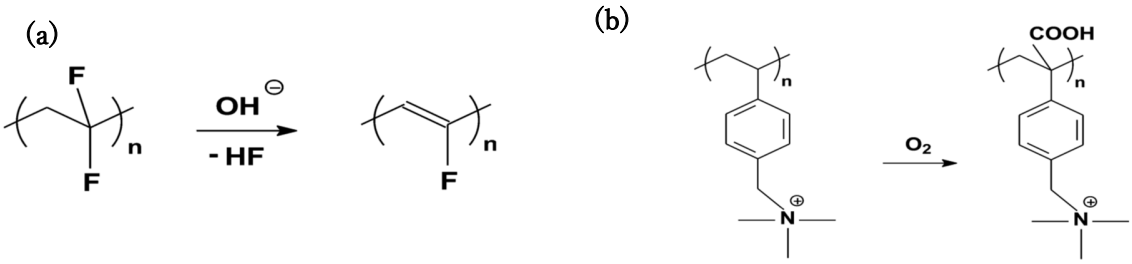

Figure 1-7. Possible degradation of (a) PVDF backbone and (b) Oxidative carboxylation of polystyrenes.[44, 45]

1.2.2.4.2 Stability of quaternary ammonium

The quaternary ammonium as the ion conducting component in AEMs, undergoes many degradation mechanisms that were extensively discussed in the literature, however the most accepted pathways are nucleophilic substitution (SN2) and Hofmann elimination (E2). In SN2 mechanism, OH^- ions attack α-carbon either in the tether (benzylic sites) as shown in (Figure 1-8), or in the pendant methyl groups of QA (Figure 1-9) to produce amine and alcohol in both cases. This degradation pathway usually leads to complete loss of QA resulting in decrease in ion exchange capacity (IEC) and conductivity.[46]

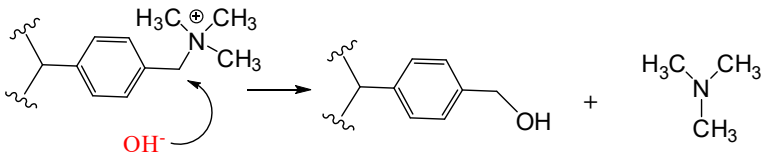

Figure 1-8. Tether degradation mechanism of AEMs *via* nucleophilic substitution.[46]

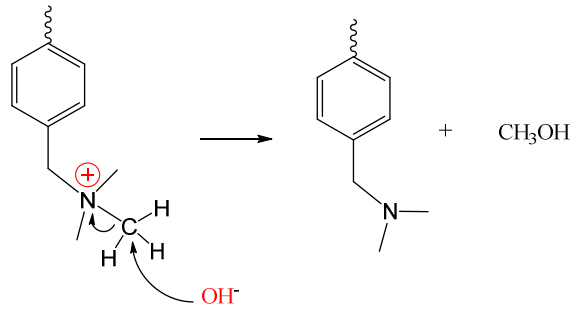

Figure 1-9. Pendant quaternary ammonium degradation *via* Nucleophilic substitution (SN2).[46]

The E2 mechanism takes place when the QA possess β-hydrogen, in which OH^- attack that β-hydrogen resulting in formation of amine and alkene (Figure 1-10). One or both of SN2 and E2 mechanisms occur in presence of α- and β-positions depending on the chemical structure. For example, the steric hindrance or bulky structure at one position favor the degradation at the other position.[47]

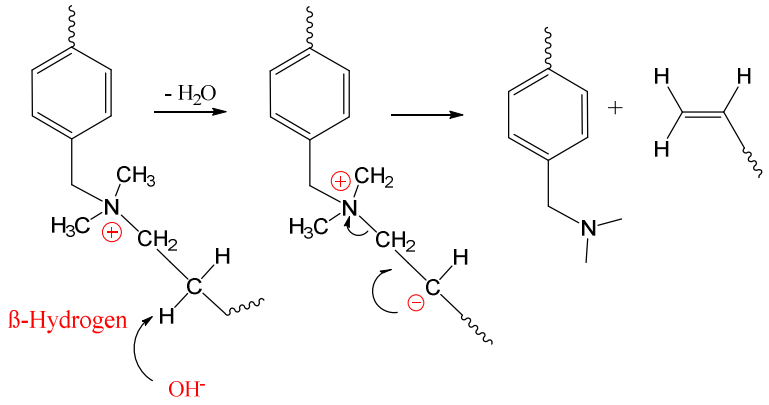

Figure 1-10. Alkaline degradation via Hofmann elimination (E2).[47]

Stevens and Sommelet-Hauser rearrangements (Figures 1-11, 1-12) were also suggested via formation of intermediate ylides ($C^-—N^+(R)_3$), however the degradation *via* Stevens and Sommelet-Hauser rearrangements have been only observed on BTMA in aqueous alkaline conditions but have not been experimentally detected in AEM materials.[13, 48-50]

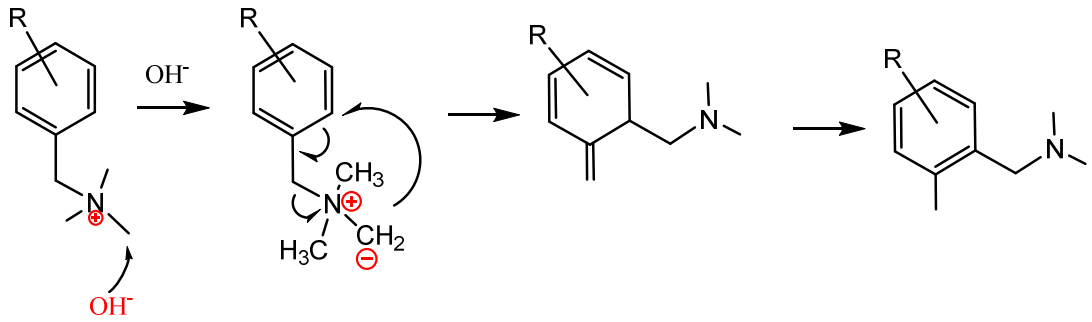

Figure 1-11. possible degradation of AEMs *via* Summelet-Hauser rearrangement.[49]

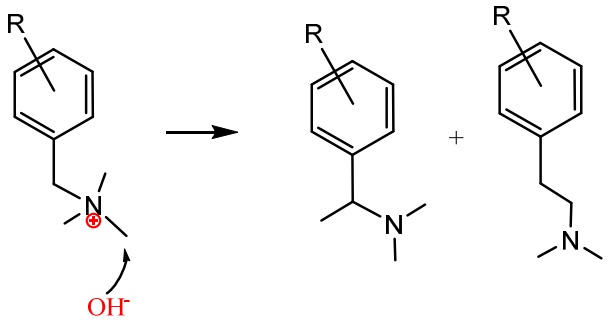

Figure 1-12. Possible degradation of AEMs *via* Stevens rearrangement.[50]

1.2.2.5 Fuel cell Performance

1.2.2.5.1 Differences between AEM and PEM

Fuel cell performance is considered the crucial property for AEMs, since the main objective of the research on AEMs is to obtain the durable and high performance AEM in practical fuel cell. However, the overall reaction for AEMFC and PEMFC is the same as described above, some main differences between the alkaline and acidic fuel cells should be considered. The first noticeable difference is the solid membrane that is fabricated with catalyst layer in each case. Usually AEM is used for alkaline cell in which OH^- transport from cathode to anode, while PEM conducts H^+ from anode to cathode in PEMFC (Figure 1-1). Another difference is the water management in alkaline and acidic fuel cells. In AEMFC, water is produced at the anode and consumed as direct reactant at cathode side, while in PEMFCs, water is generated at cathode side as byproduct.[13, 51]

Suggesting that hydration levels at cathode side is critical for AEMFCs. It was reported that low hydration levels in AEMFC specially at cathode side accelerated the degradation levels and decreased the stability of AEM.[52]

The main advantage of AEMFCs in comparison to PEMFC is that at high pH environment, the oxygen reduction reaction (ORR) is much faster than that in acidic medium of PEMFC, that permits the use of cheaper non-precious metal catalysis besides the availably of different fuel choices as described above.[8-10]

1.2.2.5.2 Recent achievements in cell performance of AEMFC

From the aforementioned differences between AEM and PEM, it seems that the lower conductivity and stability issues of AEMs are critical factors that may hinder achieving comparable power density to that of PEMFCs.[13] However, recently, a significant advance in the conductivity and stability of AEMs has been achieved that enabled high and comparable fuel cell performance to that of PEMFCs. Very recently, Varcoe et. al.[53] reported aliphatic-heterocyclic benzyl-quaternary ammonium radiation-grafted AEM with maximum power density of 980 and 800 mW/cm^2 with and without 0.1 MPa back pressurization, respectively using PtRu/C anodes and Pt/C cathodes and polysulfone ionomer in H_2/O_2 at 60 ^oC .[53] Scott and coworkers, also reported QA radiated grafted AEMs with maximum power density up to 823 mW/cm^2 with O_2 and 500 mW/cm^2 in air at 60 ^oC.[54] Also, Kim reported polyphenylene based AEM with high power density up to 577 mW/cm^2 and 450 mW/cm^2 at 80 ^oC with H_2/O_2 and air respectively.[55] More interestingly, a platinum-free hydrazine fuel cell based on poly(arylene ether) AEM achieved a high power density up to 510 mW/cm^2 with hydrazine as fuel and O_2 as oxidant.[56] These high power densities are among the best reported in the literature and are considered comparable or higher than those reported for PEMFCs, suggesting that AEMs are not inferior to PEMs.[10]

In spite of the promising fuel cell performance, the long term durability of these AEMs was not carefully investigated due to the critical concerns related to the membrane stabilities and conductivity, especially at high temperatures and low hydration levels.[13]

So that many efforts have been reported to improve the stability and conductivity of AEMs.

1.2.3 Synthetic strategies to enhance the properties of anion exchange membranes

The state-of-art proton exchange membranes such as Nafion from DuPont, still higher conductive and more chemically and mechanically stable than the existing AEMs that almost hinder the practical commercialization of alkaline fuel cells. In the last decade, many approaches have been reported in the literature to address these drawbacks.[57]

Typical AEMs are composed of polymer backbone (ca. hydrophobic segment) tethered with organic cations (ca. hydrophilic segment) such as ammonium, sulfonium or phosphonium groups. Hydrophobic segments represented in polymer backbones contribute to membrane forming capability, gas impermeability, mechanical and thermal stability, while hydrophilic onium groups serve as ion exchangeable sites for anion conduction.[57]

Many approaches have been reported to investigate the effect of polymer backbone and cationic groups on properties of AEMs which will be discussed below.

1.2.3.1 Approaches to stabilize the polymer backbones of AEMs.

A number of aromatic polymers have been investigated for AEMs such as poly(phenylene oxide)s (PPOs)[58] and poly(arylene ether sulfone)s (PAESs),[59,60] and their copolymers. These polymers could be easily synthesized via nucleophilic substitution polymerization reaction, however, arylene ether bonds are likely to be degraded under the basic conditions (Figure 1-13).[61] For example, polysulfone based AEMs broke after 168 h in 2 M KOH at 60 ºC due to the aforementioned backbone degradation (section 1.1.3.4).[41]

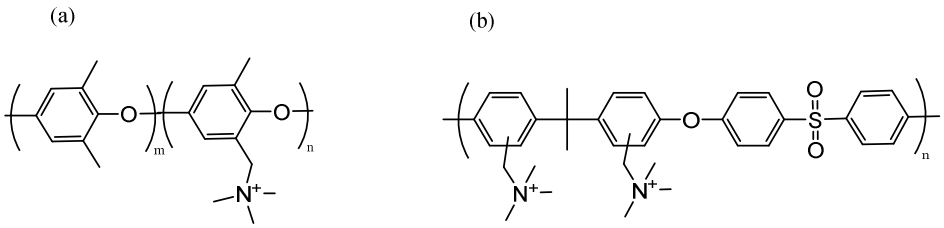

Figure 1-13. chemical structure of poly (phenylene oxide) and poly (arylene ether sulfone).[58,59]

Mohanty et. al.[62] has reported a study on the stability of various polymer backbones through the analysis of the molecular weights before and after alkaline treatment. The results demonstrated that the presence of electron-withdrawing groups such as sulfone near to the arylene-ether proximity lead to severe degradation in the polymer main chain. However, some structural change or side reactions detected for substituted PPOs, While no detectable degradation was observed for ether-free backbones such as poly (biphenyl alkyene)(PBPA) and polystyrene-*b*-poly(ethylene-*co*-butylene)-*b*-polystyrene (PSPEB).[62]

Due to the low cost and facile synthesis of PAE or PAES backbones, many efforts have been devoted to improving the properties of AEMs based on these backbones, such as block copolymerization, crosslinking, grafting or alkli-dopping.

1.2.3.1.1 Block co-polymerization

The block copolymerization was reported as effective method to improve the morphology of the membranes and mitigate the water uptake, however, the achievements of this strategy in alkaline stability was limited. For example, Yokota et. al. reported that PAE based AEMs synthesized via block copolymerization, degraded after 50 h in 1M KOH at 40 ^{o}C.[63] Separately when he used PAE with oligophenylene moieties in the hydrophilic segments, the alkaline stability improved to some extent (lost 45% of its conductivity after 1000 h at the same conditions).[56] Aslo Dong *et. al.* reported that the PAES based AEMs bearing bis-quaternary ammonium degraded after 240 h in 1M KOH at 60 ^{o}C suggesting the low alkaline stability in spite of its high conductivity.[64]

1.2.3.1.2 Crosslinking

Crosslinking of AEMs was also effective strategy to achieve the balance between water uptake and high conductivity besides the robust mechanical properties.[37] Crosslinking was also promising to improve the stability of PAE, PAES and PPO based AEMs. Recently, Lee *et. al.*[65] reported that the end group cross-linking via thermal treatment of PAES functionalized with imidazolium groups (Figure 1-14) helped to improve the alkaline stability of the membrane since the cross-linked membrane retained 68% (67 mS/cm) of its initial conductivity in 1M NaOH at 80 ºC for 500h, compared to 35% (27 mS/cm) of uncross-linked membrane.[65]

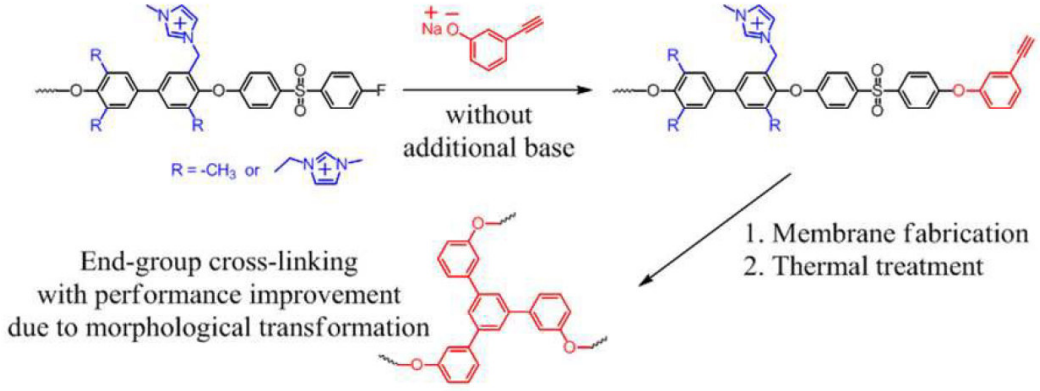

Figure 1-14. Chemical reaction of end group Crosslinking strategy of poly(arylene eteher sulfone).[65]

Poly (phenylene oxides) (Figure 1-13a) as AEMs gained more attention due to their availability and facile bromination of methyl groups avoiding the toxic and carcinogenic chloromethylation reagents.[44] Crosslinking was also effective stategy to enhance the stability of PPO-based AEMs. Hickner and coworkers reported that the crosslinking of PPO based AEMs *via* thiol-ene click chemistry, mitigated the membrane degradation to some extent (Figure 1-15). Through the allakine treatment at 80ºC for 500 h, the crosslinked membranes exhibited 27% and 52% loss of conductivity in 1M and 4M NaOH respectively, while the uncross-linked membranes lost 57% and 73% of their conductivity in 1M and 4M NaOH respectively, demonstrating the positive effect of crosslinking on membrane properties.[66]

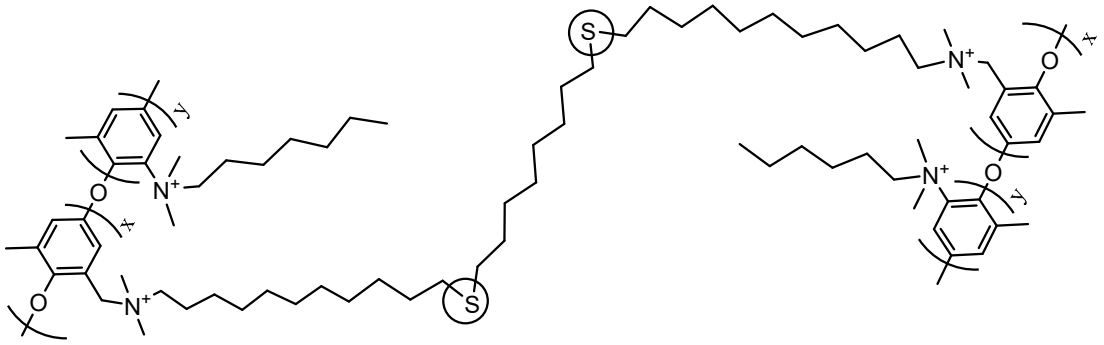

Figure 1-15. Crosslinked PPO-based AEMs *via* thiol-ene click chemistry.

Another crosslinking method was applied by Xue et. al.[67] using PPO containing azide groups (PPO-N_3) as macromolecular crosslinker for poly (vinylbenzyl chloride) (PVBC) based AEMs. The membrane was prepared by photo crosslinking via UV-irradiation followed catsting, quaternizatin and alkylation (Figure1-16). The resulted membrane showed good alkaline stability with 15 % loss of conductivity in 1M NaOH at 80 ºC for 500 h, while the uncross-linked membrane lost 58% of its conductivity at the same conditions.[67]

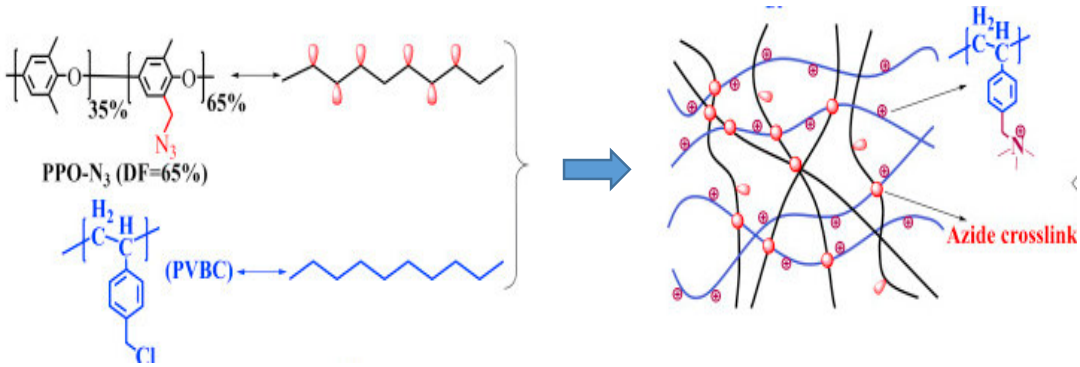

Figure 1-16. preparation of crosslinked PVBC- based AEMs using macromolecular PPO-N_3 cross-linker.[67]

1.2.3.1.3 Grafting of polymeric materials

Grafting of a commercially available polymer or a synthesized polymeric materials was reported as one one the successful approaches to improve the stability and conductivity of AEMS.[68,69] Ran

et. al reported that grafting PPO copolymers by poly (quaternary 4-vinylbenzyl chloride) (PPO-*g*-QVBC), significantly improved the conductivity and alkaline stability of the membrane (Figure 1-17). PPO-g-QVBC based AEM retained 80% of its conductivity and IEC values after 550 h in 2M NaOH at 60 ºC and without further loss up to 1440 h. While conventional PPO based AEMs lost 60% of IEC values at the same conditions.[68]

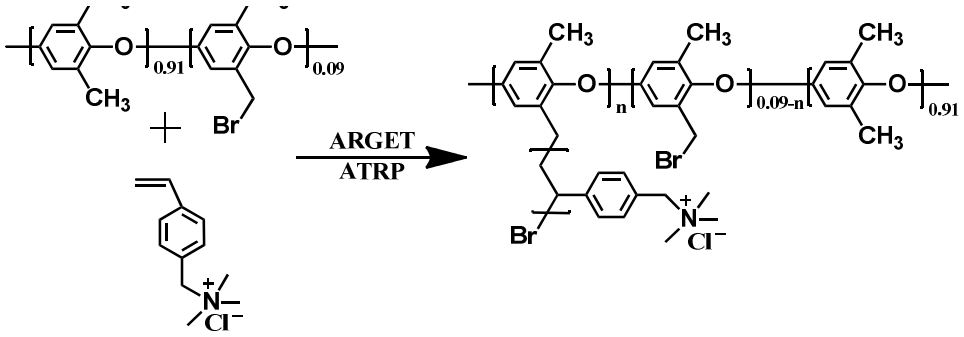

Figure 1-17. Synthesis of the poly (phenylene oxide) grafted by poly (quaternary 4-vinylbenzyl chloride) (PPO-*g*-QVBC).[68]

Pandey et. al. prepared (PPO-*g*-QVBC) membranes through the processing by solvent casting and melt pressing. The resulted membrane showed a good stability, since it exhibited only 3% loss of conductivity after in 1M KOH at 80 ºC for 12 days.[69]

1.2.3.1.4 Alkali doped based AEMs.

The quaternized poly (benzimidazole) (PBI) was unstable in alkaline medium over 60ºC, due to alkaline attack at C2 position of imidazolium ring.[70] However, another series of AEM based on alkli-dopped PBI, have been reported and exhibited excellent alkaline stability since it retained the high conductivity in 1M NaOH even at 100 ºC over 1000 h (Figure 1-18).[71] Unfortunately, the alkali bounded to PBI *via* hydrogen bonds gradually released in long term fuel cell operation, resulting in significant decrease in conductivity and voltage loss of the cell.[72] Another challenge is the fabrication of alkali-dopped AEM in electrode assembly due to their week solubility except in

high boiling point polar solvents.[72]

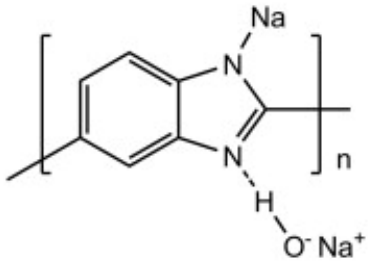

Figure 1-18. Alkali-dopped poly(2,5-benzimidazole) based AEM.[72]

1.2.3.1.5 Poly (phenylene) based AEMs

Recently, a relatively stable AEMs were simply synthesized in absence of grafting or crosslinking. This kind of membranes composed of polymer backbones containing no ether, ketone or sulfone bonds in the main chain that provide long durability in alkaline medium. Hibbs *et. al.* succeeded to synthesize the polyphenylene based AEMs without heteroatoms, ether, ketone or sulfone groups (Figure 1-19a), so that the membrane exhibited excellent stability even in 4 M KOH at 90 ºC for 336 h without change in IEC and 5% loss in conductivity.[73]

Also Bae and coworkers synthesized AEMs free of heteroatoms and ether groups based on poly (biphenyl alkylene) *via* free metal catalysis using acid condensation of trifluoroketones and biphenyls (Figure 1-19b). Poly (biphenyl alkylene)-based AEMs showed excellent alkaline stability since it survived for 720 h in 1M NaOH at 80 ºC with negligible change in IEC and conductivity.[74]

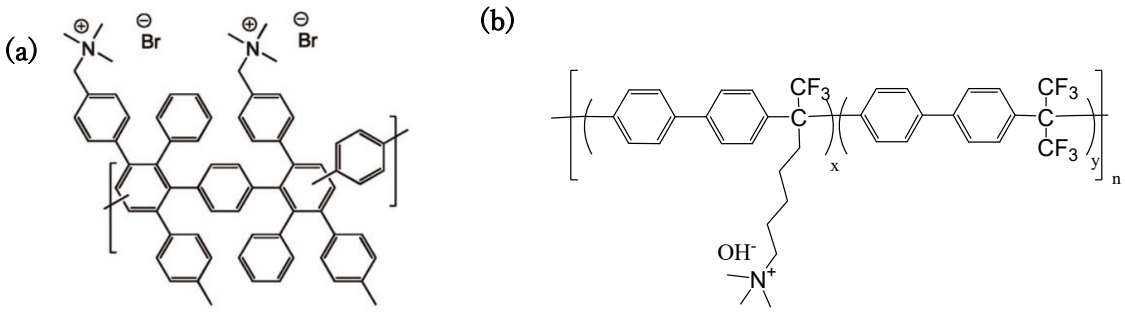

Figure 1-19. Chemical structures of a) poly phenylene and (b) poly(biphenyl alkylene).[73, 74]

Another stable polymer backbone free of ether linkages based on fluorene structure has been reported (Figure 1-20).[75] The fluorene-based membranes exhibited excellent alkaline stability since the ^{1}H NMR data of the membranes after 30 days in 1M NaOH at 80 °C, showed no evidence for degradation suggesting the long durability of these membranes in alkali. The stability of fluorene-based AEMs is attributed to both lack of ether bonds and long spacing between polymer backbone and quaternary ammonium (which will be discussed in detail in the next section).[75]

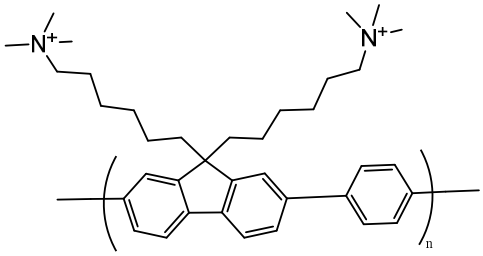

Figure 1-20. Chemical structure of fluorene-based AEMs.[75]

From the previous studies, a significant variation in the membrane properties and specifically in the resistance towards strong alkali, was observed by changing the polymer backbone, synthetic strategy or functionalization method. However, the standard AEM has not been reported. So that, many research attempts have been devoted to different strategy, that is investigating the optimum cationic group for the suitable polymer backbone.

1.2.3.2 Effect of ammonium structure on properties of AEMs

The quaternary ammonium moieties (QA), as the most common cation, play the main role as the ion exchangeable sites on the polymer main chain which are responsible for the ionic conduction of the AEMs. However, the degradation of QA in alkaline medium *via* different degradation pathways (See section 1.1.3.4) represent the main challenge for the scientists that hinder the commercialization of the alkaline fuel cell until now. Basically AEMs are functionalized by different cationic species such as quaternary ammonium (QA), phosphonium and sulfonium. QA

was found to be more chemically and mechanically stable than phosphonium and sulfonium.[76] There have been a few reports on sulfonium based-AEMs due to their low alkaline and thermal stability than that of QAs (Figure 1-21). [77, 78]

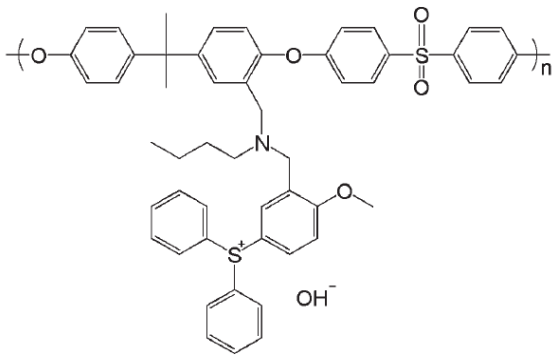

Figure 1-21. Chemical structure of sulfonium based AEM.[78]

On the other hand, Phosphonium cations exhibited different stability according to the chemical structure. For example, Arges et. al. reported that polysulfone functionalized by trimethylphosphonium degraded faster than trimethylammonium counterpart.[79]

However, increasing the steric hinderance around phosphonium cation, enhanced the stability to some extent. For example, polysulfone functionalized with bulky Tris(2,4,6-trimethoxyphenyl) phosphonium cation maintained its initial conductivity and flexibility for 30 days in 1M KOH at 60 ^{o}C (Figure 1-22).[80,81] On contrast, Ramani and coworkers reported in study using *2D*-NMR analysis that phosphonium cations degraded more rapidly than QA *via* Summelet-Hauser rearrangement and direct nucleophilic attack.[82]

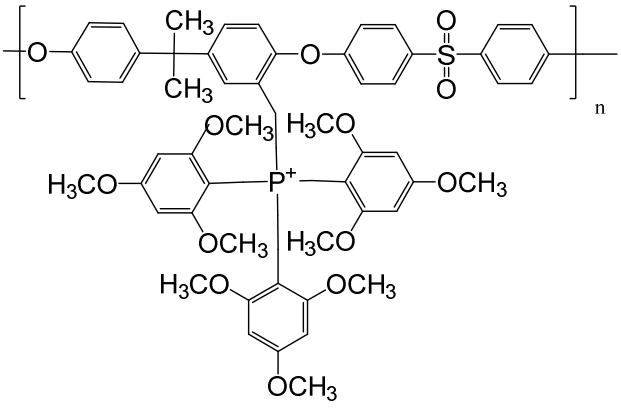

Figure 1-22. Chemical structure tris (2,4,6-trimethoxyphenyl) phosphonium based AEM.[80]

Recently, tetrakis (dialkylamino) phosphonium functionalized polyethylene based AEM exhibited excellent stability in 1M KOH at 80 °C for 22 days maintaining 82% of its conductivity (Figure 1-23).[83] The excellent stability is attributed to the charge delocalization on the phosphonium cation. Unfortunately, this membrane was prepared by multi-step synthesis (six steps) that may increase the cost and hinder its commercialization.

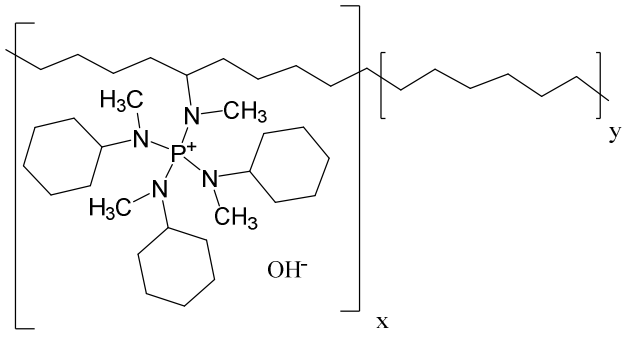

Figure 1-23. Chemical structure of Phosphonium based AEMs.[83]

1.2.3.2.1 Investigation of ammonium cations for low cost and synthetic facility.

A variety of ammonium cations have been suggested in the literature, such as ammonium,[84] imidazolium,[85] guanidinium,[86] pyridinium,[87] morpholinium,[88] spiro-ammonium[89] and metal

cations[90]. Some are claimed to be stable under harsh conditions (e.g., highly concentrated alkaline solution) for substantial period of time,[57] however, the most common ionic groups for AEMs are quaternary ammonium groups (QAs) because of the low cost and facile synthesis via direct quaternization of benzylic or alkyl halides, and their reasonable stability if they are properly attached to the polymer structure.[57]

Substituents and electronic structure of the ammonium groups strongly affect the properties and stability of the AEMs. The alkaline stability of QAs has been extensively studied with small model compounds or polymer membranes. For example, Marino et al. reported the stability of various ammonium compounds under harsh alkaline conditions (in 6 M NaOH at 160 ºC) and concluded that 6-azonia-spiro [5, 5]undecane (ASU) was the most stable QA since it exhibited the longest half-life (110 h) among the tested groups under harsh alkaline conditions at 160 ºC in 6M NaOH (Figure 1-24).[91]

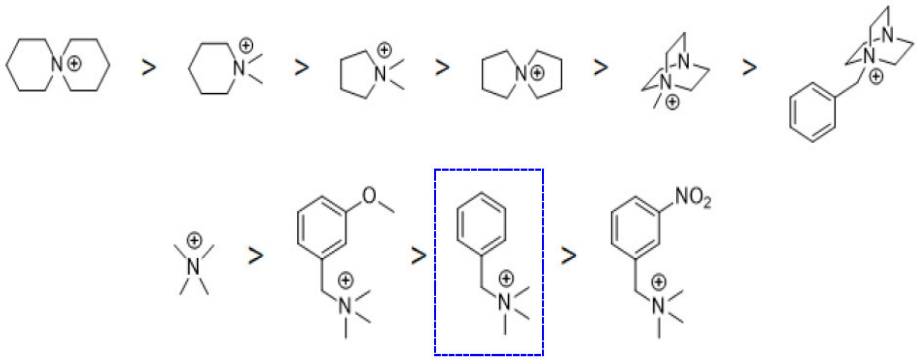

Figure 1-24. Comparison between the stability of different cations.[91]

Such spiro-cyclic ionic groups, when incorporated into the polymer backbone, improved significantly the alkaline stability of the AEM up to 1896 h at 80 ºC in 1 M KOD/D_2O but a sign of degradation was observed at 120 ºC.[91] Unfortunately, these copolymers were readily soluble in water that may hinder their effective fabrication in alkaline fuel cells. So that, the membrane was blended with commercial poly (benzimidazole) by ionic crosslinking to improve its mechanical properties.[92]

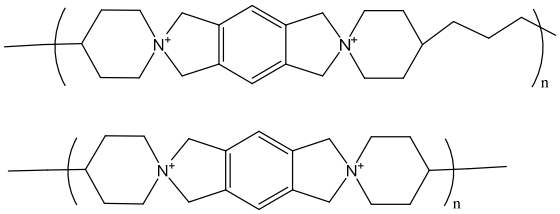

Figure 1-24. Spiro-cylic ionic groups incorporated in the polymer main chain.[92]

However, when the same ionic groups were attached to aromatic PAES backbone (Figure 1-25), the degradation occurred more easily even at 40 ºC due to the benzylic sites prone to nucleophilic attack by hydroxide ions besides the susceptibility of PAES backbone to alkaline attack (see section 1.1.3.4.1).[89]

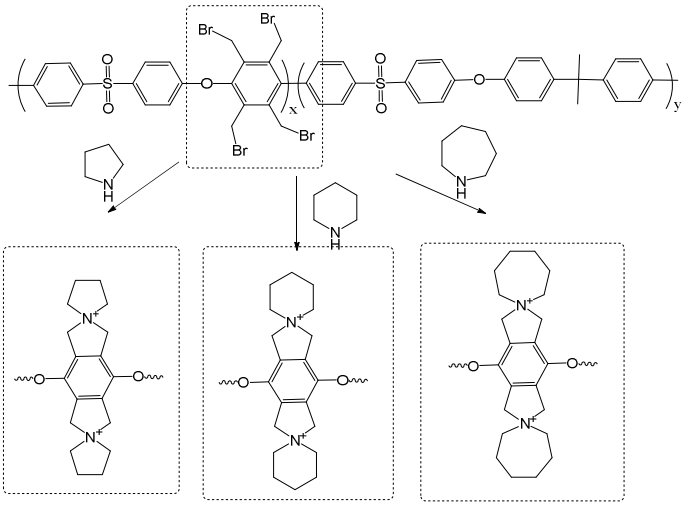

Figure 1-25. Synthesis of spiro-cyclic based AEMs attached to polymer.[89]

Bae and his coworkers[93] reported mechanistic study for another series of cationic groups (Figure 1-26) and revealed that the alkyl spacer substituted QAs (aliphatic and/or bulky alicyclic) were more alkaline stable than benzylic-substituents. The reason is attributed to the steric hindrance of side chains around the ammonium cation, besides lack of the de-shielding effect of main chain aromatic rings when QA stay far from aromatic proximity.[93]

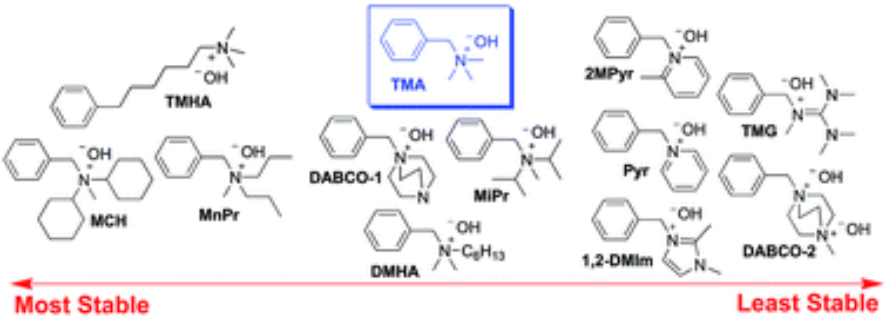

Figure 1-26. Schematic diagram for the alkaline stability of various cationic groups.[93]

Jannasch et al.[94] also reported that long aliphatic groups directly attached to benzylic sites or as spacers between the polymer backbone and the ammonium groups contributed to stabilizing the resulting PPO based AEMs. Constructing the flexible aliphatic chains as spacer and as extender chains on the QA (Figure 1-27), provided the free bath for effective ionic conduction and significantly improved the stability without detectable degradation up to 196 h in 1M NaOH at 80 ^{o}C.[94]

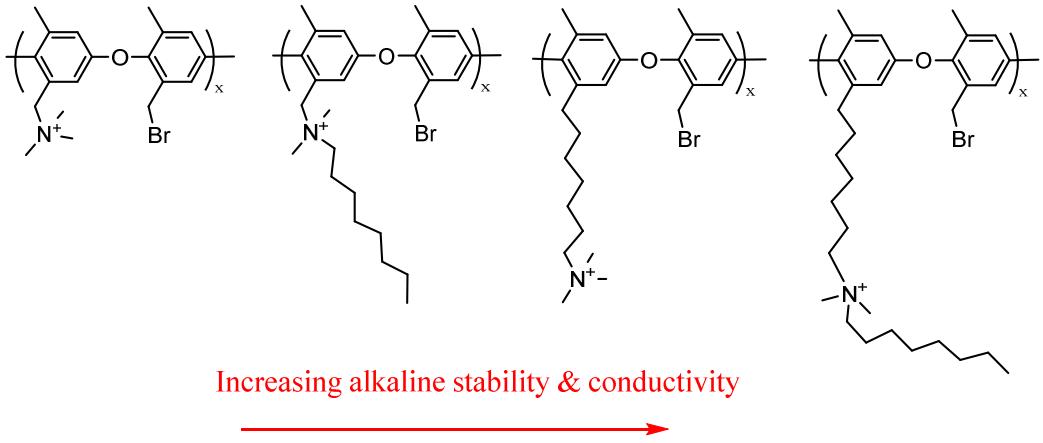

Figure 1-27. Chemical structure of PPO based AEMs with pendant alkyl side chains or flexible on QAs.[94]

Li et al.[95] supported the same idea for a different type of AEM based on polypropylene with long alkyl spacer in the side chain and on QA. The copolymers were prepared by heterogeneous Ziegler-Natta catalyst mediated polymerization and the membranes was prepared by melt pressing in bromo methyl form followed by quaternization method at 160 ºC or thermally crosslinked at 220 ºC using styrenic diene crosslinker. Both cross-linked and noncross-linked membranes exhibited excellent stability since it retained more than 85% of conductivity even in 5 M or 10 M NaOH at 80 ºC for 700 h (Figure 1-28).[95]

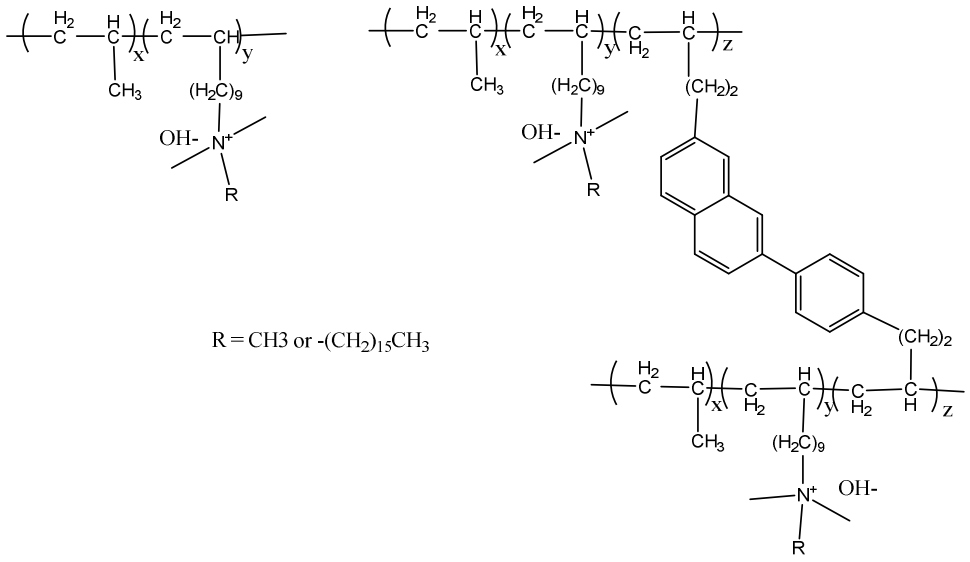

Figure 1-28. Chemical structure of polypropylene based AEMs with alky spacers QA.[95]

In contrast, an accelerated stability test for a model compound to PPO structure demonstrated that both of benzylic and alkyl spacer QAs degraded at the same rate when exposed to 4 equivalents of $NaOCH_3$ in DMSO-d_6/$CDOD_3$ (20:1) solution at 80 ºC for 48 h.[62] Moreover, Ramani et al.[96] reported that alkyl spacing QAs were not suitable since PPO functionalized with hexyl spacer (using different synthetic method from the previous reports[94]) degraded faster than the corresponding PPO without spacing when exposed to 1 M KOH at 60 ºC for 720 h.

Recently, insertion of pendant aliphatic chains to QAs attached to the polymer backbone was found to play an important role in developing the phase-separation and water utilization as well as enhancing the stability of AEMs.[97] In this regard, Binder et al. reported that PPO functionalized with pendant alkyl group (C16) achieved good alkaline stability after 500 h in 1 M NaOH at 80 ºC maintaining 80% of its initial conductivity.[98] In a separate study, Hickner et al. investigated the effect of flexible alkyl spacer from C6 to C16 on PPO backbones and found that all spacers enhanced the stability and conductivity compared with BTMA counterpart.[99] C6-C16 spacing possessed good alkaline and mechanical stability even after 2000 h in 1 M NaOH at 80 ºC, maintaining 80% of their initial conductivity (Figure 1-29). Recently, a review by Kreuer[100] concluded that the most promising approach to enhance the alkaline stability of AEMs is using alkyl spacers around the ammonium groups either tethered to amine or separated from polymer chain, which were likely to increase the steric shielding and mitigate the attack by the hydroxide anions.[100]

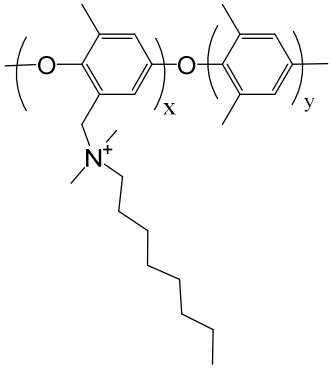

Figure 1-29. Chemical structure of poly (phenylene oxide) functionalized with pendant alkyl chain on quaternary ammonium.[99]

The inconsistent results on the stability of polymer backbones and ionic groups suggested that the effects of ionic groups as well as the polymer backbones had to be more carefully investigated for improving the stability of AEMs.[57]

1.3 Aim of the current study

Looking at the previous studies on anion conductive membranes for alkaline fuel cells as described above, it seems that the alkaline stability is the most critical challenge for AEMs due to the complex situation of the degradation mechanisms either from the polymer main chain or from quaternary ammonium. In our group, the polymer backbone of AEMs was extensively studied and different polymer structures have been investigated and recently it was found that the presence of ether bonds near to hydrophilic proximity, accelerated the degradation rate of the membranes.[63] So that, a new class of polymers were developed, based on oligophenylene moieties in hydrophilic segments such as poly(arylene ether) block copolymer based AEM (QPE-bl-9) and partially fluorinated aromatic copolymer (QPAF).[56, 101] In particular, QPE-bl-9 and QPAF membranes exhibited high anion conductivity and good mechanical stability. However, the membranes lost most of its anion conductivity in 1 M KOH at 60 or 80 ºC within several hundred hours due to the decomposition of BTMA groups.[56, 101] From the previous studies, the structure of ammonium groups plays effective role in the properties and stability of AEMs. For a distinct polymer structure, optimizing the suitable cation is a main challenge to enhance the properties of the resulted membranes. The objective of the present study is to investigate the effect of different ammonium structures on the properties and stability of two reported oligophenylene based AEMs (QPE-bl-9 and QPAF).

In chapter 1, QPE-bl-9 membrane was selected to investigate the influence of various ammonium structures on its properties due to its high conductivity, mechanical stability and good cell performance. The ammonium structures include the common trimethylamine (TMA), dimethylhexylamine (DMHA) stabilized by steric factor of pendant alkyl chain. I also selected some structures stabilized by steric factor of bulky structure such as dicyclohexylmethlamine (DCHMA) and tributylamine (TBA) and finally another heterocyclic groups were selected that stabilized by resonance and charge delocalization; methylimidazole (MIm) and dimethylimidazole (DMIm). The PE-bl-9 copolymers and chloromethylated copolymer (CMPE-bl-9) were prepared according to the literature[56] then the membranes were prepared through casting and Menshutkin

reaction with different amines. The membrane properties were carefully studied through the NMR analysis, TEM images, conductivity and water uptake measurements and alkaline stability testing besides the mechanical properties through DMA analysis. The ammonium structures under investigation are expected to improve the properties of QPE-bl-9 membranes such as conductivity and alkaline stability.

In Chapter 2, The results in chapter 1, motivated me to investigate the effect of pendant aliphatic ammonium groups on the properties of partially fluorinated and aromatic copolymer AEM (QPAF). To elucidate the effect of flexible aliphatic ammonium groups onto the properties of QPAF membrane, two ammonium structures with pendant alkyl chains were selected; dimethylbutyl amine (DMBA) and dimethylhexylamine (DMHA). The results were compared with the common BTMA and heterocyclic structure (1,2-dimethylimidazolium). The membrane properties were carefully studied through the detailed examination of the morphology, ion conductivity, and alkaline and mechanical stability besides the fuel cell performance. It is expected that the new ammonium structure may enhance the stability and performance of QPAF membranes.

1.4 References

1- Jaccard, M. *Sustainable Fossil Fuels: The Unusual Suspect in the Quest for Clean and Enduring Energy*; Cambridge University press, 2006.

2- Greene, D.; Kahn, J.; and Gibson, R. *Energy J.* **1999***, 20*, 1–31.

3- Williams, S. R. *Nuclear and Alternative Energy Supply Options for an Environmentally Constrained World: A Long-Term Perspective,*" in Leventhal, P.; Dolley, S.; and Tanzer, S. *Nuclear Power and the Spread of Nuclear Weapons: Can We Have One Without the Other?*; Washington, D.C.: Brassey's Inc., 2002.

4- Lyman, E.; Dolley, S. *Bull. At. Sci.* **2000**, *56*, 42–46.

5- Li, N. W.; Guiver, M. D. *Macromolecules* **2014**, *47*, 2175-2198.

6- Lu, S.; Pan, J.; Huang, A.; Zhuang, L.; Lu, J. *Proc. Natl. Acad. Sci. USA* **2008**, *105*, 20611–20614.

7- Hoffmann, P.; Dorgan, B. *Tomorrow's Energy: Hydrogen, Fuel Cells, and the Prospects for a Cleaner Planet*; Cambridge, Massachusetts (The MIT Press), 2012.

8- Borup, R.; Meyers, I.; Bryan, P. *Chem. Rev.* **2007**, *107*, 3904-3951.

9- Wang, Y.-J.; Qiao, J.; Baker, R.; Zhang, J. *Chem. Soc. Rev.* **2013**, ***42***, 5768-5787.

10- Shin, D. W.; Guiver, M. D.; Lee, Y. M. *Chem. Rev.* **2017**, *117*, 4759–4805.

11- Chen, J.; He, G.; Zhang, F. *Int. J. Hydr. Enrg.* **2015**, *40*, 7348-7360.

12- Li, N. W.; Guiver, M. D. *Macromolecules* **2014**, *47*, 2175-2198.

13- Varcoe, J. R.; Atanassov, P.; Dekel, D. R.; Herring, A. M.; Hickner, M. A.; Kohl, P. A.; Kucernak, A. R.; Mustain, W. E.; Nijmeijer, K.; Scott, K.; Xu, T. W.; Zhuang, L. *Energy Environ. Sci.* **2014**, *7*, 3135-3191.

14- Wang,Y.; Zhang, Z.; Jiang, C.; Xu, T. *Ind. Eng. Chem. Res.* **2013**, *52*, 18356−18361.

15- : Rahman, F.; Skyllas-Kazacos, M. *J. Power Sources* **2009**, *189*, 1212–1219.

16- : Carmo, M; Fritz, D. L.; Mergel, J.; Stolten, D. *Int. J. Hydrogen Energy*. **2013**, *38*, 4901-4934.

17- Published by Smithsonian Institution, 2017. “Fuel cell Basics : Alkli fuel cells”, http://www.americanhistory.si.edu/fuelcells/basics.htm

18- Dean, J. A. Lange’s Handbook of Chemistry, 15th ed.; McGrawHill: New York, 1999.

19- Vanysek, P. *Ionic Conductivity and Diffusion at Infinite Dilution*. In CRC Handbook of Chemistry and Physics, 83rd ed.; Lide, D. R., Ed.; CRC Press: Boca Raton, FL, 2002.

20- Zhang, Z. C.; Chalkova, E.; Fedkin, M.; Wang, C.; Lvov, S. N.; Komarneni, S.; Chung, T. C. *Macromolecules* **2008**, *41*, 9130−9139.

21- Ran, J.; Wu, L.; Wei, B.; Chen, Y.Y.; Xu, T.W. *Sci. Rep.* **2014**, 4, 6486.

22- Grew, K. N.; Chiu, W. K. S. *J. Electrochem. Soc.* **2010**, *157*, B327−B337.

23- Marx, D. *ChemPhysChem*, **2006**, *7*, 1848.

24- Tuckerman,M.; Laasonen, K.; Sprik, M.; Parrinello, M. *J. Chem. Phys.* **1995**, *103*, 150.

25- Tuckerman, M.; Laasonen, K.; Sprik, M.; Parrinello, M. *J. Phys. Chem.* **1995**, *99*, 5749.

26- Asthagiri, D.; Pratt, L. R.; Kress, J. D.; Gomez, M. A. *Proc. Natl. Acad. Sci. U.S.A.* **2004**, *101*, 7229.

27- Barbir, F. *PEM Fuel Cells Theory and Practice,* Elsevier, Burlington, MA, 2005.

28- Thampan, T.; Malhotra, S.; Tang, H.; Datta,R. *J. Electrochem. Soc.* **2000**, *147*, 3242.

29- Commer, P.; Cherstvy, A. G.; Spohr, E.; Kornyshev, A. A. *Fuel Cells* **2002,** *2*, 127.

30- Choi, P.; Jalani, N. H.; Datta, R. *J. Electrochem. Soc.* **2005**, *152*, E84.

31- Choi,P.; Jalani, N. H.; Datta, R. *J. Electrochem. Soc.* **2005**, *152*, E123.

32- Paddison, S. J.; Paul, R.; Zawodzinski, T. A.; Jr. *J. Electrochem. Soc.* **2000**, *147*, 617.

33- Paddison, S. J.; Paul, R. *Phys. Chem. Chem. Phys.* **2002**, *4*, 1158.

34- Weber, A. Z.; Newman, J. *J. Electrochem. Soc.* **2003**, *150*, A1008.

35- Weber, A. Z.; Newman, J. *J. Electrochem. Soc.* **2004**, *151*, A311.

36- Wang, Y.-J.; Qiao, J.; Baker, R.; Zhang, *J.* ***Chem. Soc. Rev.*** **2013**, ***42***, 5768-5787.

37- Zhu, L.; Zimudzi, T. J.; Li, N.; Pan, J.; Lina, B.; Hickner, M. A. *Polym. Chem.* **2016**,*7*, 2464-2475.

38- Tanaka, M.; Fukasawa, K.; Nishino, E.; Yamaguchi, S.; Yamada, K.; Tanaka, H.; Bae, C.; Miyatake, K.; Watanabe, M. *J. Am. Chem. Soc.* **2011**, *133*, 10646-10654.

39- Hickner, M.A.; Pivovar, B.S. *Fuel Cells* **2005**, 5, 213-229.

40- Kreuer, K.D. *J. Memb. Sci.* **2001**, *185*, 29-39.

41- Arges, C. G.; Ramani., V. *Proc. Natl. Acad. Sci. USA* **2013**, *11*, 2490-2495.

42- Fujimoto, C.; Kim, D.-S.; Hibbs, M.; Wrobleski, D.; Kim, Y. *J. Membr. Sci.* **2012**, *423*, 438−449

43- Choe, Y. K.; Fujimoto, C.; Lee, K. S.; Dalton, L. T.; Ayers, K.; Henson, N. J.; Kim, Y. S. *Chem. Mater.* **2014**, *26*, 5675−5682.

44- Ameduri, B. *Chem. Rev*. **2009**, *109*, 6632–6686.

45- Merle, G.; Wessling, M.; Nijmeijer, K. *J. Membr. Sci.* **2011**, *377*, 1.

46- Bauer, B.; Tirathmann, H.; Effenberger, F. *Desalination* **1990**, *79*, 125.

47- Bauer, B.; Tirathmann, H.; Effenberger, F. *Desalination* **1990**, *79*, 125

48- Ye, Y.; Elabd, Y. A. *ACS Symposium Series* **2012**, *1096*, 233–251.

49- Kantor, S. W.; Hauser, C. R. *J. Am. Chem. Soc.* **1951**, *73*, 4122.

50- Stevens, T. S.; Creighton, E. M.; Gordon, A. B.; MacNicol, M. *J. Chem. Soc.* **1928**, 3193.

51- Weissmann, M.; Coutanceau, C.; Brault, P.; L´eger, J.-M. *Electrochem. Commun.*, **2007**, *9*, 1097.

52- Varcoe, J. R. *Phys. Chem. Chem. Phys.* **2007**, *9*, 1479.

53- Gonza´lez, J. P.; Whelligan, D. K.; Wang, L.; Soualhi, R. B.; Wang,Y.; Peng, Y.; Peng, H.; Apperley, D. C.; Sarode, H. N.; Pandey, T. P.; Divekar, A. G.; Seifert, S.; Herring, A. M.; Zhuang, L.; Varcoe, J. R. *Energy Environ. Sci.* **2016**, *9*, 3724-3735.

54- Mamlouk, M.; Horsfall, J. A.; Williams, C.; Scott, K. *Int. J. Hydrogen Energy* **2012**, *37*, 11912-11920.

55- Kim, Y. S. US DOE Hydrogen and fuel cells program and vehicle technologies program annual merit review, 2011, http://www.hydrogen.energy.gov/pdfs/review11/fc043_kim_2011_o.pdf.

56- Yokota, N.; Shimada, M.; Ono, H.; Akiyama, R.; Nishino, E.; Asazawa, K.; Miyake, J.; Watanabe, M.; Miyatake, K. *Macromolecules* **2014**, *47*, 8238-8246.

57- Mahmoud, A. M. A.; Elsaghier, A. M. M.; Miyatake, K. *Macromolecules* **2017**, 50, 4256-4266.

58- Li, N.; Leng, Y.; Hickner, M. A.; Wang, C. Y. *J. Am. Chem. Soc.* **2013**, *135*, 10124-10133.

59- Zschocke, P.; Quellmalz, D. *J. Mater. Sci.* **1985**, *22*, 325–32.

60- Fujimoto, C.; Kim, D.-S.; Hibbs, M.; Wrobleski, D.; Kim, Y. *J. Membr. Sci.* **2012**, *423*, 438−449

61- Choe, Y. K.; Fujimoto, C.; Lee, K. S.; Dalton, L. T.; Ayers, K.; Henson, N. J.; Kim, Y. S. *Chem. Mater.* **2014**, *26*, 5675-5682.

62- Mohanty, A. D.; Tignor, S. E.; Krause, J. A.; Choe, Y.-K.; Bae, C. *Macromolecules* **2016**, *49*, 3361-3372.

63- Yokota, N.; Ono, H.; Miyake, J.; Nishino, E.; Asazawa, K.; Watanabe, M.; Miyatake, K. *ACS Appl. Mater. Interfaces*, **2014**, *6*, 17044–17052.

64- Dong, X.; Hou, S.; Mao, H.; Zheng, J.; Zhang, S. *J. Memb. Sci.* **2016**, *518*, 31-39.

65- Lee, K. H.; Cho, D. H.; Kim, Y. M.; Moon, S. J.; Seong, J. G.; Shin, D. W.; Sohn, J. Y.; Kim J. F .and Lee, Y. M. Energy Environ. Sci. **2017**, *10*, 275-285.

66- Zhu, L.; Zimudzi, T.; Li, N.; Pan, J.; Lin, B.; Hickner, M. A. *Polym. Chem.* **2016**, *7*, 2464-2475.

67- Xue, J.; Liu, L.; Liao, J.; Shen, Y.; Li, N. *J. Memb. Sci.* **2017**, *535*, 322-330.

68- Ran, J.; Wu, L.; Wei, B.; Chen, Y.Y.; Xu, T.W. *Sci. Rep.* **2014**, *4*, 6486.

69- Pandey, T. P.; Seifert, S.; Yang, Y.; Yang, Y.; Knauss, D. M.; Liberatore, M. W.; Herring, A. M. *Electrochim. Acta.* **2016**, *222*, 1545-1554.

70- Valade, D.; Boschet, F.; Roualdès, S.; Ameduri, B. *J. Polymer Sci., Part A: Polymer Chem.* **2009**, *47*, 2043.

71- Luo, H.; Vaivars, G.; Agboola, B.; Mu, S.; Mathe, M. *Solid State Ionics* **2012**, *208*, 52–55.

72- Zeng, L.; Zhao, T. S.; An, L.; Zhao, G.; Yan, X. H. *Energy Environ. Sci.* **2015**, *8*, 2768-2774.

73- Hibbs, M. R. *J. Polym. Sci., B: Polym. Phys.* **2013**, *51*, 1736-1742.

74- Lee, W. H.; Kim, Y. S.; Bae, C. *ACS Macro Lett.* **2015**, *4*, 814-818.

75- Lee, W.-H.; Mohanty, A. D.; Bae, C. *ACS Macro Lett.* **2015**, *4*, 453–457

76- Couture, G.; Alaaeddine, A.; Boschet, F.; Ameduri, B. *Prog. Polym. Sci.* **2011**, *36*, 1521–1557.

77- Merle, G.; Wessling, M.; Nijmeijer, K. *J. Membr. Sci.* **2011**, *377*, 1–35.

78- Zhang, B.; Gu, S.; Wang, J.; Liu, Y.; Herring, A. M. and Yan, Y. *RSC Adv.* **2012**, *2*, 12683–12685.

79- Arges, C. G.; Parrondo, J.; Johnson, G.; Nadhan, A.; Ramani, V. *J. Mater. Chem.* **2012**, *22*, 3733–3744.

80- Gu, S.; Cai. R.; Luo, T.; Chen, Z.; Sun, M; Liu, Y.; He, G.; Yan, Y. *Angew. Chem. Int. Ed.*

2009, *48*, 6499-6502.

81- Gu, S.; Cai. R.; Luo, T.; Jensen, K.; Contreras, C.; Yan, Y. *ChemSusChem* **2010**, *3*, 555-558.

82- Arges, C. G.; Ramani, V. *J. Electrochem. Soc.* **2013**, *160*, F1006-F1021.

83- Noonan, K. J. T.; Hugar, K. M.; Kostalik, H. A.; Lobkovsky, E. B.; Abrunna, H. D.; Coates, G. W. *J. Am. Chem. Soc.* **2012**, *134*, 18161-18164.

84- Deavin, O. I.; Murphy, S.; Ong, A.; Poynton, S. D.; Zeng, R.; Herman, H.; Varcoe, J. R. *Energy Environ. Sci.* **2012**, *5*, 8584.

85- Lin, B.; Dong, H.; Li, Y.; Si, Z.; Gu, F.; Yang, F. *Chem. Mater.* **2013**, *25*, 1858-1867.

86- Liu, L.; Li, Q.; Dai, J.; Wang, H.; Jin, B.; Bai, R. *J. Mem. Sci.* **2014**, *453*, 52-60.

87- Miyake, J.; Fukasawa, K.; Watanabe, M.; Miyatake, K. *J. Polym. Sci. Polym. Chem.* **2014**, *52*, 383-389.

88- Morandi, C. G.; Peach, R.; Krieg, M. H.; Kerres, J. *J. Mater. Chem. A* **2015**, *3*, 1110-1120.

89- Pham, T. H.; Jannasch, P. *ACS Macro Lett.* **2015**, *4*, 1370-1375.

90- Disabb-Miller, M. L.; Zha,Y.; Declaro, A. J.; Pawar, M.; Tew, G. N.; Hickner, M. A. *Macromolecules* **2013**, *46*, 9279-87.

91- Marino, M. G.; Kreuer, K. D. *ChemSusChem.* **2014**, 7, 1-12.

92- Pham, T. H.; Olsson, J. S.; Jannacsh, P. *J. Am. Chem. Soc.* **2017**, *139*, 2888-2891.

93- Mohanty, A. D.; Bae, C. *J. Mater. Chem. A* **2014**, *2*, 17314−17320.

94- Dang, H. S.; Jannasch, P. *Macromolecules* **2015**, *48*, 5742-5751.

95- Zhang, M.; Liu, J.; Wang, Y.; An, L.; Guiver, M. D.; Li, N. *J. Mater. Chem. A* **2015**, *3*, 12284-12296.

96- Parrondo, J.; Jung, M. J., Wang, Z.; Arges, C. G.; Ramani, V. *J. Electrochem. Soc.* **2015**, *162*, F1236-F1242.

97- Jannacsh, P.; Weiber, E. A. *Macromol. Chem. Phys.* **2016**, *217*, 1108-1118.

98- Li, N.; Yan, T.; Li, Z.; Albrecht, T. T.; Binder, W. H. *Energy Environ. Sci.* **2012**, *5*, 7888-7892.

99- Li, N.; Leng, Y.; Hickner, M. A.; Wang, C. Y. *J. Am. Chem. Soc.* **2013**, *135*, 10124-10133.

100- Kreuer, K.-D. *Chem. Mater.* **2014**, *26*, 361-380.

101- Ono, H.; Miyake, J.; Shimada, S.; Uchida, M.; Miyatake, K. *J. Mater. Chem. A* **2015**, *3*, 21779-21788.

Chapter 2

Effect of ammonium groups on the properties of anion conductive membranes based on partially fluorinated aromatic polymers

2.1 Introduction.

From chapter 1, the urgent demand for a highly conductive and alkaline stable anion exchange memebrane (AEM) motivated various attempts to develop different synthetic strategies for investigating the applicable AEMs. These synthetic strategied were directd towards enhancing the alkaline stability as the most critical property for AEMs to make it applicable in alkaline fuel cells. It was reported that the stability of AEMs not only depend on the polymer backbone but also on the cationic groups. Various cationic groups were used to functionalize AEMs and among them is quaternary ammonium (QA) that gained more attention due to the facile synthesis and lower cost. In chapter 2, A partially fluorinated aromatic block copolymer Poly(arylene ether) based AEM (QPE-bl-9) was selected for investigating the ammonium structure effect on its properties. It was reported that QPE-bl-9 exhibited high conductivity (138 mS/cm, 80 ^{o}C, 2.0 meq/g) and good mechanical strength besides its high cell performance (520 mW/cm^2).[1] The effect of ammonium groups on QPE-bl-9 membranes was carefully studied using various bulky and/or π-conjugated ammonium groups. The properties of the resulting QPE-bl-9 membranes with different functionalities were characterized through NMR analysis, TEM imaged, water uptake, conductivity and alkaline stability measurements besides the mechanical strength testing by DMA analysis.

2.2 Experimental

2.2.1 Materials and methods

2.2.1.1 Materials

Decafluorobiphenyl (DFBP), hexafluorobisphenol A (HFBPA), 4-chlorophenol (CP), 1,4-dichlorobenzene, 1,3-dichlorobenzene, bipyridine, dicyclohexylmethylamine (DCHMA), tributylamine (TBA), 1-methylimidazole (MIm), and 1,2-dimethylimidazole (DMIm) were purchased from TCI Inc. and used as received. Potassium carbonate, bis(1,5-cyclooctadiene) nickel(0) ($Ni(cod)_2$), chloromethyl methyl ether (CMME), thionyl chloride (SOCl2), hydrochloric acid, potassium hydroxide, dimethyl sulfoxide (DMSO), N,N-dimethylformamide (DMF), anhydrous lithium bromide, and N,N-dimethylacetamide (DMAc) were purchased from Kanto Chemical Co. and used as received. 1,1,2,2-Tetrachloroethane (TCE) was purchased from Kanto Chemical Co. and dried over 4 Å molecular sieves (Kanto chemicals) before use. Zinc chloride tetrahydrofuran solution, 45% trimethylamine (TMA) aqueous solution, and dimethyl hexylamine (DMHA) were purchased from Sigma-Aldrich and used as received. 1,1,2,2-Tetrachloroethane-d2 (TCE- *d2*), dimethylsulfoxide-d6 with 0.03% TMS (DMSO-*d6*), and chloroform-d1 with 0.03% TMS ($CDCl_3$) were purchased from Acros Organics and used as received. Tokuyama A201 AEM (IEC = 1.7 meq g^{-1}) was kindly supplied by Tokuyama Corp.

2.2.2 Synthesis of PE-bl-9

Oligomers 1 and DFBP-terminated telechelic oligomers 2 were synthesized according to the procedure described in the literature.[1] A typical procedure for the copolymerization of 2 and dichlorobenzenes is as follows (X=4, p : q : r = 1 : 2 : 8). A 100 ml round-bottomed flask equipped with mechanical stirrer under nitrogen atmosphere, was charged with oligomer 2 (0.60 g, 0.14 mmol), 1,4-dichlorobenzene (0.040 g, 0.27 mmol), 1,3-dichlorobenzene (0.16 g, 1.1 mmol), 2,2'-bipyridine (0.57 g, 3.6 mmol), and DMAc (20 mL). The mixture was heated at 80 °C to obtain a homogenous solution, to which $Ni(cod)_2$ (1.0 g, 3.6 mmol) was added. After heating at 80 °C for 3 h, the mixture was cooled to room temperature and diluted with additional DMAc (10 mL). The mixture was poured dropwise into a large excess of diluted hydrochloric acid to precipitate a pale yellow powder. The crude product was washed with ultrapure water and methanol several times.

Drying in vacuum oven at 60 °C provided PE-bl-9 in 92% yield.

2.2.3 Chloromethylation of PE-bl-9

A typical procedure for the preparation of CMPE-bl-9 (X= 4.17, p : q : r = 1 : 2.4 : 12.2) is as follows. A 100 mL round flask with a reflux condenser and a magnetic stirrer, was charged with PE-bl-9 (2.30 g, 0.53 mmol) and TCE (169 mL) under nitrogen atmosphere. The mixture was stirred to obtain a homogeneous solution, to which $SOCl_2$ (12.34 mL), CMME (64.09 mL, 1.35 mol), and $ZnCl_2$ (1.15 g, 8.46 mmol) were added. After the reaction at 80 °C for 24 h, the mixture was cooled to room temperature and poured dropwise into a large excess of methanol. The precipitated crude product was washed with hot methanol several times and dried in a vacuum oven at 60 °C overnight. The obtained CMPE-bl-9 (2.37 g) was dissolved in TCE (24 mL) and casted on to a flat glass plate. Drying the solution at 60 °C gave a membrane (50-100 μm thick).

2.2.4 Quaternization Reactions

Two methods were carried out for the quaternization reactions.

1) Membrane soaking in amine / ethanol solution (used for MIm, DMIm, DCHMA, and TBA): The CMPE-bl-9 membranes were immersed in 1.0 M of amines in ethanol (20 mL) at 60 °C for 48 h, washed with ethanol several times, and immersed in ethanol for 24 h to remove the excess amines. Then, the membranes were immersed in ultrapure water for 24 h prior to the ion conductivity measurements (Cl^- form).

2) Membrane soaking in amine under aqueous or neat conditions (used for TMA and DMHA respectively):

a) In the case of TMA, CMPE-bl-9 membrane was immersed in TMA (45%) aqueous solution at room temperature for 48 h. The obtained membrane was washed with diluted hydrochloric acid and ultrapure water, and dried at 60 °C in vacuum oven.

b) In the case of DMHA, CMPE-bl-9 membrane was immersed in DMHA (98%) at 40 °C for 3 days. The obtained membrane was washed with diluted hydrochloric acid and ultrapure water, and

dried at 60 °C in vacuum oven.

2.2.5 Ion Exchange

The quaternized membranes were immersed in 1 M KOH aqueous solutions at 40 °C for 2 days to exchange the chloride ions to hydroxide ions. After the ion exchange, the membranes were washed with deionized water and stored in a closed vial containing deionized water.

2.2.6 Measurements

The prepared oligomers and polymers were characterized by ^{1}H and ^{19}F NMR spectra on a JEOL JNM-ECA/ECX500 using $CDCl_3$, TCE-*d2*, or DMSO-*d6* as a solvents and tetramethylsilane (TMS) as an internal reference. FT-IR spectra of the membranes were measured using JASCO FT/IR-6100. Molecular weights (M_w and M_n) were estimated *via* gel permeation chromatography (GPC) using a Shodex KF-805L or SB-803 column and a Jasco 805 UV detector with DMF containing 0.01 M lithium bromide as eluent and calibrated with standard polystyrene samples. For transmission electron microscopic (TEM) observation, the selected membranes were stained with tetrachloroplatinate ions by ion exchange of ammonium groups in 0.5 M potassium tetrachloroplatinate (II) aqueous solution, rinsed with deionized water, and dried in vacuum oven at 60 °C. The stained membranes were embedded in epoxy resin, cut into 50 nm thickness, and placed on a copper grid. Dynamic mechanical analysis (DMA) of the membranes was performed at 60% relative humidity (RH) in temperature range from room temperature to 95 °C at a heating rate of 1 °C min-1. Detailed procedures of these measurements were described in the literature.[2]

2.2.7 Determination of IEC values

Ion exchange capacities (IECs) were estimated from the 1H NMR spectra by the integral ratio of the methylene protons (8, 8') relative to the sum of the aromatic protons (1, 2, 3, 4, 5, 6, 7, 9, and 10).

IECs were also determined by Mohr titration method. About 50 mg of the membrane in hydroxide ion form was ion-exchanged to chloride ion form by immersing in 10% NaCl / 4% HCl aqueous

solution for 24 h and washed with deionized water. The membranes were immersed in 0.2 M $NaNO_3$ for 24 h. $NaNO_3$ solution including the membrane was titrated with 0.01 M $AgNO_3$ in the presence of 1.6 mL of 0.25 M K_2CrO_4 as an indicator. Then, the membranes were recovered, washed with distilled water, dried in vacuum oven at 60 °C for 24 h, and weighed. The IEC was calculated from the equation: IEC (meq g^{-1}) = (molar amount of $AgNO_3$ used for titration) / dry weight.

2.2.8 Water uptake and λ

The water uptake of the membranes in chloride ion form was measured by immersing the dry membrane samples in deionized water for 24 h, wiped quickly with a tissue paper to remove the surface water, and weighed immediately (W_w). The membranes were dried in vacuum oven at 80 °C overnight and weighed (W_d). The water uptake (WU, %) was calculated from the equation:

$$WU = (W_w - W_d) / W_d \times 100$$

The average number of absorbed water molecules per ammonium group, λ, was calculated from the measured WU and IEC from the equation:

$$\lambda = (WU / IEC \times 18.015)$$

2.2.9 Conductivity measurements

Hydroxide ion conductivity of the membranes was measured in degassed, deionized water using AC impedance spectroscopy system (Solatron 1255B, Solatron Inc.). The corresponding resistances of the membranes were measured at 30, 40, 60 and 80 °C using a four-probe conductivity cell. The impedance plots were obtained in the frequency range from 1 to 105 Hz. The hydroxide ion conductivity (σ) was calculated from the equation, $\sigma = L/RA$, where L is the length between the inner electrodes (L= 1 cm), R is the resistance of the membranes, and A is the cross-sectional area of the membranes. The activation energies, E_a, were calculated from the slopes of Arrhenius plots (the logarithm of the conductivity versus 1000/T).

2.2.10 Stability test

The membranes in chloride ion form were immersed in deionized water for 24 h. and the conductivity was measured as 0 h. Then, the membranes were immersed in 1M KOH aqueous solution at 60 °C in a closed vial for 24, 48, 72, 96, 200, 300, 400, 500, 700, 1000 h. At the set time, the membranes were removed from the vial, washed and immersed in deionized water for 24 h prior to the hydroxide ion conductivity measurement.

2.3 Results and discussion

2.3.1 Synthesis of QPE-bl-9 with various ammonium groups

A series of quaternized copolymers, QPE-bl-9, based on partially fluorinated oligo(arylene ether) as a hydrophobic component and oligophenylene as a hydrophilic segments attached to a variety of ammonium groups, were successfully synthesized (Scheme 2-1).

First, sequenced precursor copolymer, PE-bl-9, was prepared from oligomer 2 (Figure 2-1) by Ullmann coupling copolymerization with 1,3-dichlorobenzene and 1,4-dichlorobenzene using $Ni(cod)_2$ as a catalyst and DMAc as a solvent. The copolymerization reaction was achieved with feed ratio (X= 3 - 5, p : q : r = 1: 2: 8). The obtained copolymers were soluble in some organic solvents such as chloroform and DMF. The structure of the copolymers was confirmed by ^{1}H and ^{19}F NMR spectra (Figure 2-2). The copolymers contained somewhat higher content of m-phenylene moieties than the targeted. Formation of high molecular weight copolymers was confirmed from GPC data (Figures 2-3). Detailed characterization of the copolymers was reported in our previous paper.[1]

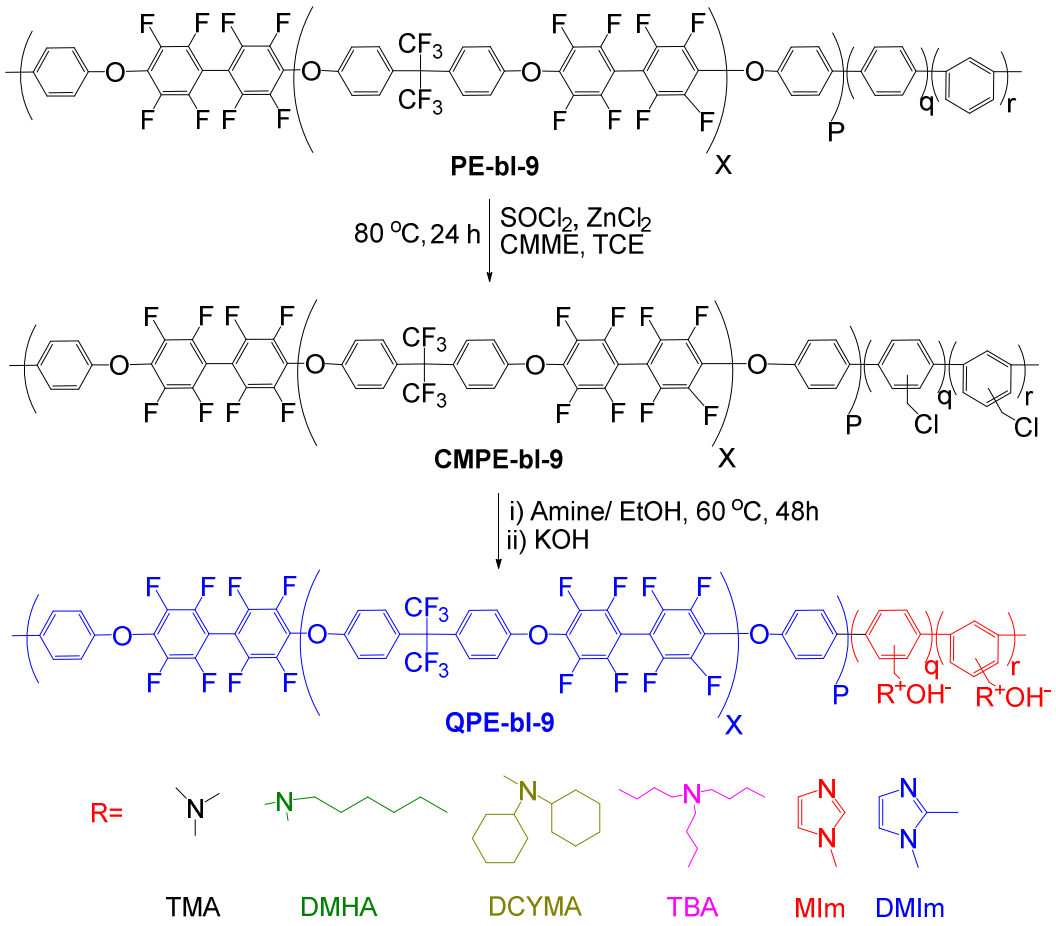

Scheme 2-1. Synthesis of QPE-bl-9 with various ammonium groups.

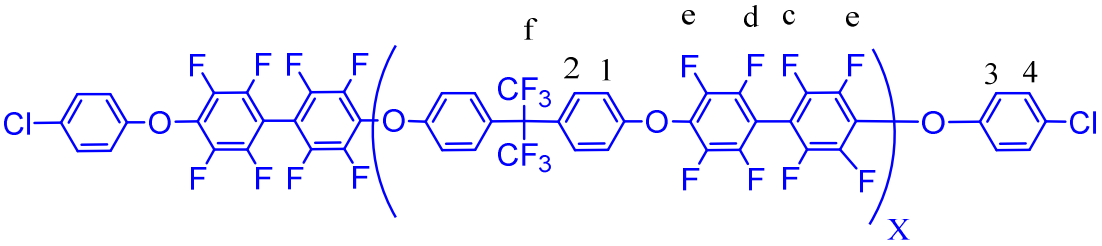

Oligomer 2

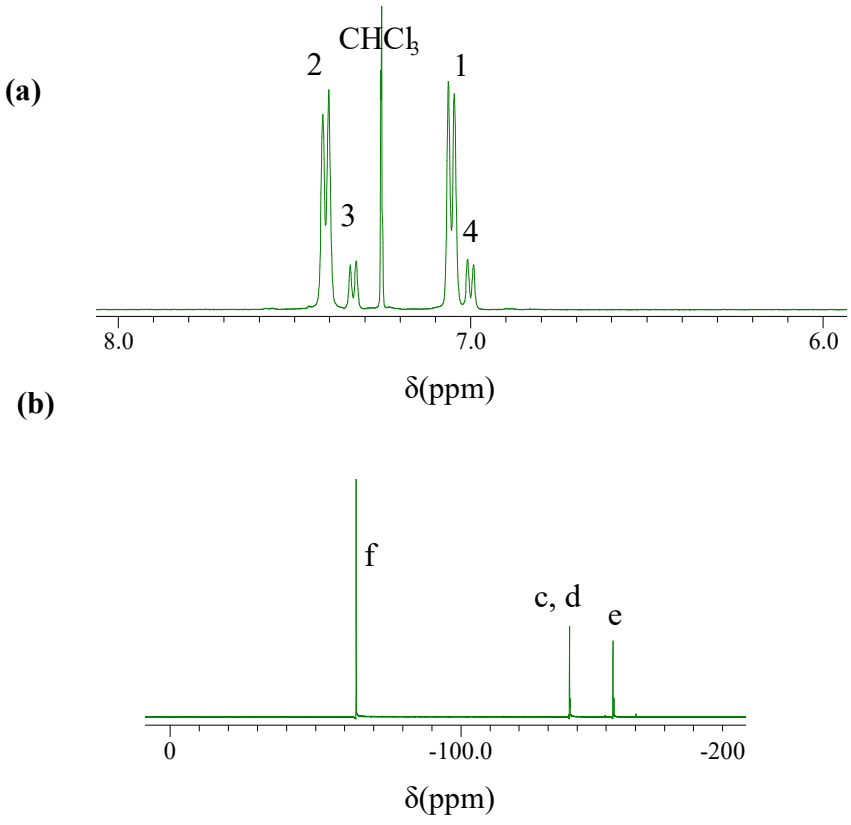

Figure 2-1. (a) ^{1}HNMR and (b) ^{19}FNMR spectra of Oligomer 2 in $CDCl_3$ at room temperature.

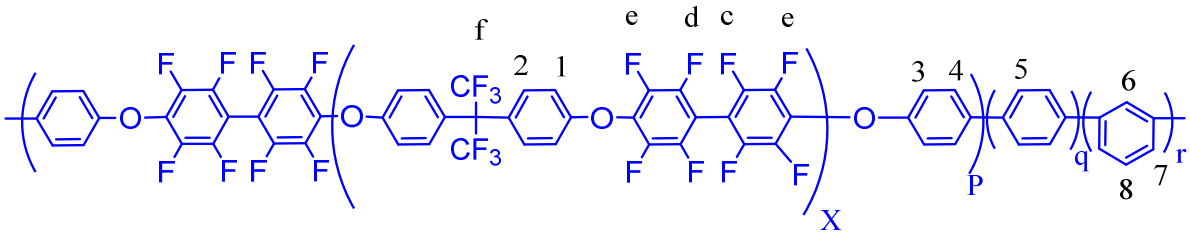

PE-bl-9

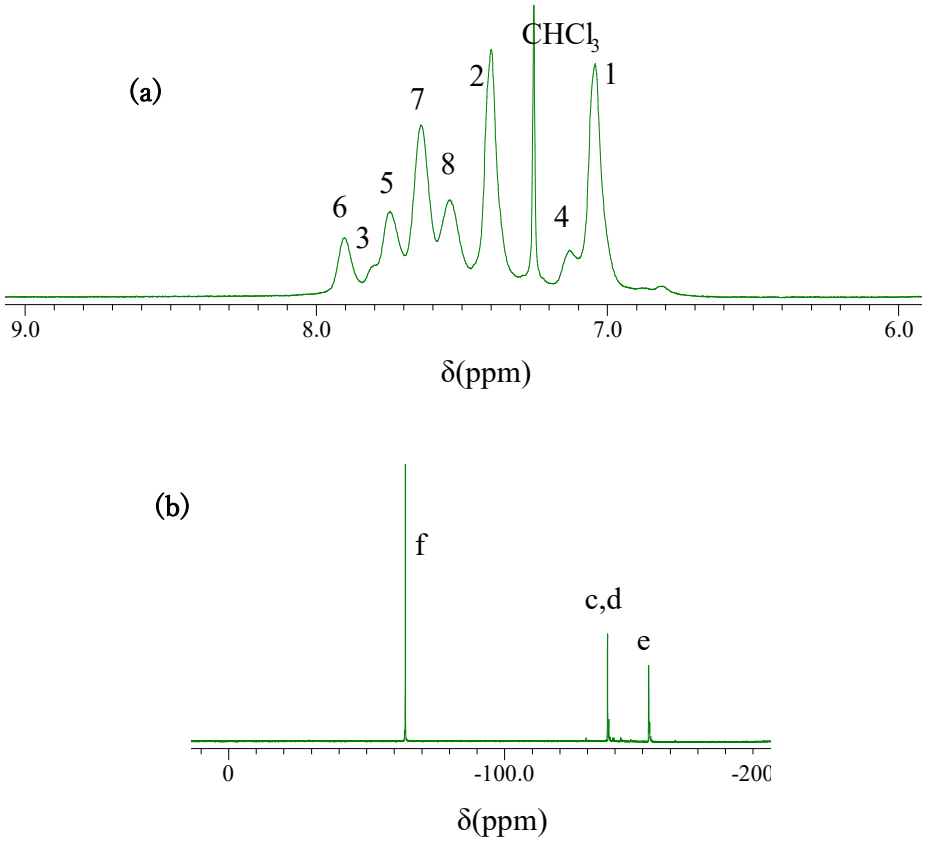

Figure 2-2. (a) ^{1}HNMR and (b) ^{19}FNMR spectra of PE-bl-9 in $CDCl_3$ at room temperature.

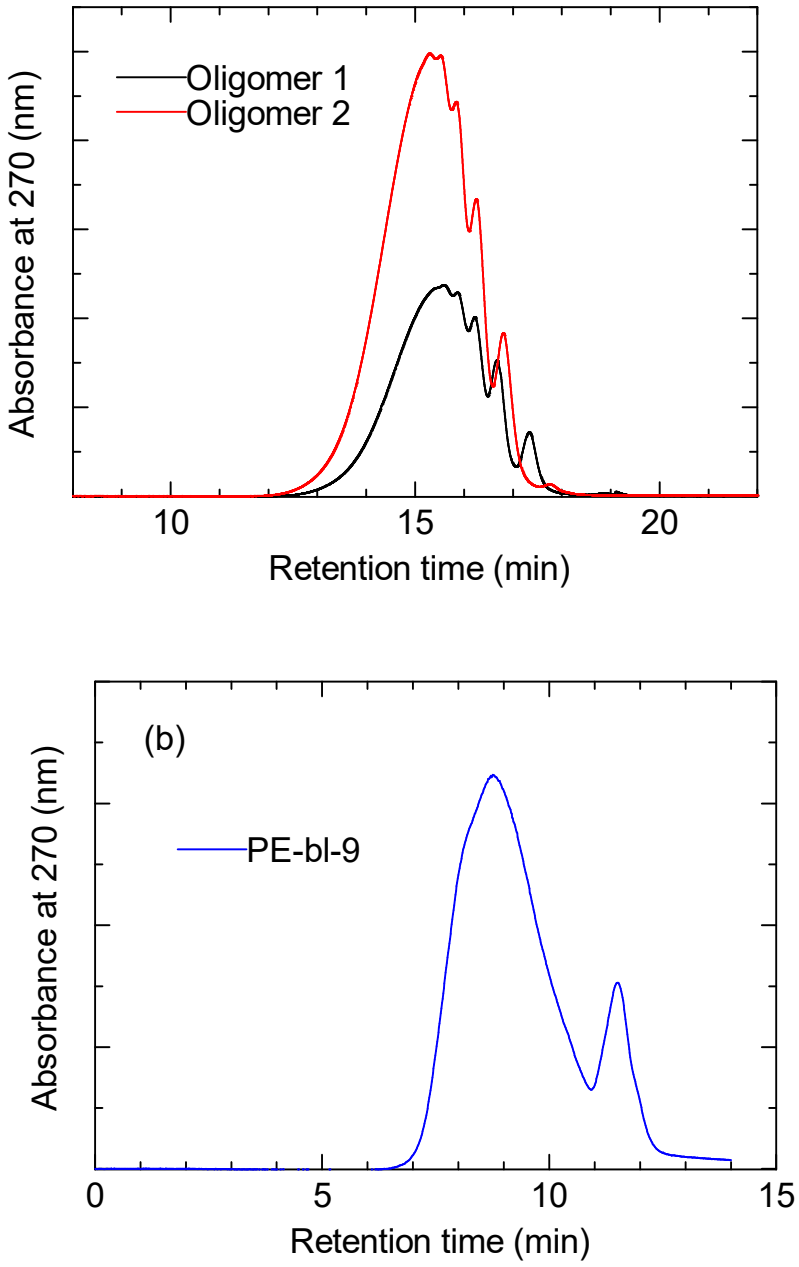

Figure 2-3: GPC profiles of (a) oligomer1, 2 and (b) PE-bl-9.

The chloromethylated copolymers, CMPE-bl-9, were prepared via Friedel-Crafts chloromethylation reaction of PE-bl-9 with CMME (160 equiv. to phenylene rings in the oligophenylene segments) as a chloromethylating agent in the presence of $SOCl_2$ (20 equiv. to

phenylene rings) and $ZnCl_2$ (1 equiv. to phenylene rings) in TCE at 80 °C for 24 h. The conditions were selected for shorter reaction time compared with our previous work, in which 5 days were needed to achieve the similar degree of chloromethylation.[1] The chloromethylation reaction was selective and quantitative on the oligophenylene segments without unfavorable side reactions such as crosslinking. The GPC analyses showed high molecular weight CMPEs with no detectable degradation and side reactions (Figure 2-4 and Table 2-1). The peak at longer retention time in PE-bl-9 was absent in CMPE-bl-9, suggesting that the purification process was effective for removing the lower molecular weight products (possible oligo(phenylene)s). The structure of CMPE-bl-9 was confirmed by ^{1}H and ^{19}F NMR spectra (Figure 2-5). The broad peak at ca. 4.5 ppm in the ^{1}H NMR spectrum was assigned to the methylene protons of the chloromethyl groups. The ^{19}F NMR spectra did not show detectable changes between PE-bl-9 and CMPE-bl-9, suggesting that the fluorinated oligo(arylene ether) moieties were not chloromethylated. The degree of chloromethylation (DC) estimated from the ^{1}H NMR spectra ranged from 0.23 to 0.87 chloromethyl groups per phenylene unit in the oligophenylene moieties. Casting CMPE-bl-9 solution in TCE provided transparent, colorless and bendable membranes.

Table 2-1. Properties of PE-bl-9 and CMPE-bl-9 membranes.

Polymer	X^a	X^b	X^c	PE-bl-9		CMPE-bl-9			
				p : q : r [a]	p : q : r[b]	P : q : r [b]	Mn[c] (KDa)	Mw[c] (KDa)	DC[d]
A	5	5.58	6.84	1.0 : 2.0 : 8.0	1.0 : 1.8 : 8.6	1.0 : 2.3 :9.4	37	224	0.78
B	5	5.58	6.84	1.0 : 2.0 : 8.0	1.0 : 2.7 : 11.9	1.0 : 1.8 : 7.2	34	207	0.87
C	3	3.24	4.52	1.0 : 2.0 : 8.0	1.0: 2.03 : 12.5	1.0 : 4.2 : 16.9	41.38	330	0.46
D	4	4.17	5.33	1.0 : 2.0 : 8.0	1.0 : 2.4 : 12.2	1.0 : 6.2 : 25.0	6.5	233.5	0.23
E	4	4.17	5.33	1.0 : 2.0 : 8.0	1.0 : 2.4 : 13.4	1.0 : 10.3 : 41.3	49.5	514	0.38

[a] Calculated from the feed ratio. [b] Determined by [1] HNMR Spectra. [c] Determined by GPC analyses(calibrated with polystyrene standards). [d] Degree of Chloromethylation = (number of chloromethyl groups per phenylene ring in the oligophenylene moieties).

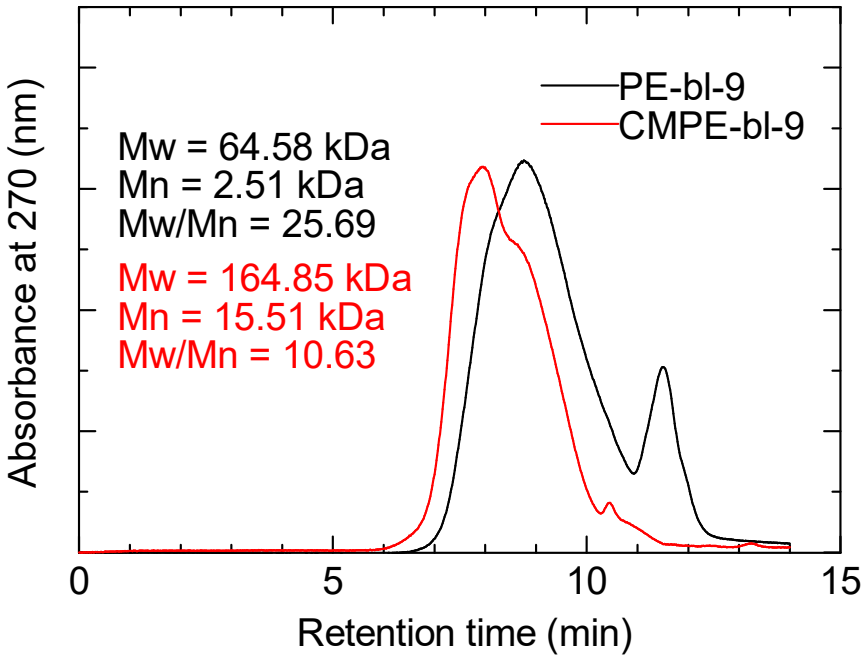

Figure 2-4. GPC profiles of PE-bl-9 and CM-PE-bl-9.

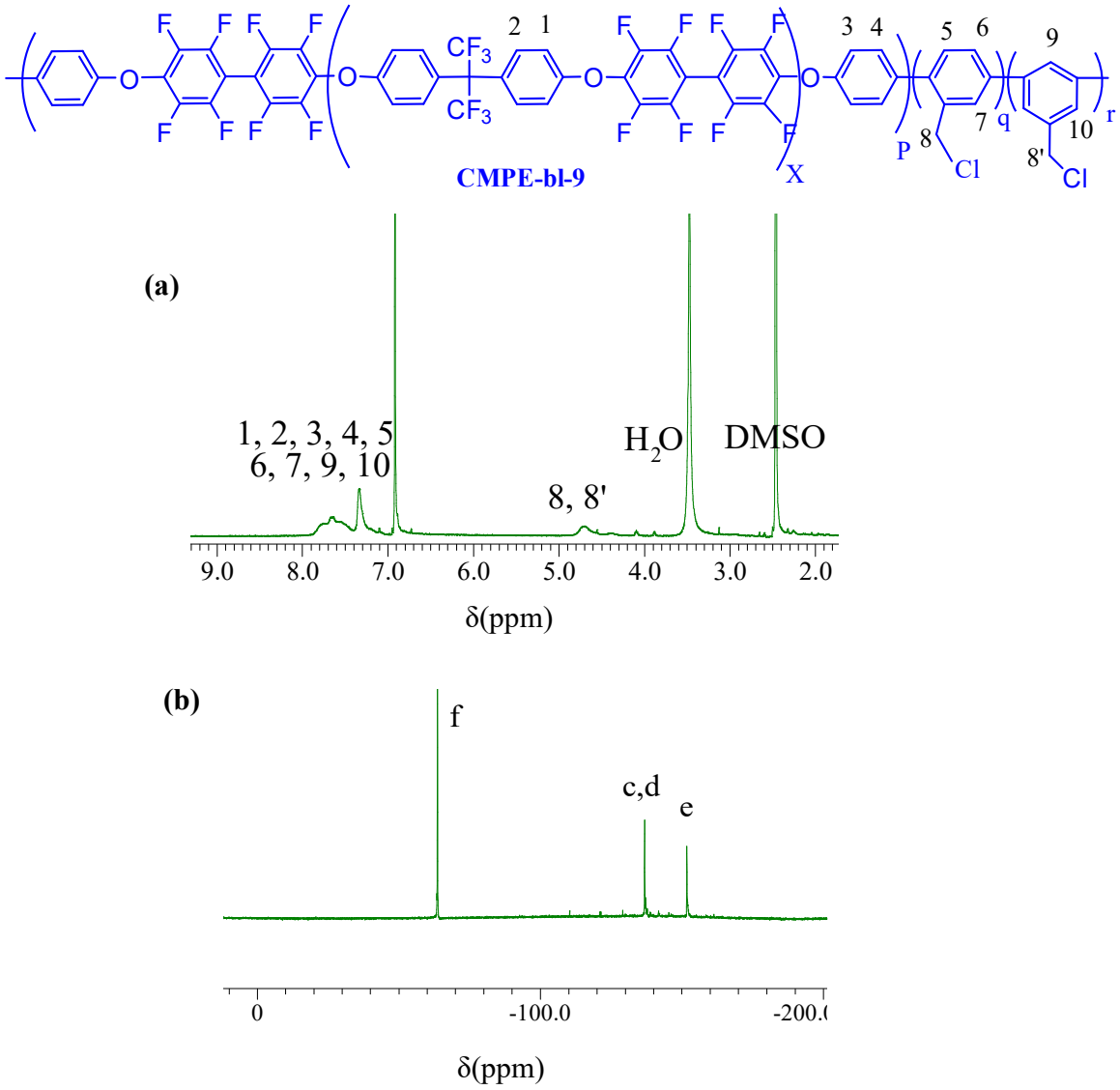

Figure 2-5. (a) ^{1}HNMR and (b) ^{19}FNMR of CMPEbl-9 membranes in *d6*-DMSO at r.t.

The membranes were quaternized with various amines under different quaternization conditions depending on the molecular size, steric hindrance, and electronic structure of the amines. The tertiary amines investigated in this study included TMA as the smallest and the most common amine, DMHA with a pendant alkyl chain, MIm and DMIm as heterocyclic aromatics, and DCHMA and TBA as bulky and sterically hindered amines. First, we have optimized the quaternization reaction conditions for each amine (Table 2-2). The quaternization reaction was

evaluated by the ion exchange capacity (IEC in meq g^{-1}) via titration, which was converted to the degree of quaternization (DQ) per phenylene unit in the oligophenylene moieties. CMPE-bl-9 was quaternized with TMA and DMHA under neat (solvent free) conditions at the temperature depending on the amines. For TMA, room temperature was sufficient for reasonable degree of quaternization (DQ = 0.82). DMHA as larger and bulkier amine than TMA was not quaternized at room temperature. DQ was 0.52 even at 40 °C for DMHA. Polar solvents such as ethanol were used for the reaction, however, the DQ was comparable or lower than that under neat conditions (Table 2-3). In contrast, ethanol was effective as the solvent for the heterocyclic aromatic amines, MIm and DMIm (DMIm is a solid at room temperature), for the quaternization reaction at 60 °C to achieve 0.75 of DQ. Under the same conditions, however, DCHMA and TBA gave lower DQ (0.16 and 0.12, respectively). Changes in the copolymer composition did not help improve the quaternization reaction (Table 2-3). Many other attempts were carried out, such as changing the solvent and the stoichiometry, but were not so successful. Higher reaction temperature than 60 °C was not tried because of the possible degradation of the resulting ammonium groups.

Table 2-2. Quaternization conditions, IEC, WU and DQ of QPE-bl-9 membranes.

CMPE-bl-9[d]	amine	temperature (°C)	solvent	IEC[a] (meq g^{-1})	IECa (meq g^{-1})	DQ[b]
A	TMA	r.t	H_2O	1.6	1.95	0.82
E	DMHA	40	N/S[c]	1.0	1,92	0.52
A	MIm	60	EtOH	1.4	1.86	0.75
E	DMIm	60	EtOH	1.3	1.73	0.75
B	DCHMA	60	EtOH	0.20	1.25	0.16
B	TBA	60	EtOH	0.15		0.12

[a]Determined by Mohr titration method. [b]Degree of quaternization (DQ) was calculated from IEC. [c]No solvent was used. [d]Polymer compositions of CMPE-bl-9-A, B and E are indicated in Table 1.

Table 2-3. Quaternization degrees of QPE-bl-9-TBA and QPE-bl-9-DCYMA at different conditions.

Polymer	Quaternization conditions		QPE-bl-9-TBA		QPE-bl-9-DCYMA		QPE-bl-9-DMHA	
	Solvent	Temperature (° C)	DQ %	IEC[c]	DQ %	IEC[c]	DQ %	IEC[c]
A[a]	Ethanol	60	6	0.08	4.9	0.06	60	0.8
B	Ethanol	60	12	0.14	16	0.2	54	0.7
C	Ethanol	60	7	0.13	5	0.09	29	0.57
D	Ethanol	60	15	0.24	5	0.08	31	0.55
D	Solvent free	40	14	0.24	NA[b]	0.08	52	1.02

[a] The polymer compositions from A-D are mentioned in Table 1. [b] Self-standing membrane was not obtained. [c] Determined by Mohr titration method.

The resulting quaternized copolymers, QPE-bl-9, were characterized by 1H NMR spectra. The ^{1}H NMR spectra were measured for the copolymers in chloride ion form due to the poor solubility of the copolymers in hydroxide ion form. The conversion of the chloromethylene groups to the corresponding ammonium methylene groups was suggested, either by the shift of the methylene protons (8, 8') from 4.5 ppm to 5.0-6.0 ppm for TMA, MIm and DMIm, or by the decrease of the methylene peak intensity for DMHA (Figures (2-6) – (2-9)). The chemical shift of the methylene protons was more pronounced in the cases of the heterocyclic aromatic ammonium groups (MIm and DMIm). QPE-bl-9-TBA and DCHMA were not soluble in any organic solvents even in the chloride ion forms, which prevented them from the NMR analyses. The characteristic peaks of each ammonium group were also confirmed. For QPE-bl-9-TMA, a singlet signal at 2.9 ppm was assigned to the methyl groups attached to the quaternary nitrogen atoms. For QPE-bl-9-MIm and QPE-bl-9-DMIm, the singlet peaks at 3.4 and 3.7 ppm, respectively, were assignable to the methyl

groups attached to the imidazolium groups. The imidazolium protons were overlapped with the aromatic protons of the polymer main chains. The 1H NMR spectrum of QPE-bl-9-DMHA revealed a singlet signal at 2.9 ppm assignable to dimethyl groups, while protons for the hexyl groups were also detected at 0.9 - 2.4 ppm. We did not calculate the IECs from the 1H NMR spectra because the most peaks were broad and/or overlapped with other protons or the solvent. More accurate and reliable IECs were obtained by Mohr titration method as mentioned above.

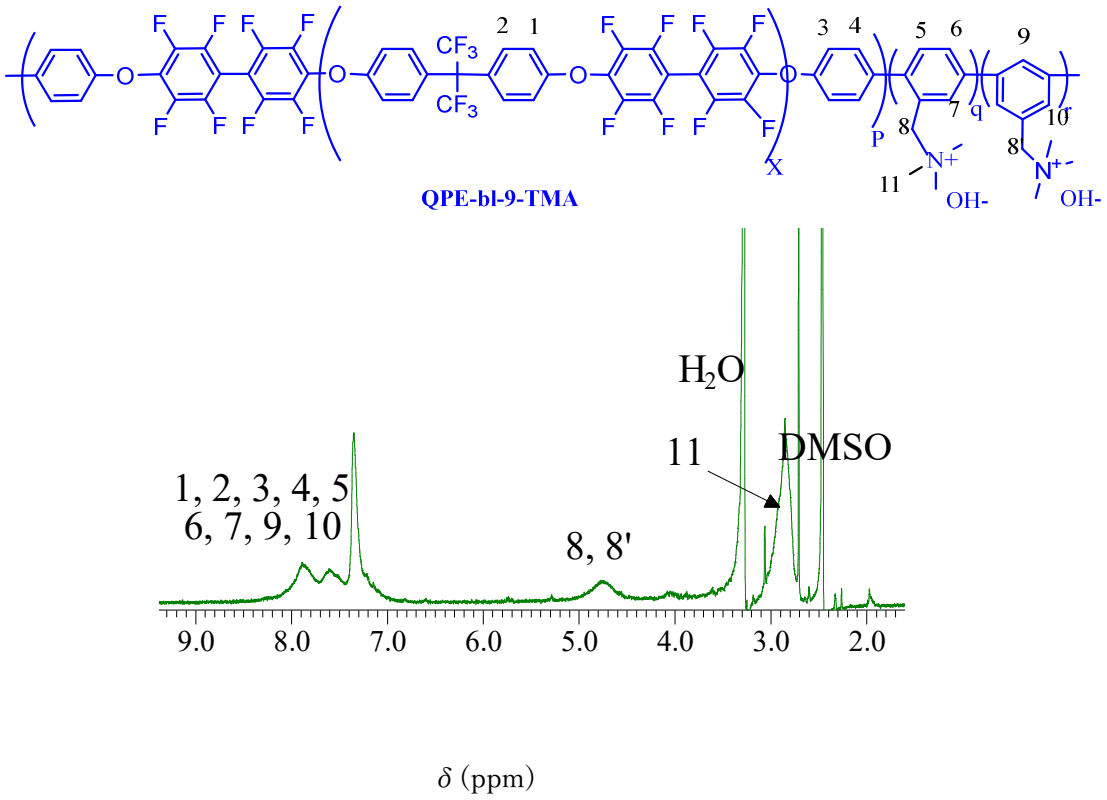

Figure 2-6. ^{1}H NMR of QPE-bl-9-TMA in *d6*-DMSO at r.t.

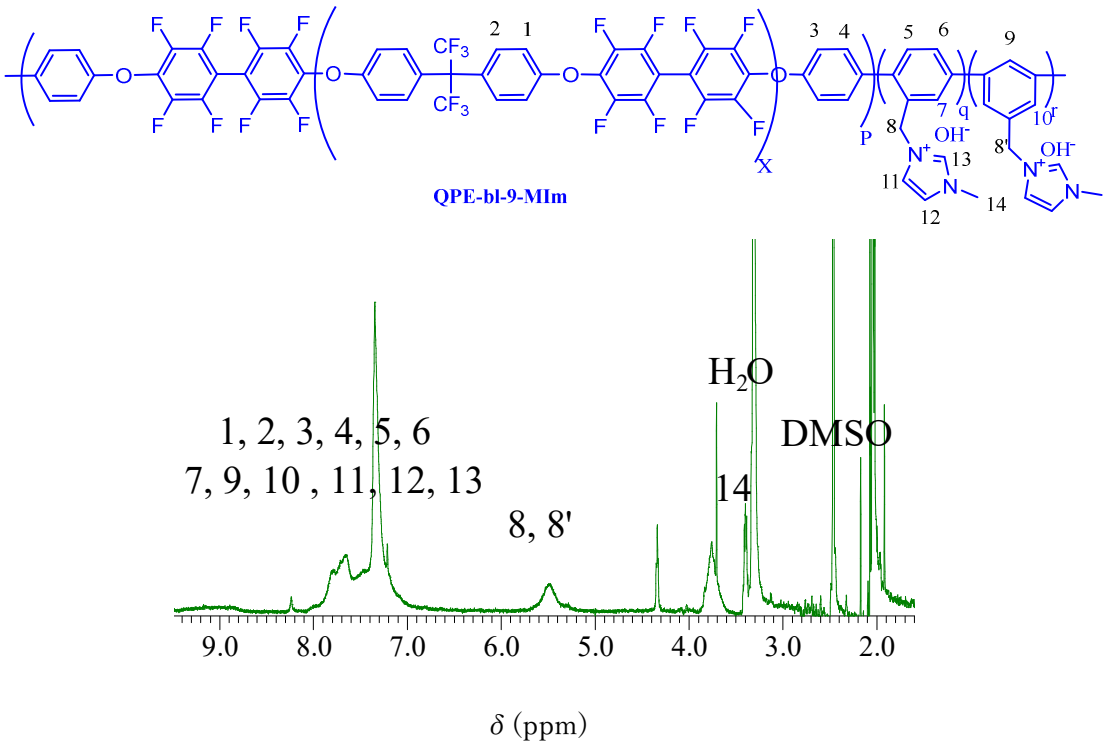

Figure 2-7. ^{1}H NMR of QPE-bl-9-MIm in *d6*-DMSO at room temperature.

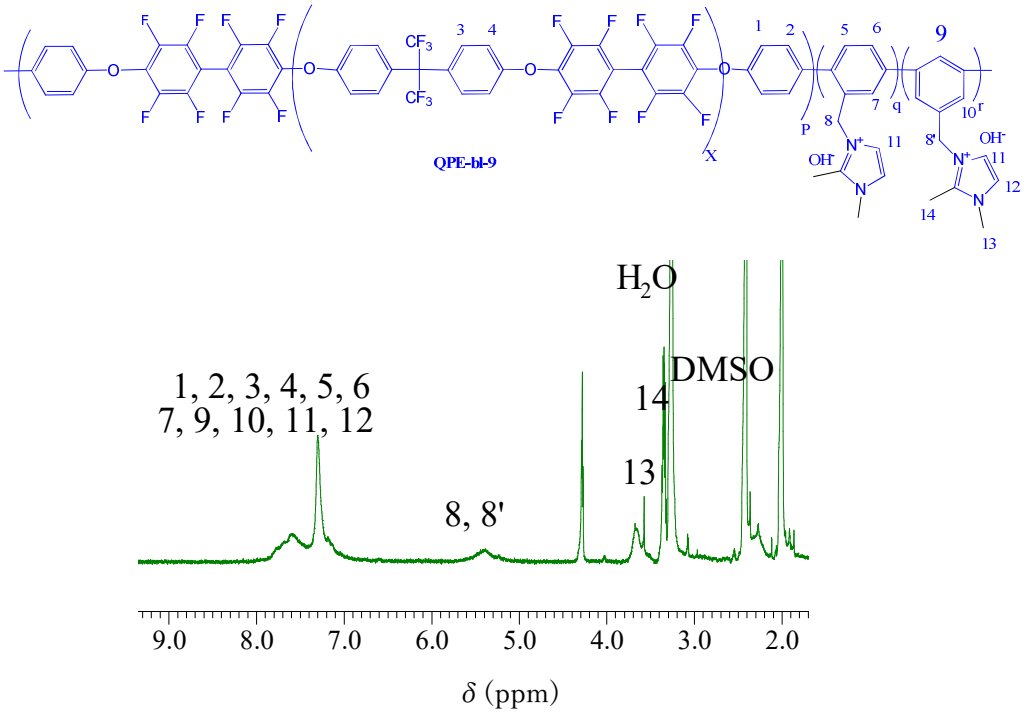

Figure 2-8. ^{1}H NMR of QPE-bl-9-DMIm in *d6*-DMSO at r.t.

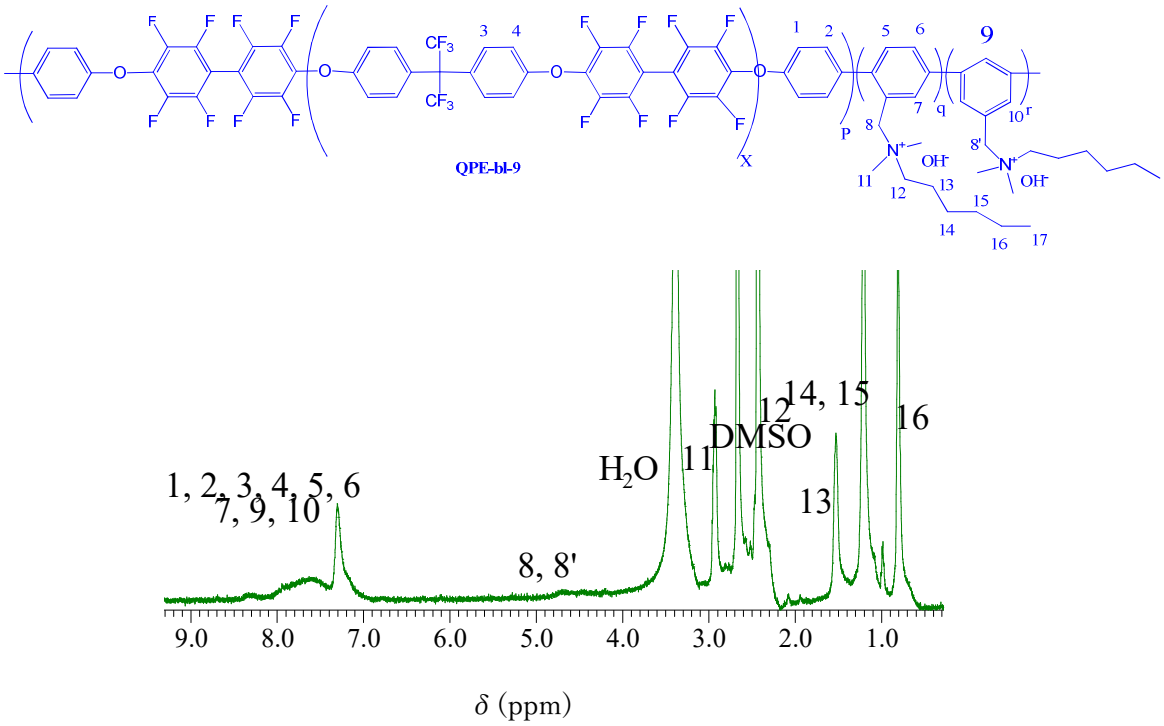

Figure 2-9. ^{1}HNMR of QPE-bl-9-DMHA in *d6*-DMSO at r.t.

2.3.2 Morphology

One of the effective approaches for achieving high hydroxide ion conductivity in AEMs is having interconnected ion channels associated with hydrophilic / hyrdrophobic phase separation. In this work, the phase-separated morphology was observed using the cross-sectional TEM images for QPE-bl-9-TMA, DMHA, DMIm, and MIm membranes with IEC values ranging from 1.02 to 1.60 meq g^{-1} stained with tetrachloroplatinate ions (Figure 2-10). The darker areas represent the hydrophilic domains containing ammonium tetrachloroplatinate groups and the brighter areas represent the hydrophobic domains. While these four QPE-bl-9 membranes showed phase separated morphology, their domain sizes differed. QPE-bl-9-DMHA exhibited slightly larger ionic clusters (ca. 2 - 3 nm in diameter) than those of QPE-bl-9-TMA (ca. 1.0 - 1.6 nm). The bulkier structure of DMHA groups was probably responsible for the formation of the larger ionic clusters. However, the ionic domains were somewhat in disorder and their connectivity seemed less

efficient for QPE-bl-9-DMHA membrane. QPE-bl-9-DMIm and MIm membranes exhibited even smaller ionic clusters (ca. 0.7 - 1.0 nm), which were well-dispersed throughout the sight. It is considered that the flat imidazolium rings could stack themselves to cause such compact ionic domains.

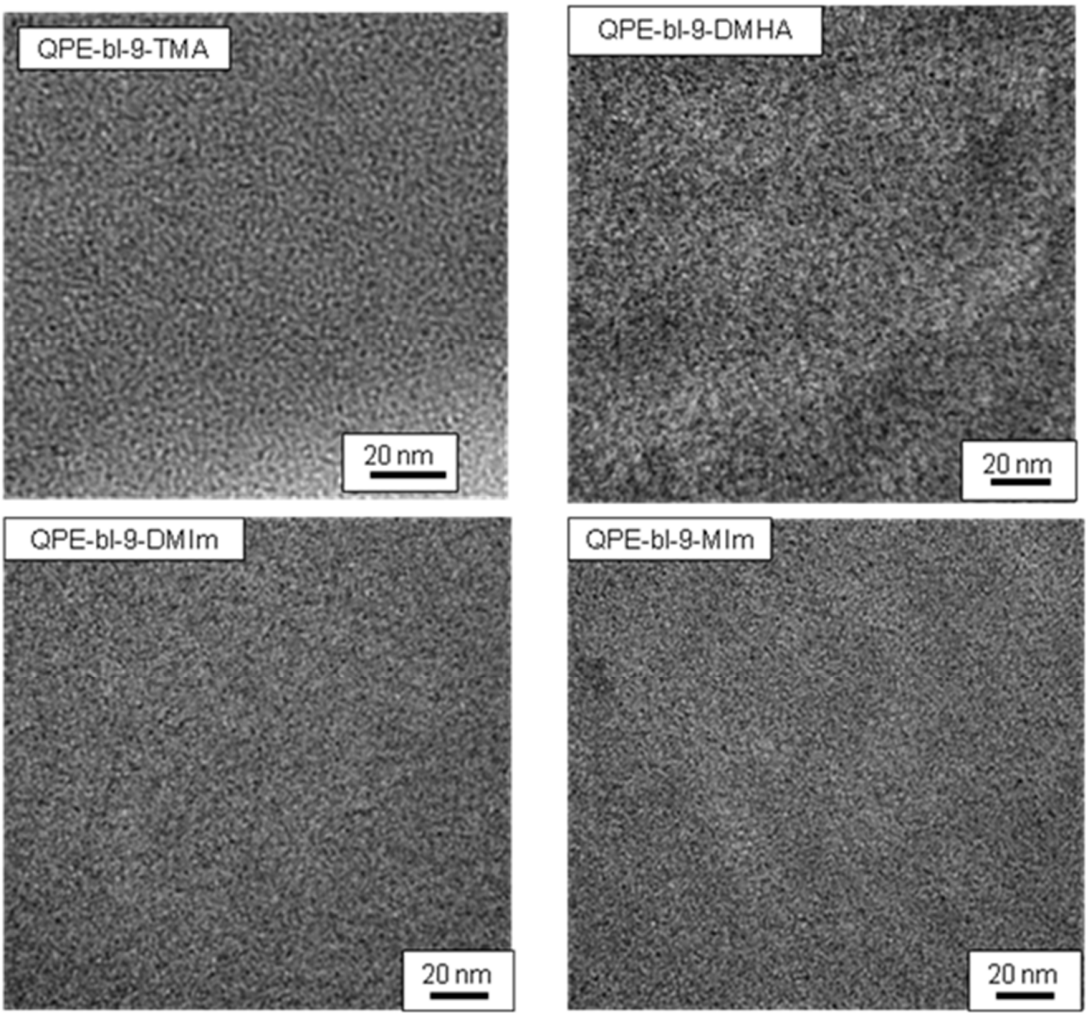

Figure 2-10. TEM images of QPE-bl-9 membranes stained with tetrachloroplatinate ions. The IECs were 1.60 meq g^{-1} (TMA), 1.02 meq g^{-1} (DMHA), 1.05 meq g^{-1} (DMIm), and 1.43 meq g^{-1} (MIm).

2.3.3 Water uptake and anion conductivity

In order to investigate the effect of the ammonium groups on the membrane properties, water uptake was measured for QPE-bl-9-TMA, -DMHA, -MIm, -DMIm, -TBA, and -DCHMA membranes in chloride ion forms at 30 °C in water and was plotted as a function of IEC (Figure 2-11a). As expected, the general trend was that the water uptake increased with increasing IECs for all series of the QPE-bl-9 membranes as a result of an increase in the hydrophilicity. QPE-bl-9-TMA membranes exhibited smaller water uptake than those of QPE-bl-9-MIm and DMIm membranes probably because of the smaller molecular size of TMA groups providing less free volume in the membrane. The water uptake was as high as 136% and 125% for -MIm (IEC = 1.43 meq g^{-1}) and DMIm (IEC = 1.38 meq g^{-1}), respectively, while that for -TMA was 76% (IEC = 1.62 meq g^{-1}). For QPE-bl-9-TBA and -DCHMA membranes, dependence of water uptake on IEC is not discussed because only low IEC membranes could be obtained as discussed above.

Under the same conditions, the hydroxide ion conductivity was also measured and plotted as a function of IEC in Figure 2-11b. Similar to the water uptake, the hydroxide ion conductivity increased with increasing IEC of the membranes. Despite its lower water uptake, QPE-bl-9-TMA membrane showed higher hydroxide ion conductivity than those of the other QPE-bl-9 membranes. The highest conductivity was 52 mS cm^{-1} at IEC = 1.62 meq g^{-1}. This conductivity was reasonable compared to the conductivities achieved in our previous work,[1] taking into account the IEC values (22 mS cm^{-1} at 1.3 meq g^{-1}, 52 mS cm^{-1} at 1.8 meq g^{-1}, and 77 mS cm^{-1} at 2.0 meq g^{-1}). QPE-bl-9-DMHA and DMIm membranes were also highly conductive and these membranes showed a jump in the conductivity at a certain IEC value approximately higher than 1.0 meq g-1. It is considered that the connectivity of ion conducting channels was improved around this IEC value. Such conductivity jump was not observed for QPE-bl-9-MIm membrane.

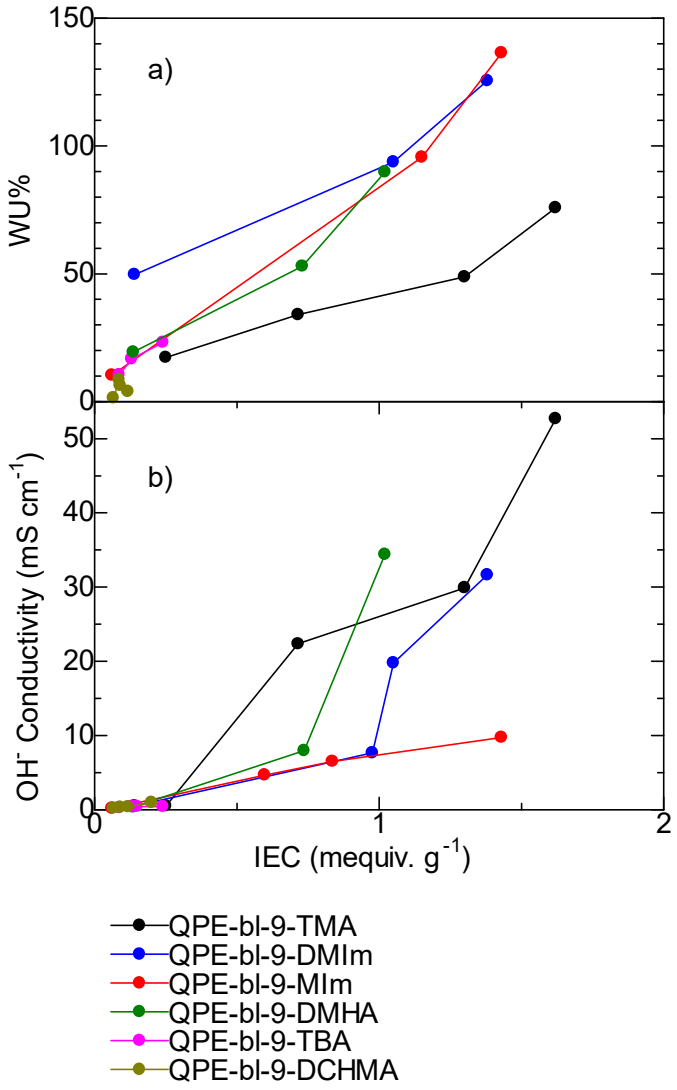

Figure 2-11. a) Water uptake (WU) and b) hydroxide ion conductivity of QPE-bl-9 membranes at 30 °C in water as a function of IEC. The maximum error in the conductivity was 2%.

In Figure 2-12, is re-plotted the hydroxide ion conductivity of the membranes at 30 °C as a function of number of water molecules absorbed per ammonium group (λ). QPE-bl-9-TMA membrane utilized the absorbed water molecules efficiently for hydroxide ion conduction as the high conductivity (52 mS cm^{-1}) was achieved with low hydration number (λ = 26). The efficiency of

water molecules for ion conduction was followed by QPE-bl-9-DMHA and -DMIm. These two membranes achieved high conductivity of 34 mS cm^{-1} at λ = 48 and 32 mS cm^{-1} at λ = 50, respectively. Tokuyama A201 membrane (IEC = 1.7 meq g^{-1}), state-of-the-art AEM, also showed good efficiency with high conductivity (30 mS cm^{-1}) and low hydration number (λ = 22). The efficiency of water molecule for hydroxide ion conduction was similar for QPE-bl-9-TMA and Tokuyama A201 membranes taking their IEC values into account. The efficiency was low for the other membranes (QPE-bl-9-MIm, -TBA, and -DCHMA), and increase in λ did not contribute to improving the hydroxide ion conductivity.

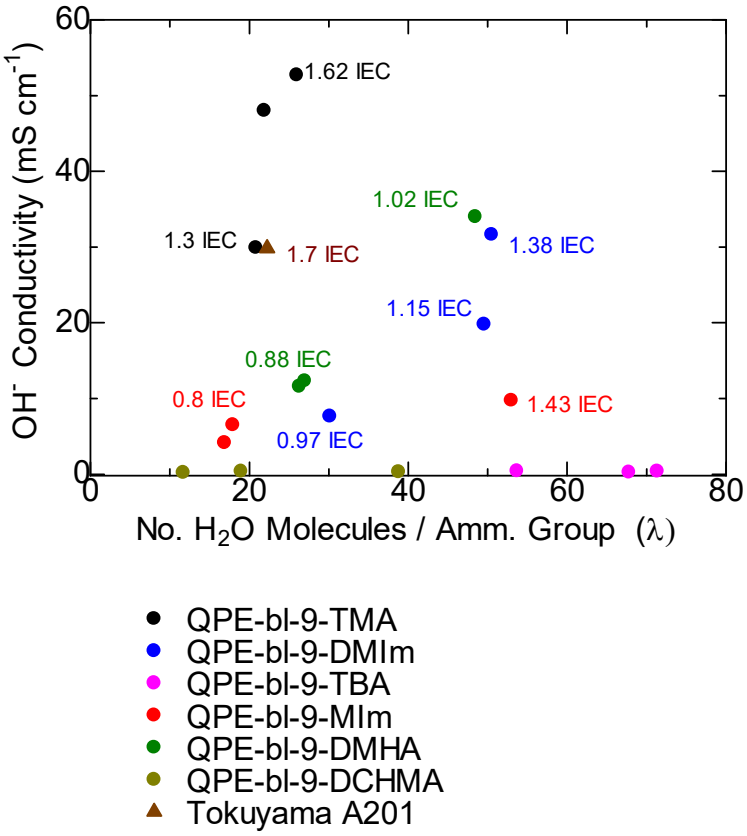

Figure 2-12. Hydroxide ion conductivity of QPE-bl-9 membranes at 30 °C in water as a function of λ.

Figure 2-13, shows the temperature dependence of the hydroxide ion conductivity of the QPE-bl-9 membranes in water. All membranes exhibited approximate Arrhenius-type temperature dependence of the conductivity up to 80 °C. QPE-bl-9-TMA with IEC = 1.62 meq g^{-1} exhibited the highest conductivity (101 mS cm^{-1} at 80 °C), which was among the highest conductivities for aromatic copolymer-based AEMs with comparable IEC values (higher conductivity, 138 mS cm^{-1}, was achieved with higher IEC = 2.0 meq g^{-1} in our previous study[1]). For their relatively low IEC value, QPE-bl-9-DMHA (IEC= 1.02 meq g^{-1}) and -DMIm (IEC = 1.38 meq g^{-1}) membranes exhibited high hydroxide ion conductivities ranging from 32 to 62 mS cm^{-1}. In contrast, QPE-bl-9-MIm with IEC = 1.43 meq g^{-1}, showed lower conductivity ranging from 10 to 19 mS cm^{-1} compared to those of the above-mentioned three membranes. Compared to Tokuyama A201 membrane whose conductivity ranged from 29 to 62 mS cm^{-1}, QPE-bl-9-TMA was more conductive while QPE-bl-9-DMHA and DMIm were similar in the conductivity. The apparent activation energies (E_a) for the hydroxide ion conduction of the membranes were estimated from the slopes of the lines to be 11.7 kJ mol^{-1} for TMA, 11.6 kJ mol^{-1} for DMHA, 11.8 kJ mol^{-1} for MIm, 11.9 kJ mol^{-1} for DMIm, 14.6 kJ mol^{-1} for DCHMA, 13.0 kJ mol^{-1} for TBA, and 13.0 kJ mol^{-1} for Tokuyama A201. The E_a values were similar to those of our previous aromatic copolymer-based AEMs (11-14 kJ mol^{-1}) suggesting that the differences in the ammonium groups do not practically affect the hydroxide ion conducting mechanism.[1-4]

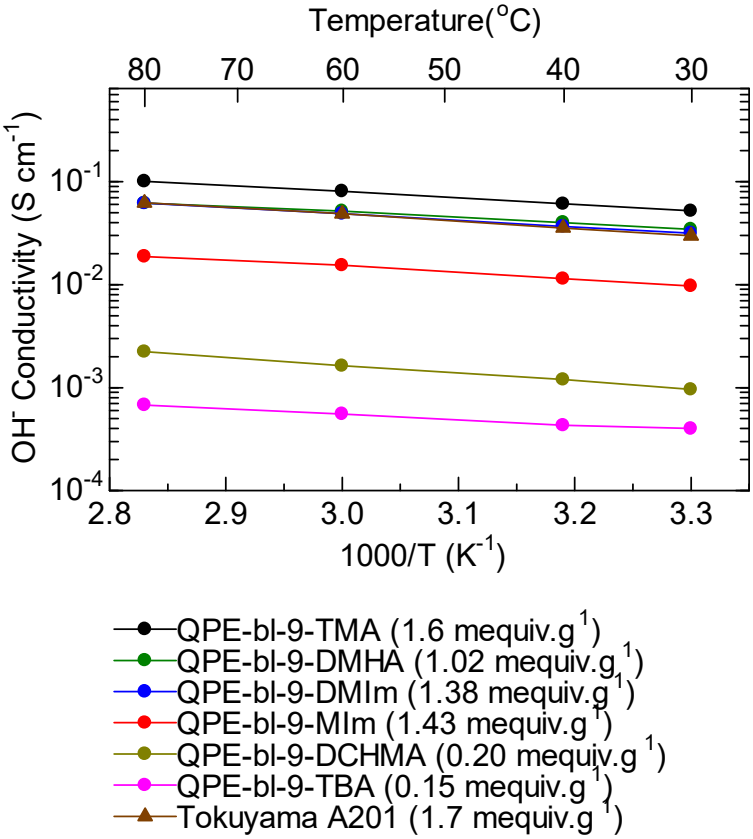

Figure 2-13. Temperature dependence of the hydroxide ion conductivity of QPE-bl-9 membranes in water.

2.3.4 Alkaline stability

The alkaline stability of the QPE-bl-9 membranes (in chloride ion form) was tested in 1 M KOH at 60 °C up to 1000 h and the change in the hydroxide ion conductivity was measured in water at 40 °C (Figure 2-14). The hydroxide ion conductivity of all the membranes jumped in the first 24 h due to the ion exchange from chloride ion to more conductive hydroxide ion form. Then, the conductivity decreased gradually with the testing time. While the data contained certain errors due

to the swelling of the membranes to change their thicknesses, it was concluded that QPE-bl-9-TMA exhibited the highest alkaline stability with the high ion conductivity (13.6 mS cm^{-1} and 20 mS cm^{-1} at IEC = 1.6 and 1.3 meq g^{-1}, respectively) after 1000 h. QPE-bl-9-DMHA also showed better stability than the other membranes.

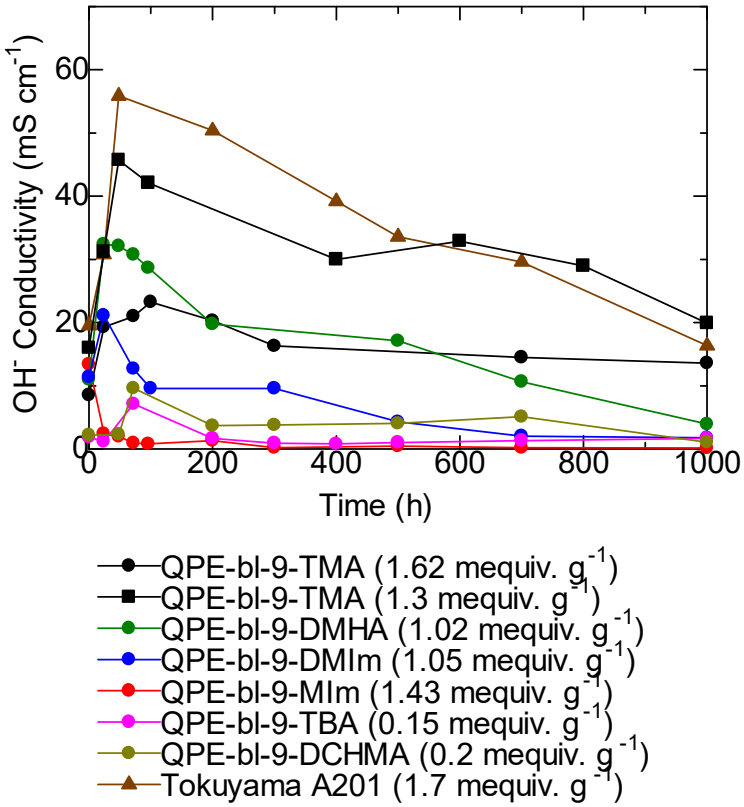

Figure 2-14. Alkaline stability of QPE-bl-9 membranes at 60 °C (the conductivities at 40 °C in water are plotted as a function of testing time).

To understand better the alkaline stability of the membranes, the retention of the conductivity was plotted in Figure 2-15, where the conductivity at each testing time was normalized using the maximum conductivity as 100%. The retention after 1000 h was 58% and 44% for TMA, 12% for DMHA, and 8% for DMIm, respectively. QPE-bl-9-MIm showed fast degradation within 24 h and

retained only 3% of its maximum conductivity after 1000 h. QPE-bl-9-TBA and -DCHMA showed relatively high retention (23% and 11%, respectively) due to their low IEC values and thus low conductivities. Tokuyama A201 membrane was also tested under the same conditions and its ion conductivity and retention were 16.3 mS cm^{-1} and 29%, respectively, after 1000 h. The retention of the conductivity of QPE-bl-9-TMA was higher than that of Tokuyama A201 membrane.

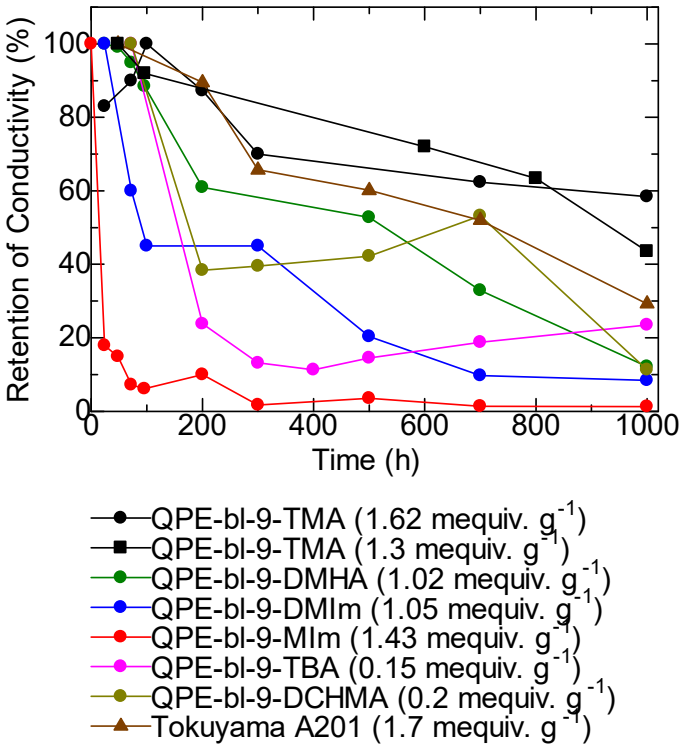

Figure 2-15. Alkaline stability of QPE-bl-9 membranes at 60 °C (normalized conductivities at 40 °C in water are plotted as a function of testing time, where the maximum conductivities in Figure 2-14 are defined as 100%).

For deeper discussion on the alkaline stability, the retention of the conductivities of QPE-bl-9 membranes after alkaline stability test are plotted as a function of the remaining conductivities after 1000 h (Figure 2-16). QPE-bl-9-TMA showed the higher retention and higher remaining conductivity than those of the other membranes including Tokuyama A201. QPE-bl-9-DMHA and

DMIm showed low remaining conductivity (4 mS cm-1 and 2 mS cm-1, respectively) and low retention after 1000h (12% and 8%, respectively). QPE-bl-9-DCHMA and -TBA with bulkier ammonium groups were more or less similar to -DMHA and -DMIm. The results suggest that the trimethylammonium groups are the most promising for QPE-bl-9 membranes among the ammonium groups investigated.

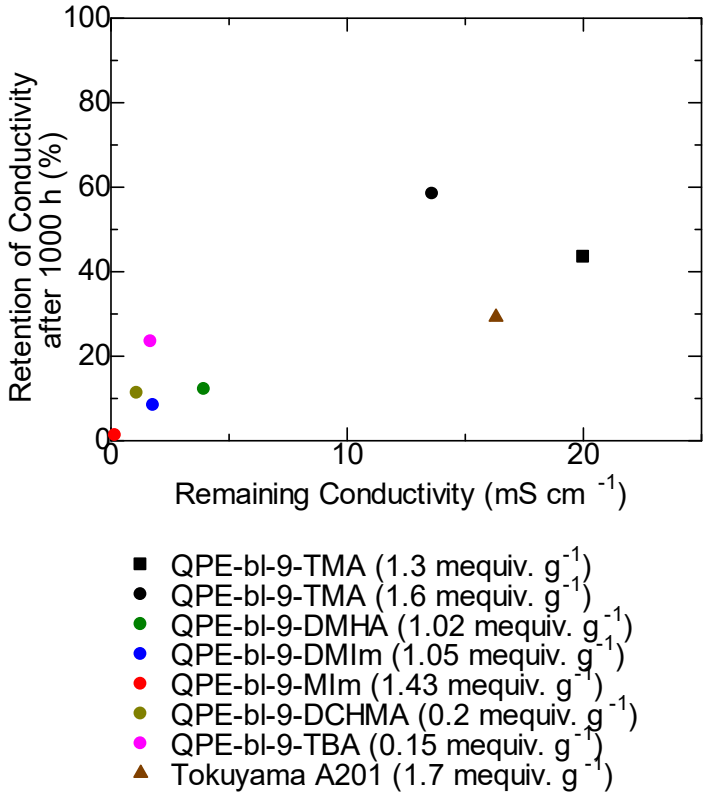

Figure 2-16. The retention of hydroxide ion conductivity of QPE-bl-9 membranes after the alkaline stability test for 1000 h as a function of the remaining conductivity.

Since the post-test membrane was not completely soluble in organic solvents, NMR analyses were not available. FT-IR spectra were measured for QPE-bl-9-TMA and QPE-bl-9-MIm as the most and the least stable membranes and were compared before and after the alkaline stability test. As

shown in Figure 2-17a, the FT-IR spectrum of QPE-bl-9-TMA revealed only minor changes. Since the conductivity decreased, it is considered that the trimethylammonium groups were decomposed to some extent. The absorbance bands at 892 cm^{-1} assignable to ($C\text{-}N^+$) deformation vibration of the ammonium groups and at 1212 cm^{-1} assignable to $C\text{-}N^+$ stretching vibration of aliphatic ammonium groups were lower in intensity for the post-test membrane than for the pristine membrane, supporting the above mentioned idea of the decomposition of the ammonium groups. The peak at 1609 cm^{-1} assignable to C-C stretching vibration of aromatic rings was slightly smaller for the post-test membrane than for the pristine membrane, suggesting minor degradation in the polymer main chain. On the other hand, the FT-IR spectrum of QPE-bl-9-MIm (Figure 2-17b) showed major changes after the stability test. The changes included the disappearance of the peak at 1572 cm^{-1} assignable to in-plane asymmetric stretching vibration of the imidazole rings and the peak at 625 cm^{-1} assignable to out-of-plane bending vibration of the imidazole rings.[5] Moreover, the lower intensity of the peak at 1212 cm^{-1} ($C\text{-}N^+$ stretching vibration) indicates the degradation of the imidazolium rings and thus of the ammonium cations. The peak at 1609 cm^{-1} (C-C stretching vibration of aromatic rings) was very weak for the post-test membrane, suggesting the major degradation in the polymer main chain. Then, the post-test QPE-bl-9-DMHA membrane was also subjected to the IR analyses (Figure 2-17c). Similar to QPE-bl-9-TMA, minor degradation in the polymer main chain was suggested by somewhat lower intensity of the peak at 1609 cm^{-1} assignable to C-C stretching vibration of the aromatic rings. The degradation of the ammonium groups was indicated by the lower intensity of the peak at 1212 cm^{-1} assignable to C-N stretching vibration of the aliphatic ammonium groups. The $C\text{-}N^+$ stretching vibration could not be observed at 892 cm^{-1} for QPE-bl-9-DMHA membrane probably because of the overlapping with the larger peak at 829 cm^{-1}. These changes in the IR spectra are well accountable for the changes in the conductivities and their retentions during the alkaline stability test.

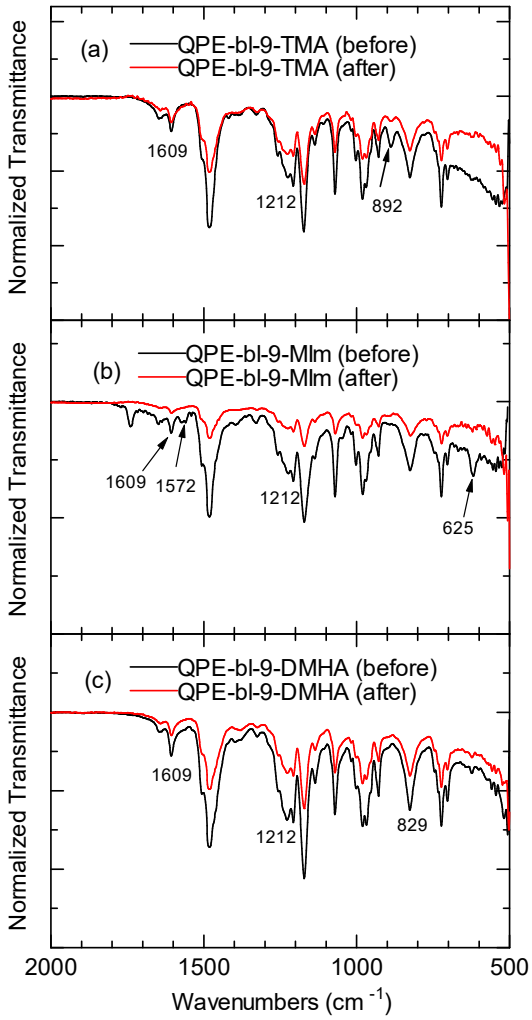

Figure 2-17. FT-IR spectra of (a) QPE-bl-9-TMA, (b) QPE-bl-9-MIm and (c) QPE-bl-9-DMHA membranes before and after the stability test for 1000 h.

2.3.5 Mechanical properties

The mechanical stability of the QPE-bl-9 membranes was investigated through the dynamic mechanical analyses (DMA). The temperature dependence of the storage modulus (E'), loss modulus (E''), and tan δ (E''/E') of the QPE-bl-9 membranes (in chloride or bicarbonate ion form) was measured at 60% RH (Figure 2-18). The E' and E'' values were nearly constant for the pristine and post-test QPE-bl-9 membranes regardless of the different ammonium groups and IEC values. The results suggest that the DMA properties mainly reflect the main chain structure and that the main chain degradation in the alkaline stability test was not significant. This idea is not contradictory to the above mentioned conductivity and IR analyses, both of which implied that the decomposition of the ammonium groups were the major degradation modes for the QPE-bl-9 membranes. Nevertheless, the post-test QPE-bl-9-TMA and -DMHA membranes were less ductile and easier to break during the DMA measurements implying some main chain degradation. The pristine and post-test Tokuyama A201 membranes exhibited a decrease in E' as increasing the temperature. The results may imply the possibility of the Tokuyama membrane to lose mechanical strength in operating fuel cells especially at higher temperature, whereas that is not the case for the series of the QPE-bl-9 membranes.

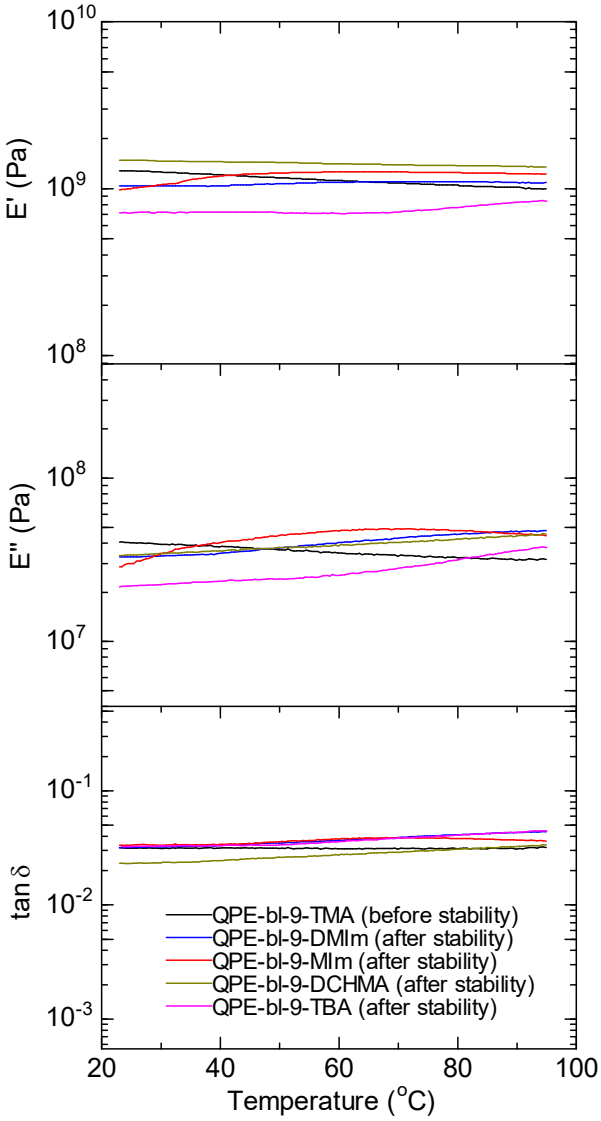

Figure 2-18. DMA curves of QPE-bl-9 and A201 membranes at 60% RH as a function of temperature before and after the alkaline stability test.

2.4 Screening of new series of ammonium groups

As described above, none of the investigated ammonium groups (DMHA, DMIm, MIm, TBA and DCHMA) exhibited higher conductivity or more stability than BTMA. We hypothesized that the bulky structure of QPE-bl-9 as aromatic block copolymer is presumably responsible for impeding the facile quaternization and /or the free bath for ionic conduction with bulky ammonium groups. To confirm our hypothesis, another series of ammonium groups were investigated looking for the optimum cation for QPE-bl-9 membranes. The new series included the ammonium structures stabilized by steric factor of pendant alkyl chain (dimethylbutyl amine (DMBA) and dimethyloctylamine (DMOA)) (Figure 2-19). The second series stabilized by antiperiplanar structure that suppress Hofmann elimination (diazaabicyclo-octane (DABCO) and double quaternized diazaabicyclo-octane (DDABCO)) (Figure 2-19).[6] Another series is stabilized by charge delocalization along double bond and lone pair of electrons on the second nitrogen (Diazabicyclo [4.3.0]non-5-ene (DBN)) (Figure 2-19). Also, a series of ammonium groups stabilized by the basicity include (N-methylmorpholine (NMM), N-methylpiperazine (MP), mono quaternized N,N-dimethylpiperazine (DMP), double quaternized dimethylpiperazine (DDMP), 1-(2-Dimethylaminoethyl)-4-methylpiperazine (DMAMP) and double quaternized (DDMAMP) (Figure 2-19). Finally, tetramethylimidazole (TMIm) that stabilized by resonance, donating methyl groups and steric effect.

The CMPE-bl-9 membranes were quaternized by the aforementioned series of ammonium groups following the same quaternization conditions described above. DQ ranged from 55-94% as shown in Table 2-4. The resulting quaternized membranes were tested for their conductivity, water absorbability and alkaline stability and compared with that of QPE-bl-9-TMA.

2.4.1 Ionic conduction and water management

In figures 2-20 and 2-21, hydroxide ion conductivity was plotted as a function of IEC and hydration number (λ)(number of water molecules per ammonium group) respectively. Among the new

series of ammonium groups; NMM, DABCO and DMBA exhibited higher conductivity than the rest of ammonium groups at IEC > 1.0 meq g^{-1}, however, they exhibited low to moderate hydration numbers. The other ammonium groups were lower conductive even at larger IEC and higher water content. In spite of that, TMA still the highest conductive at comparable IEC and low hydration numbers. Notably, TMA possess the smallest molecular volume among the other bulky ammonium groups, demonstrating that the volume of ammonium group is crucial for effective functionalization of QPE-bl-9 membranes.

2.4.2 Morphology

The morphology of the highest conductive membranes (QPE-bl-9-NMM, -DABCO and –DMBA) were examined through TEM images (Figure 2-22). As expected the three membrane showed good phase separated morphology with nearly similar ionic clusters (2-3 nm). Suggesting that the phase separation is responsible for the high ionic conduction in these three membranes.

2.4.3 Alkaline stability

The alkaline stability of the new series of ammonium groups was measured in 1M KOH at 60 ^{o}C for 1000 h. The relation between initial hydroxide ion conductivity at 40 ^{o}C and the remaining conductivity after 1000 h of stability test, was plotted in Figure 2-23. Among the second series of ammonium groups, TMA (1.3 meq g^{-1}) and DMBA (1.23 meq g^{-1}) exhibited the highest initial and remaining conductivity since DMBA retained 11.0 mS/cm and 25.7% compared to 20 mS/cm (44%) for TMA.

All the rest of ammonium groups were less stable and most of these groups exhibited lower initial hydroxide conductivity than those in Figure 2-20, suggesting that these ammonium groups were degraded at early stage in the first 24 h of alkaline stability test.

The results suggest that small volume ammonium groups (TMA) are more suitable for QPE-bl-9 membranes followed by pendant aliphatic group (DMBA). However, the pendant alkyl chain ammonium groups were calimed to be more stable than BTMA, contrary to that QPE-bl-9-TMA

was more stable. The reason for that may be illustrated from **Figures 2-12** and **2-21**, the low hydration numbers of QPE-bl-9-TMA may be responsible for reduced solvation of ammonium group since the low solvation decrease the dissociation of the ammonium group and/or obstacle the free access of OH^- to attack quaternary ammonium (i.e. less interaction between ammonium cation and alkali). On contrast, in the pendant alkyl, bulky and heterocyclic ammonium cations, the higher water content leads to more hydration levels that in turn facilitate the OH^- attack through the ease access to QA. These results are in agreement with the study reported by Nuñez *et. al.,*[7] in solution on small molecule analogs in which quaternary ammonium with pendant n-alkyl chain, degraded faster than BTMA.[7]

However, some ammonium groups with low or similar hydration numbers were also degraded faster than BTMA, such as MP, DMAMP, DDMAMP and NMM. The instability of these low hydrated groups may be attributed to the presence of β-hydrogen and β-carbon. Introducing β–hydrogen facilitates the Hoffmann elimination that competes with the nucleophilic substitution, increasing the possibility of the ammonium degradation. While the presence of β-carbon leads to extended interaction between β-carbon and α-carbon (C_β-$C_\alpha N^+$) through hyper-conjugative donation, leading to longer bond between benzylic carbon and ammonium cation (C_{Bn}-N^+) resulting in faster degradation.[7-10] (This situation may be also the case for some of the ammonium groups with high hydration levels such as the case for DMBA, DMHA, DABCO and DDABCO). These results were inconsistent with those performed on membrane materials,[11,12] suggesting that the stability of AEMs face a complicated competition between different and probably counteracting factors such as phase separation, steric shielding, chemical structure and hydration levels.[7,11,12] The hydration levels and chemical structure seem to be the dominant factors controlling the stability of QPE-bl-9 membranes.

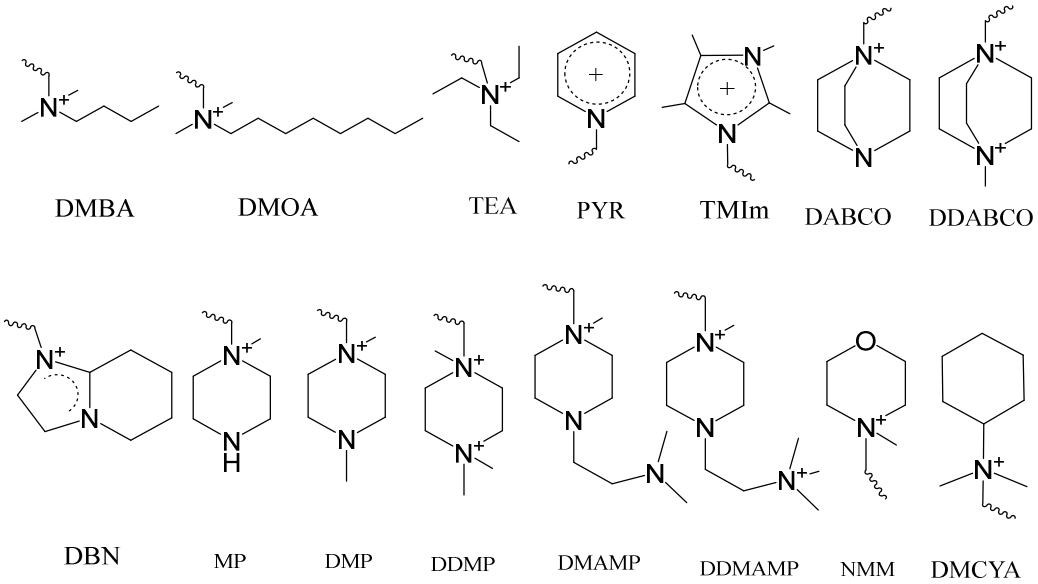

Figure 2-19. Chemical structures of new series of ammonium groups.

Table 2-4. IEC and degree of quarterniztion of QPE-bl-9 membranes.

Membrane	IECtit	IEC calcu.	DQ (%)
QPE-bl-9-DABCO	1.0	1.5	66
QPE-bl-9-DDABCO	1.35	1.96	68
QPE-bl-9-DMCHA	1.2	1.6	75
QPE-bl-9-NMM	1.69	1.8	93
QPE-bl-9-DBN	0.83	1.5	55
QPE-bl-9-DMBA	1.23	1.5	82
QPE-bl-9-Pyridine	1.42	1.86	76
QPE-bl-9-TEA	1.26	1.9	66
QPE-bl-9-A-DMOA	0.89	1.5	59
QPE-bl-9-TMIm	0.97	1.7	57
QPE-bl-9- MP	1.46	1.96	74
QPE-bl-9-DMP	1.83	1.98	94
QPE-bl-9-DDMP	0.97	1.6	60
QPE-bl-9-DMAMP	1.9	2.2	86
QPE-bl-9-DDMAMP	1.7	2.4	70

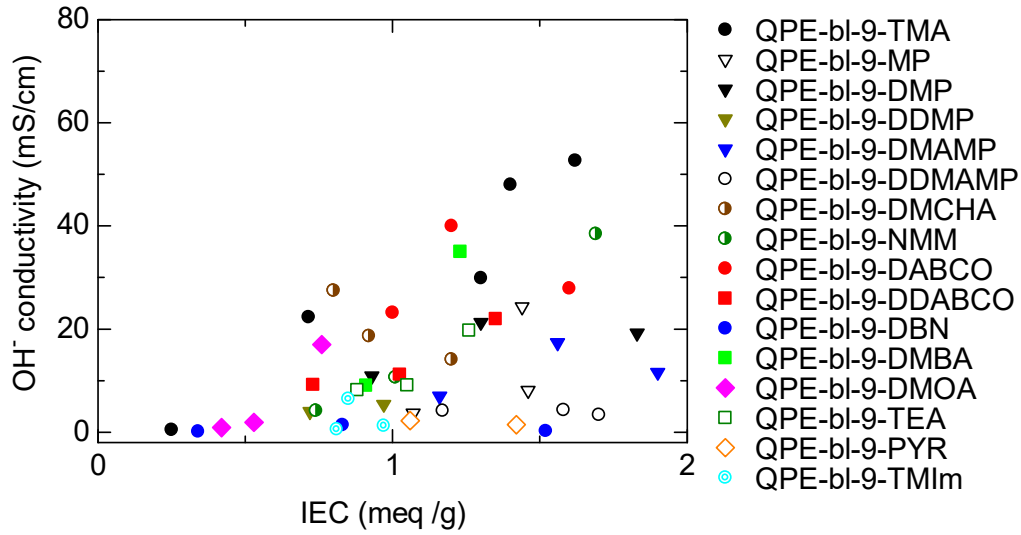

Figure 2-20. Hydroxide ion conductivity at 30 ºC of QPE-bl-9 membranes as a function of ion exchange capacity(IEC).

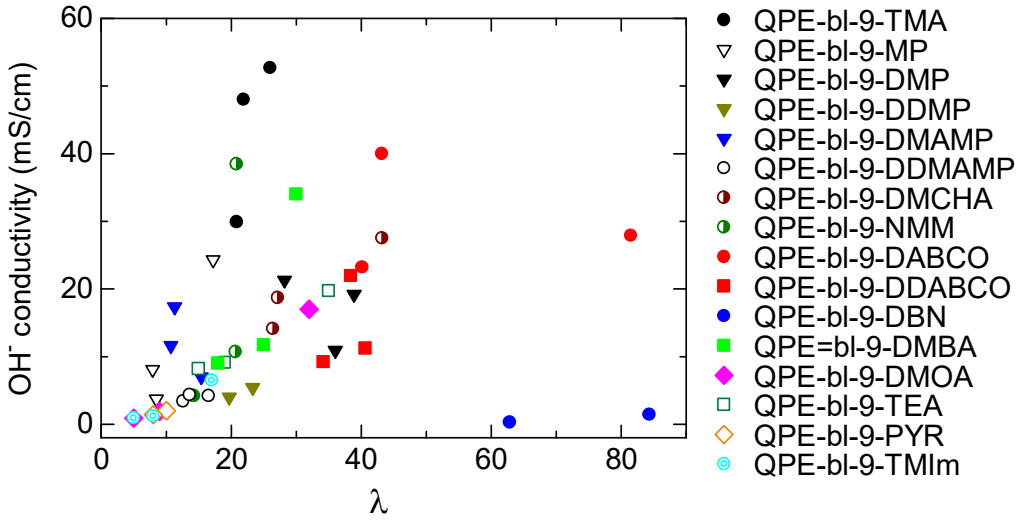

Figure 2-21. Hydroxide ion conductivity at 30 ºC of QPE-bl-9 membranes. as a function of λ .

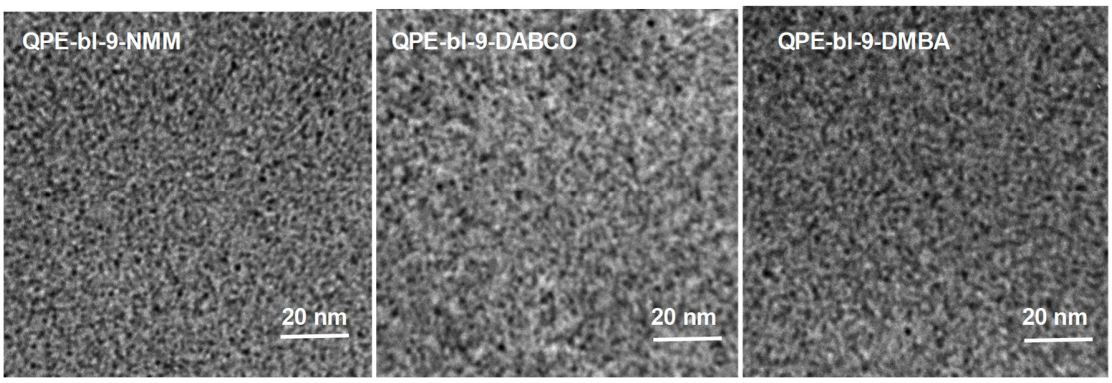

Figure 2-22. TEM images of QPE-bl-9-NMM, -DABCO and –DMBA (stained with tetrachloropalatinate ions).

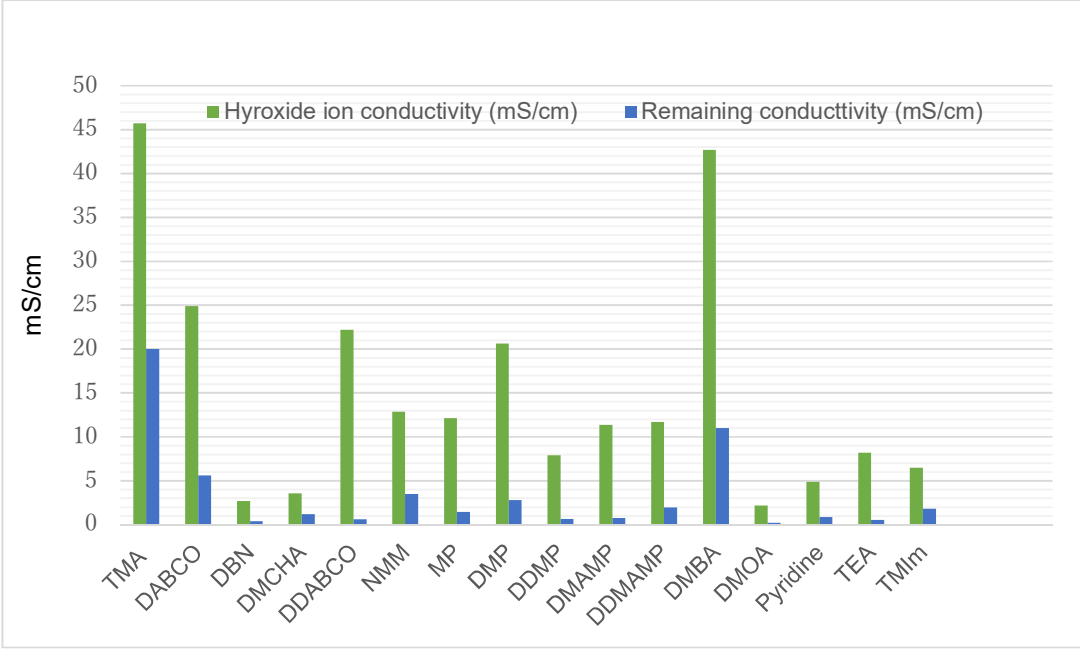

Figure 2-23. Hydroxide ion conductivity at 40 °C and remaining conductivity after 1000 h in 1M KOH of QPE-bl-9 functionalized with various ammonium groups.

2.5 Conclusion

Effect of the ammonium groups on the properties of anion exchange membranes has been investigated for aromatic copolymers containing oligophenylene as the hydrophilic component and partially fluorinated arylene ether as the hydrophobic component (QPE-bl-9). Regardless of the differences in the ammonium groups, the QPE-bl-9 membranes exhibited similar phase-separated morphology based on the hydrophilic/hydrophobic differences in the polymer component. The size of the hydrophilic domains was in the order of bulky aliphatic ammonium groups (DMHA), small aliphatic ammonium groups (TMA), and flat imidazolium groups (MIm and DMIm). From the water uptake and hydroxide ion conductivity, it was concluded that QPE-bl-9-TMA utilized water molecules more efficiently (followed by -DMHA with a pendant hexyl group) than the other series of QPE-bl-9 membranes. The three membranes, QPE-bl-9-TMA (1.6 meq g^{-1}), -DMHA (1.02 meq g^{-1}) and -DMIm (1.38 meq g^{-1}), exhibited higher hydroxide ion conductivity than that of the benchmark Tokuyama A201membrane (1.7 meq g^{-1}) taking the IEC values into account. The E_a values of the hydroxide ion conductivity in water were similar among those membranes and our previous aromatic copolymer-based AEMs (11-14 kJ mol^{-1}), suggesting that the differences in the ammonium groups were unlikely to affect the ion conducting mechanism.

QPE-bl-9-TMA was the most stable among the tested groups in 1 M KOH at 60 °C for 1000 h. The retention of the conductivity (58%) was higher than that of Tokuyama A201 (29%). Other QPE-bl-9 membranes showed smaller retention than 12%. The post-test IR analyses revealed that the major degradation involved the decomposition of the ammonium groups, while minor main chain scission was also suggested. The mechanical stability tested by DMA analyses revealed that the E' and E'' values changed little after the alkaline stability test and were independent on the ammonium groups and IEC values. The results imply that the viscoelastic properties of QPE-bl-9 membranes mainly reflect the polymer main chain structure. From the present study, the trimethylammonium groups seem the most promising ammonium groups for QPE-bl-9 as AEMs. The same result was confirmed through another series of ammonium groups included bulky, conjugated and heterocyclic ammonium groups, in which the aliphatic ammonium groups with

pendant alkyl chain (DMBA) was also promising and come in the second order after TMA in terms of conductivity and alkaline stability.

2.6 References

1- Yokota,N.; Shimada,M.; Ono, H. ; Akiyama, R. ; Nishino, E. ; Asazawa, K.; Miyake, J.; Watanabe, M. ; Miyatake, K. *Macromolecules* **2014**, *47*, 8238-8246.

2- Yokota, N. ; Ono, H.; Miyake, J.; Nishino, E. ; Asazawa, K. ; Watanabe, M. ; Miyatake, K. *ACS Appl. Mater. Interfaces* **2014**, *6*, 17044–17052.

3- Ono, H.; Miyake, J.; Bae, B.; Watanabe, M.; Miyatake, K. *Bull. Chem. Soc. Jpn.* **2013**, *86*, 663-670.

4- Tanaka, M.; Fukasawa, K.; Nishino, E.; Yamaguchi, S.; Yamada, K.; Tanaka, H.; Bae, B.; Miyatake, K.; Watanabe, M. *J. Am. Chem. Soc.* **2011**, *133*, 10646-10654.

5- Heimer, N. E.; Sesto, R. E.; Meng, Z.; Wilkes, J. S.; Carpe, W. R. *J. Mol. Liq.* **2006**, *124*, 84-95.

6- Fang, J.; Yang, Y.; Lu, X.; Ye, M.; Li, W.; Zhang, Y. *J. Hydrogen Energy*, **2012**, *37*, 594-602.

7- Nuñez, S. A. ; Capparelli, C. ; Hickner, M. A. *Chem. Mater.* 2016, 28 (8), pp 2589–2598

8- Westaway, K. C.; Fang, Y.; MacMillar, S. ; Matsson, O.; Poirier, R. A. A.; Islam, S. M. *J. Am. Chem. Soc.* **2007**, *111*, 8110–8120.

9- Harris, J. M.; Shafer, S. G.; Moffatt, J. R.; Becker, A. R. *J. Am. Chem. Soc.* **2002**, *101*, 3295–3300.

10- Rastogi, P. P. Zeitschrift Für Physikalische Chemie. *Z. Phys. Chem.* **1971**, *75*, 202–206.

11- Li, N.; Leng, Y.; Hickner, M. A.; Wang, C. Y. *J. Am. Chem. Soc.* **2013**, *135*, 10124-10133.

12- Kreuer, K.-D. *Chem. Mater.* **2014**, *26*, 361-380.

Chapter 3

High Hydroxide Ion Conductivity with Enhanced Alkaline Stability of Partially Fluorinated and Quaternized Aromatic Copolymers as Anion Exchange Membranes

3.1 Introduction

In chapter 2, various ammonium groups were investigated to functionalize the block copolymer poly(arylene ether) based AEM (QPE-bl-9), looking for the highest conductive and the most stable cation. The ammonium structure showed significant impact on the conductivity, water absorbability and alkaline stability, while the mechanical strength was not affected. Unfortunately, none of the ammonium groups under investigation was higher conductive or more stable than the conventional benzyltrimethylammonium cation (BTMA). Notably, BTMA has the smallest volume among the tested groups, suggesting that the rigid aromatic structure of QPE-bl-9 is likely to mitigate the high degree of quaternization and/or free bath of ionic conduction of bulky ammonium structure. However, TMA was followed by pendant alkyl chains such as dimethylbutylamine(DMBA) that was more stable and higher conductive than the other heterocyclic and bulky groups. These results motivated me in this chapter to investigate the effect of pendant alkyl groups on the properties of another partially fluorinated aromatic polymer backbone with less aromatic content (QPAF). QPAF share the same hydrophilic component of the oligophenylene moieties with QPE-bl-9, however the former possess flexible perfluoroalkylene in hydrophobic segments that provide more flexibility and membrane capability than that of rigid QPE-bl-9 membranes. Particularly, QPAF membranes exhibited high conductivity and good mechanical strength, however it possessed week alkaline stability since it lost most of its anion conductivity in 1 M KOH at 60 or 80 ºC within several hundred hours due to the decomposition

of BTMA groups.[1,2] In this chapter, the pendant aliphatic groups are expected to enhance the stability and other properties of QPAF membranes. The results are also compared with heterocyclic structure (1,2-dimethylimidazolium) and the resulted membranes will be studied through the detailed examination of the morphology, ion conductivity, and alkaline and mechanical stability.

3.2 Experimental section

3.2.1 Materials

Dodecafluoro-1,6-diiodohexane, 1-chloro-3-iodobenzene, 1,4-dichlorobenzene, 1,3-dichlorobenzene, bipyridine, dimethylbutylamine (DMBA), 1,2-dimethylimidazole (DMIm), and zinc chloride were purchased from TCI Inc. and used as received. 45% Trimethylamine (TMA) aqueous solution and dimethylhexylamine (DMHA) were purchased from Sigma-Aldrich. Dimethylsulfoxide-d_6 (DMSO-d_6) with 0.03% tetramethylsilane (TMS), 1,1,2,2-tetrachloroethane-d_2 (TCE-d_2), and chloroform-d_1 ($CDCl_3$) with 0.03% TMS were purchased from Acros Organics and used as received. Bis(1,5-cyclooctadiene) nickel(0) ($Ni(cod)_2$), chloromethyl methyl ether (CMME), thionyl chloride ($SOCl_2$), hydrochloric acid, potassium carbonate, potassium hydroxide, dimethyl sulfoxide (DMSO), N,N-dimethylformamide (DMF), anhydrous lithium bromide, and N,N-dimethylacetamide (DMAc) were purchased from Kanto chemical Co. and used as received.

3.2.2 Synthesis of QPAF Membranes

Perfluoromonomer and precursor copolymers (PAF and CMPAF) were prepared according to the literature.[1] The resulting CMPAF copolymer was used for the following quaternization reaction.

3.2.3 Quaternization Reactions

A round-bottomed flask sealed with a Teflon cap was charged with 0.15 g of CMPAF followed by the addition of amine solution (2.5 equiv. of phenylene units). The mixture was suspended in

methanol (20 mL) and heated at 60 ºC. After a few hours, the mixture became homogenous solution. The mixture was kept under vigorous stirring at 60 ºC for 48 h. The mixture was cooled to room temperature and poured into a large excess of 2 M hydrochloric acid. The resulting suspension was dialyzed for up to 48 h until the external water became neutral. The solvent was removed under vacuum to obtain QPAF in chloride ion form (0.18-0.22 g) (95-98% yield)

3.2.4 Membrane Preparation

The resulting QPAF in Cl^- form was dissolved in NMP, filtered, and casted onto a flat glass plate at 60 ºC for 24 h. Transparent and flexible membranes were obtained (45-100 μm thick**).**

3.2.5 Ion Exchange Reactions

To exchange the chloride ions to hydroxide ions, the QPAF membranes in Cl^- forms were immersed in 1 M aqueous potassium hydroxide solution at 40 ºC for 48 h. After the ion exchange reaction, the membranes were washed and stored in degassed deionized water.

3.2.6 Measurements

The prepared monomers and copolymers were characterized by ^1H and ^{19}F NMR spectra on a JEOL JNM-ECA/ECX500 using $CDCl_3$, TCE-d_2 or DMSO-d_6 as solvents and TMS as an internal reference. JASCO FT/IR-6100 was used to measure the FT-IR spectra of the copolymers. Gel permeation chromatography (GPC) was used to determine the molecular weights (M_w and M_n) using a Shodex KF-805L or SB-803 column and a Jasco 805 UV detector with DMF containing 0.01 M lithium bromide as eluent. Standard polystyrene samples were used for calibration. Transmission electron microscopic (TEM) images were taken for the selected membranes stained with tetrachloroplatinate ions using a Hitachi H-9500 transmission electron microscope with an acceleration voltage of 200 kV. The domain sizes in TEM images were estimated using J-image program. Dynamic mechanical Analyses (DMA) of the membranes were performed at 60% relative humidity (RH) from room temperature to 95 ºC at a heating rate of 1 ºC min^{-1} using an

ITK DVA-225 dynamic viscoelastic analyzer. Further detailed procedures of these measurements were mentioned in our previous publications.[1, 3]

3.2.7 Determination of IEC Values

The theoretical ion exchange capacities (IECs) were calculated from the feed comonomer ratios (m:n:o) and the degree of chloromethylation (DC). The IEC values were also calculated from the ^{1}H NMR spectra using the integral ratio of the methylene protons (9) relative to the sum of the aromatic protons (1, 2, 3, 4, 5, 6, 7 and 8). The titrated IEC values were determined by Mohr method in which the membranes in chloride ion forms were immersed in 0.2 M $NaNO_3$ for 24 h. The remaining $NaNO_3$ solution was titrated with 0.01 M $AgNO_3$ in the presence of 0.25 M K_2CrO_4 as indicator. After reaching the end point, the membranes were recovered, washed with distilled water, dried under vacuum at 60 ºC for 24 h, and weighed. The titrated IEC values were calculated from the equation:

$IEC_{titrarion}$ = ((mmoles of $AgNO_3$ equivalent to Cl^- ions)/ dry weight).

3.2.8 Water Uptake and λ

The water uptake was measured for the membranes in hydroxide ion forms by immersing the dry samples in deionized water for 24 h, wiped quickly with a paper to remove the surface water, and weighed immediately (W_w). The membranes were dried in vacuum oven at 60 ºC for overnight and weighed (W_d). The water uptake (WU) was calculated from the equation:

$$WU\ \% = (W_w - W_d) / W_d \times 100$$

The number of absorbed water molecules per ammonium group, λ, was calculated from the measured WU and $IEC_{titration}$ using the equation:

$$\lambda = (WU / IEC \times 18.015)$$

3.2.9 Ion Conductivity Measurements

Hydroxide ion conductivity of the membranes was measured using an AC impedance system (Solartron 1255B, Solartron Inc.) in degassed, deionized water. The corresponding resistances of the membranes were measured using a four-probe conductivity cell at 30, 40, 60 and 80 ºC. The impedance plots were obtained in frequency range from 1 to 10^5 Hz. The hydroxide ion conductivity (σ) was calculated from the equation, σ = L/RA, where L is the length between the inner electrodes (L= 1 cm), R is the resistance of the membranes, and A is cross-sectional area of the membranes. The apparent activation energies, E_a, were estimated from the slopes in Arrhenius plot (the logarithm of the ion conductivity versus 1000/T).

3.2.10 Calculation of the Diffusion Coefficients of Hydroxide Ions

The diffusion coefficient (D) of the hydroxide ion in the membranes was calculated from Nernst Einstein equation:

$$D = \sigma RT/cz^2F^2$$

where σ = measured ion conductivity, R = gas constant, T = absolute temperature, c = concentration of hydroxide ions, z = the ion charge, F = Faraday constant.[4]

Concentration (c) of hydroxide ions was calculated from the equation:

$$c = (0.001 \times \rho \, IEC)/ (1 + 0.01 \, X_{v\text{-}H2O})$$

where ρ = density of dry membrane, $X_{v\text{-}H2O}$ = volume fraction of absorbed water.[5]

Ion diffusivity in dilute solution (D_0) was calculated from the equation:

$$D_0 = \mu \, k_B T/ z$$

where μ = ion mobility in dilute solution, k_B = Boltzmann constant, T = absolute temperature.[6]

3.2.11 Alkaline Stability Test

The membranes in chloride ion forms were set in the conductivity cell and immersed in deionized water for 24 h and the conductivity was measured as 0 h. The membranes fixed in the cell were immersed in 1 M KOH aqueous solution at 60 ºC or 80 ºC in a closed vial for 1000 h or 500 h,

respectively. At the set time, the membranes in the cells were removed from the vial, washed and immersed in deionized water for 24 h prior to the conductivity measurement.

3.2.12 Preparation of Catalyst Coated Membrane (CCM) and Fuel Cell Operation

A procedure of the literature was modified as follows:[1, 7] A 50 wt% Pt-loaded catalyst (Pt/CB, TEC10E50E, Tanaka Kikinzoku Kogyo) with QPAF-TMA ionomer (1.16 meq g^{-1}) as the binder were used for the catalyst paste preparation. The mass ratio of the binder (dry basis) to carbon black (QPAF-TMA ionomer/carbon) was adjusted to 0.8. To prepare the CCM, the catalyst paste was sprayed onto both sides of QPAF-DMBA (1.33 meq g^{-1}, 45μm thick) membrane using a pulse-swirl-spray apparatus. The Pt loading was 0.2 ± 0.02 mg cm^{-2}, and the geometric area of the electrode was 4.41 cm^2. The CCM was ion exchanged to hydroxide ion form by immersion in 1.0 M KOH for 48 h then in deionized water for 24 h. The CCM was sandwiched between two gas diffusion layers at 1.0 MPa for 3 min. The MEA was assembled into a single cell consisting of two carbon separator plates. The fuel cell was operated at 40 ºC under an ambient pressure with fully humidified (100% RH) H_2 and O_2. The flow rate was 100 mL min^{-1} for both H_2 and O_2. The high-frequency resistance (HFR) of the cell was measured with a Kikusui FC impedance meter at 5.0 kHz**.**

3.3 Results and discussion

3.3.1 Synthesis of QPAF Polymers

Perfluoromonomer and the precursor copolymers (PAF and CMPAF) were prepared via nickel catalyzed Ullmann coupling reaction followed by Friedel-Crafts chloromethylation reaction as described in our previous report (Scheme 3-1).[1] The copolymer composition (m:n:o) was easily controlled by feed comonomer ratios since the polymerization reaction was quantitative. The copolymer compositions calculated from the ^1H NMR spectra were in agreement with the feed

ratios (Table 3-1). The CMPAFs were characterized by ^{1}H NMR spectra in which a broad peak at ca. 4.5 ppm was assignable to the chloromethyl protons. The ^{19}F NMR spectra were very similar between PAF and CMPAF, indicating the selective chloromethylation onto oligophenylene moieties without detectable side reactions (Figure 3-1). CMPAFs were of high molecular weight (M_n = 25-39 kDa, M_w = 182-265 kDa and PDI = 5.2-8.0) as suggested by GPC analyses (Table 3-1 and Figure 3-2). The GPC curve of CMPAF revealed a broad and trimodal distribution of the molecular weight. The higher molecular weight portions are considered to be the minor cross-linked products via methylene groups, while the lower molecular weight ones to be oligophenylene compounds without PAF moieties.[8] Nevertheless, these structural defects were minor and did not affect the solubility of CMPAF. These results were similar to those of our previous PAF and CMPAF with different copolymer compositions.[1] The degree of chloromethylation (DC) was reasonably high ranging from 0.71-0.80 chloromethyl group per phenylene unit in the oligophenylene moieties.

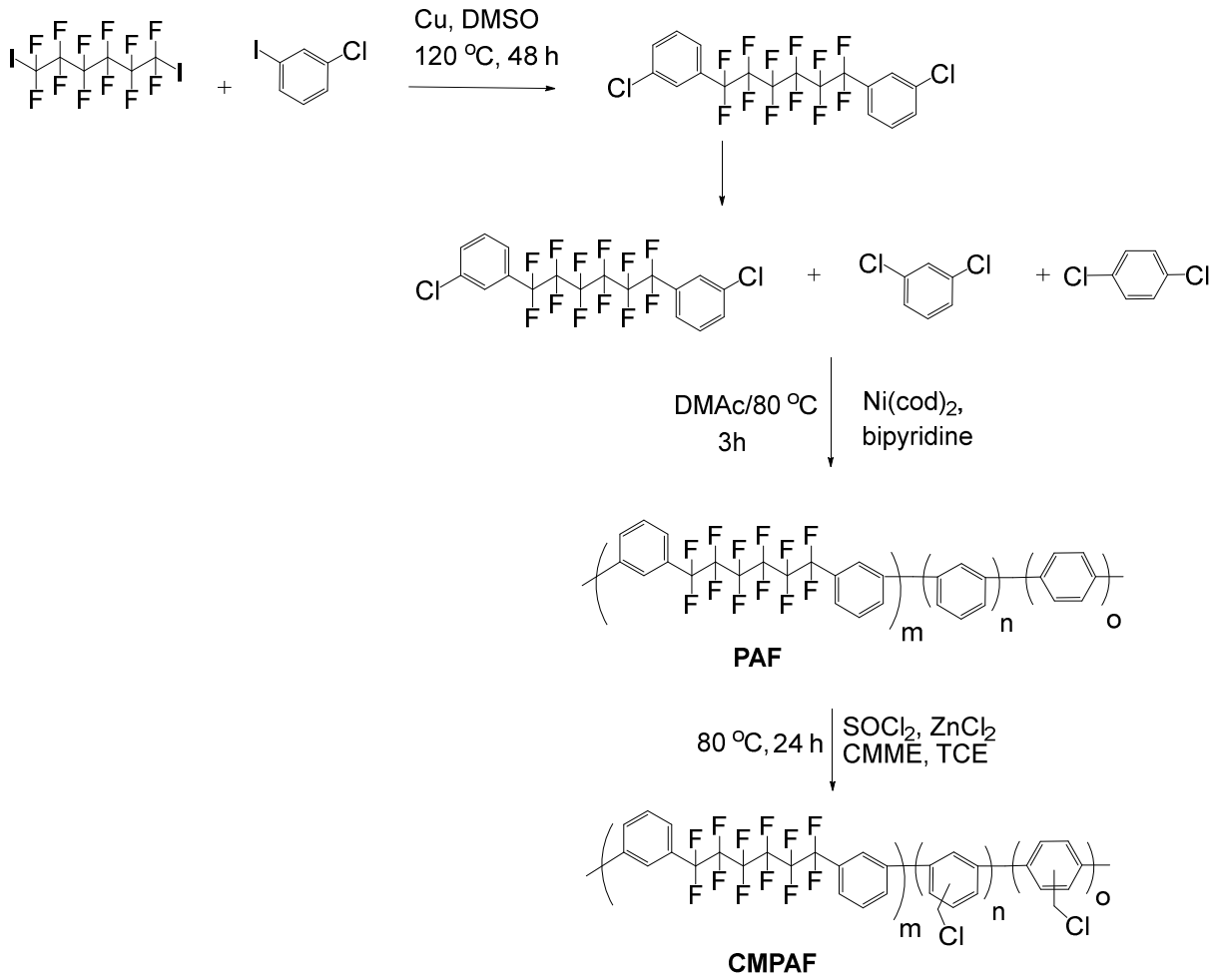

Scheme 3-1. Synthesis of PAF and CMPAF copolymers.

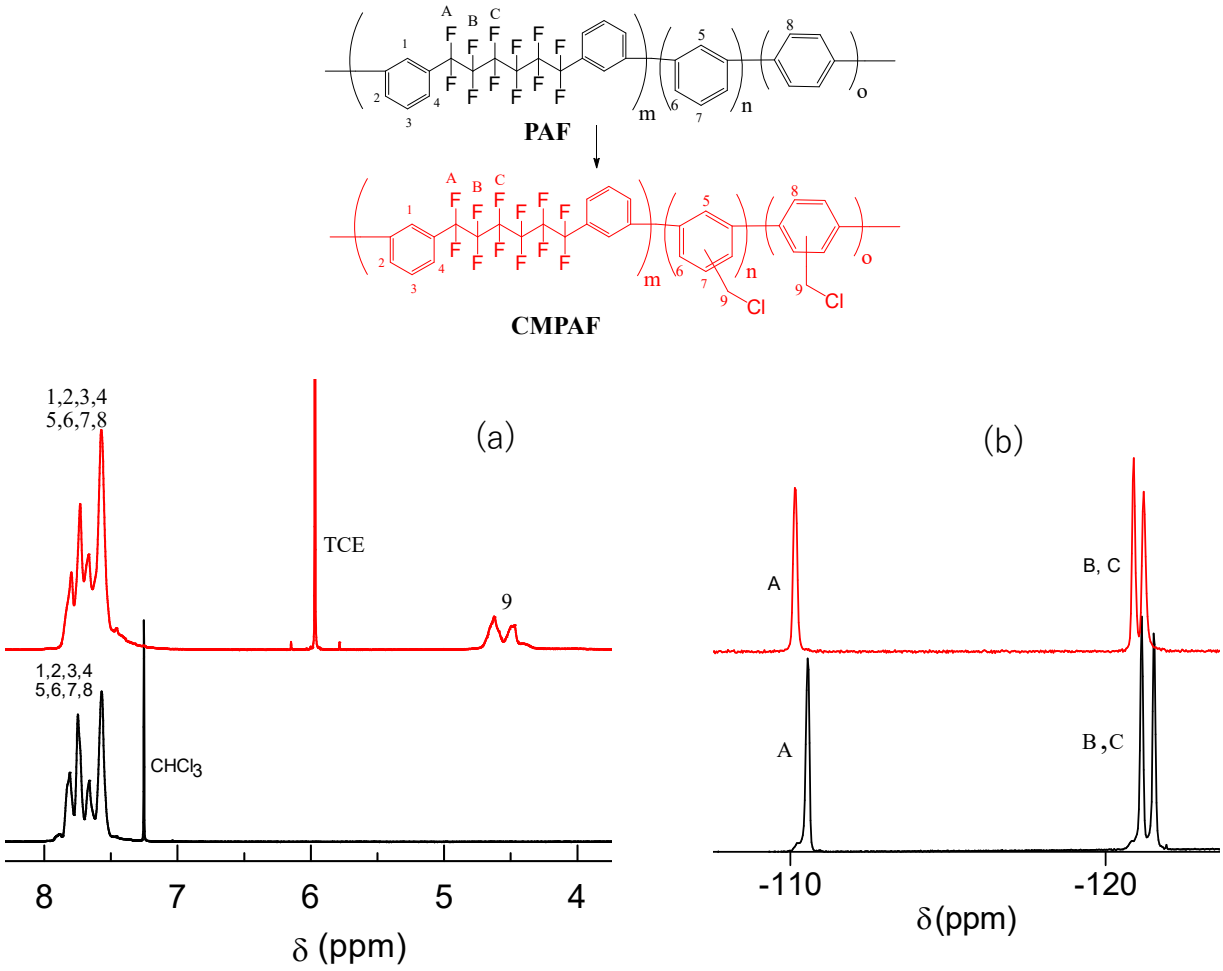

Figure 3-1. (a) ^{1}H and (b) ^{19}F NMR spectra of PAF and CMPAF (m:n:o = 1.0:0.48:0.62) at r.t.

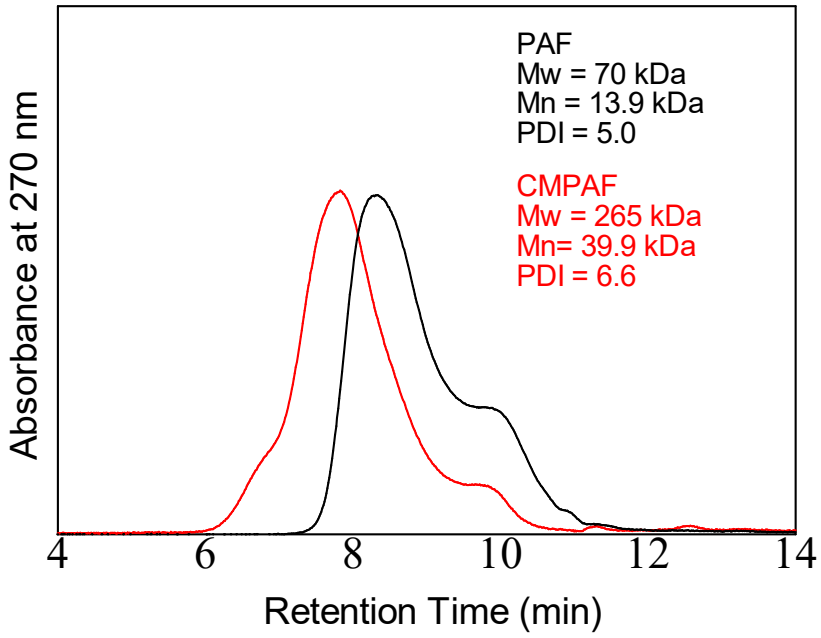

Figure 3-2. GPC profile of PAF and CMPAF (m:n:o = 1.0:0.48:0.62) copolymers (calibrated with polystyrene standards).

Table 3-1. Properties of QPAF membranes with different copolymer compositions and ammonium structures

QPAF-	m:n:o[a]	m:n:o[b]	M_w (kDa)[c]	M_n (kDa)[c]	PDI[c]	DC[d]	IEC[a]$_{theor.}$ (meq g^{-1})	IEC[b]$_{NMR}$ (meq g^{-1})	IEC[e]$_{tit.}$ (meq g^{-1})	DQ[f] (%)	WU[g] (%)	Thick. (μm)
DMBA	0.79: 0.48 : 0.62	0.79 :0.5 :0.65	182	25	7.2	0.80	1.58	1.62	1.16	72	43	72
	1.0: 0.48 : 0.62	1 :0.59 :0.76	265	39	6.6	0.71	1.16	1.15	1.09	95	33	100
	1.0: 0.67: 0	1:0.81:0	205	39	5.2	0.77	0.90	1.00	0.63	63	15	50
	1.0: 0.67: 1.03	1.0: 0.58: 0.89	252	32	8.0	0.72	1.65	1.50	1.33	89	53	45
DMHA	0.79: 0.48 : 0.62	0.79 :0.5 :0.65	182	25	7.2	0.80	1.30	1.50	0.90	60	24	68
	1.0: 0.48 : 0.62	1 :0.59 :0.76	265	39	6.6	0.71	1.13	1.11	1.10	99	40	74
	1.0: 0.67: 0	1:0.81:0	205	39	5.2	0.77	0.88	1.01	0.49	49	10	55
	1.0: 0.67: 1.03	1.0: 0.58: 0.89	252	32	8.0	0.72	1.57	1.32	1.17	89	45	45
DMIm	0.79: 0.48 : 0.62	0.79 :0.5 :0.65	182	25	7.2	0.80	1.59	1.64	1.15	70	53	80
	1.0: 0.48 : 0.62	1 :0.59 :0.76	265	39	6.6	0.71	1.23	1.15	1.24	100	120	70
	1.0: 0.67: 0	1:0.81:0	205	39	5.2	0.77	0.90	1.05	0.78	74	29	50

[a]Calculated from the feed comonomer ratio. [b]Determined by ^{1}H NMR spectra. [c]Determined by GPC analyses (calibrated with polystyrene standards) for CMPAF. [d]Degree of chloromethylation = (number of chloromethyl groups per phenylene ring in the oligophenylene moieties). [e]Determined by Mohr titration method. [f]Degree of quaternization per chloromethylated phenylene unit in the oligophenylene moieties.

A series of anion exchange membranes based on perfluoroalkylene groups as a hydrophobic segment and oligophenylene groups tethered with a various ammonium groups as a hydrophilic component were successfully synthesized through the Menshutkin reaction of CMPAF copolymers and various amines as shown in Scheme 3-2.

To investigate the effect of ammonium structures on QPAF membranes, some ammonium groups were selected, dimethylbutylamine (DMBA) and dimethylhexylamine (DMHA) with pendant alkyl groups, and heterocyclic 1,2-dimethylimidazole (DMIm). The structure of the quaternized QPAFs was analyzed by ^{1}H NMR spectra. For QPAF-DMIm, methylene protons appeared at 5.5 ppm, shifted to lower magnetic field from that of CMPE (ca. 4.5 ppm). The protons of the two methyl groups attached to the imidazolium ring appeared at 2.3 ppm and 3.8 ppm, respectively, while the imidazolium ring protons overlapped with the aromatic protons of the polymer main chain (Figure 3-3). The ^{1}H NMR spectra of QPAF-DMBA and QPAF-DMHA were similar. The peaks of the methylene protons shifted slightly from ca. 4.5 ppm to 4.8 ppm and the methyl protons of $N^{+}(CH_3)_2$ appeared as multiplet peaks at 2.8 ppm. The aliphatic protons of the pendant butyl and hexyl groups appeared as broad multiplet peaks from 0.5 ppm to 1.5 ppm as shown in Figures 3-4 and 3-5.

The quaternization reaction was tested under three different conditions, neat, in methanol, and in DMSO (Table 3-2). It was found that the quaternization reaction was more efficient in methanol than neat and in DMSO. In addition, membrane forming capability was better when methanol was used as the solvent. By changing the copolymer composition and the degree of quaternization (DQ), we were able to prepare a series of QPAF-DMBA, -DMHA, and -DMIm membranes with IEC_{theor} values ranging from 0.88 to 1.65 meq g^{-1} (Table 3-1). The higher IECs than 1.65 meq g^{-1} were avoided since QPAF-TMA with IECs higher than 1.5 meq g^{-1} exhibited excess swelling as reported previously.[1]

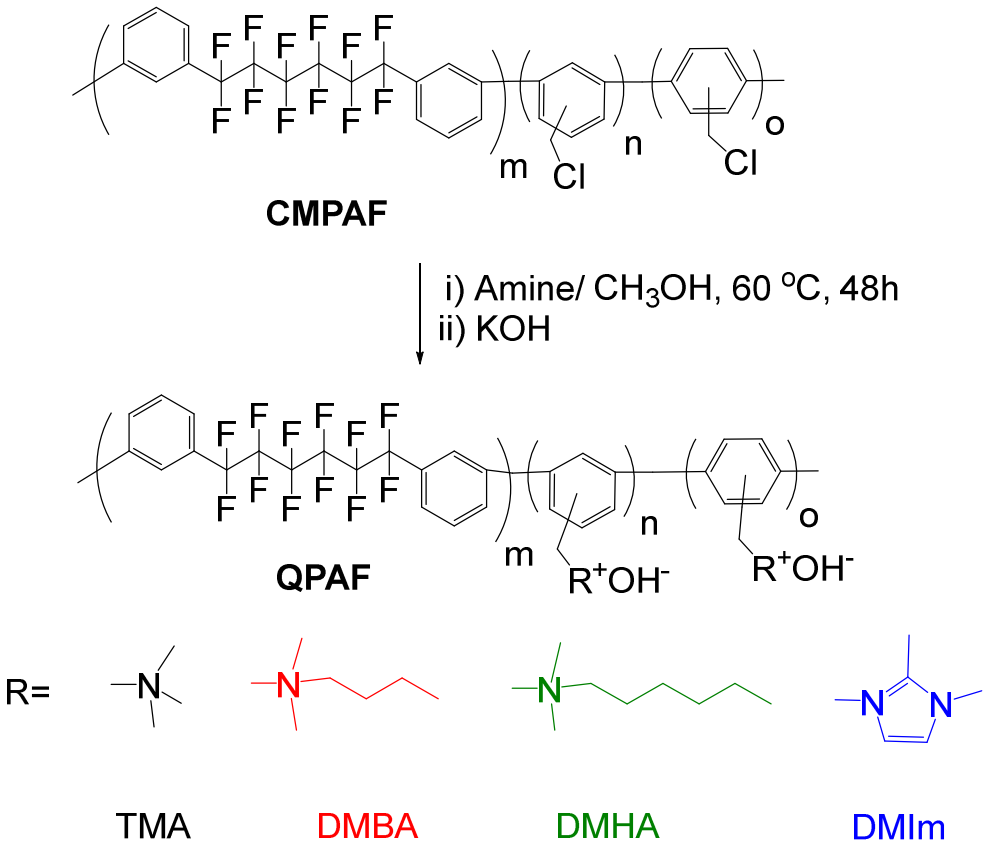

Scheme 3-2. Synthesis of QPAF membranes with various ammonium structures

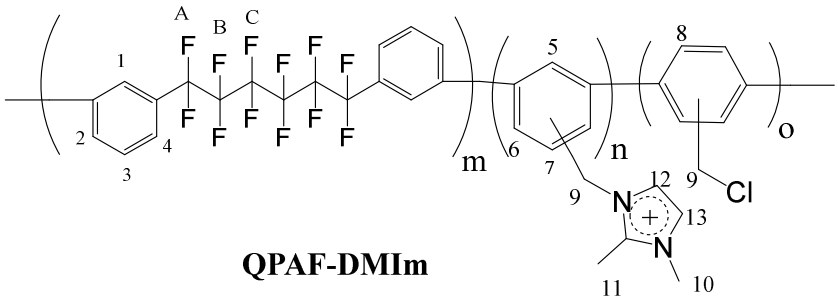

QPAF-DMIm

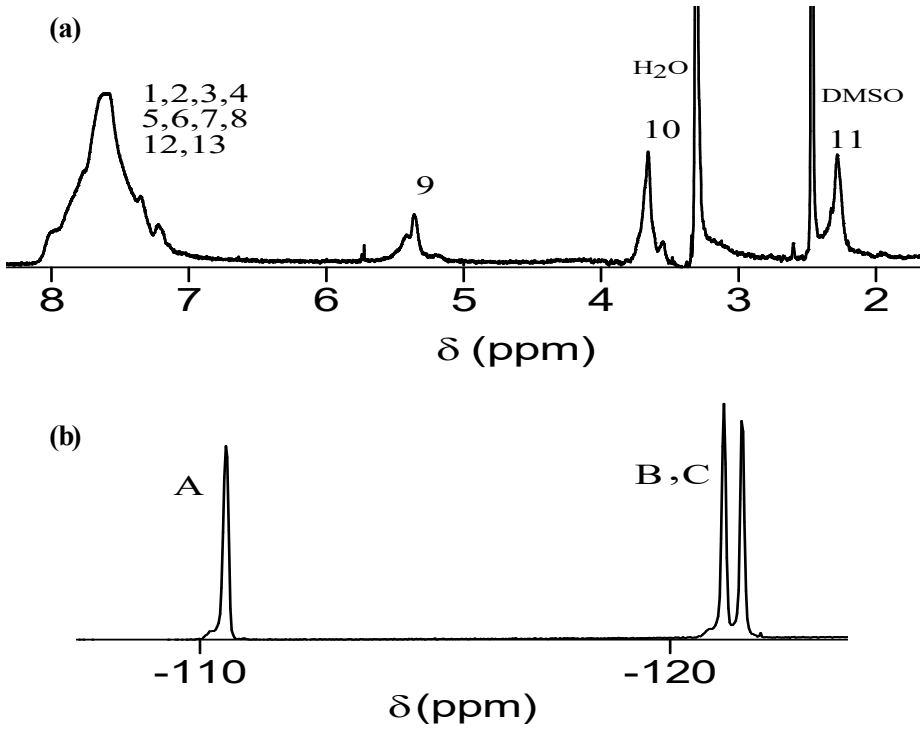

Figure 3-3. (a)^{1}H and (b) ^{19}F NMR spectra of QPAF-DMIm in DMSO-d_6 at r.t.

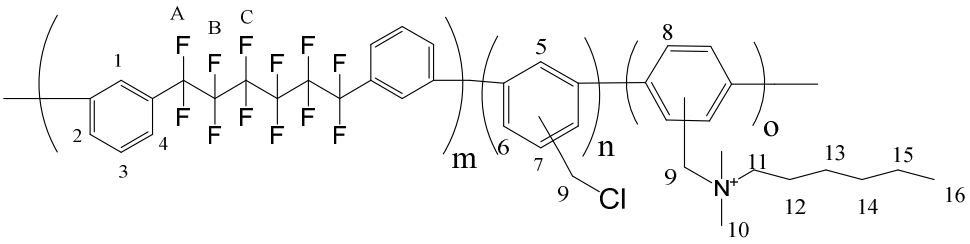

QPAF-DMHA

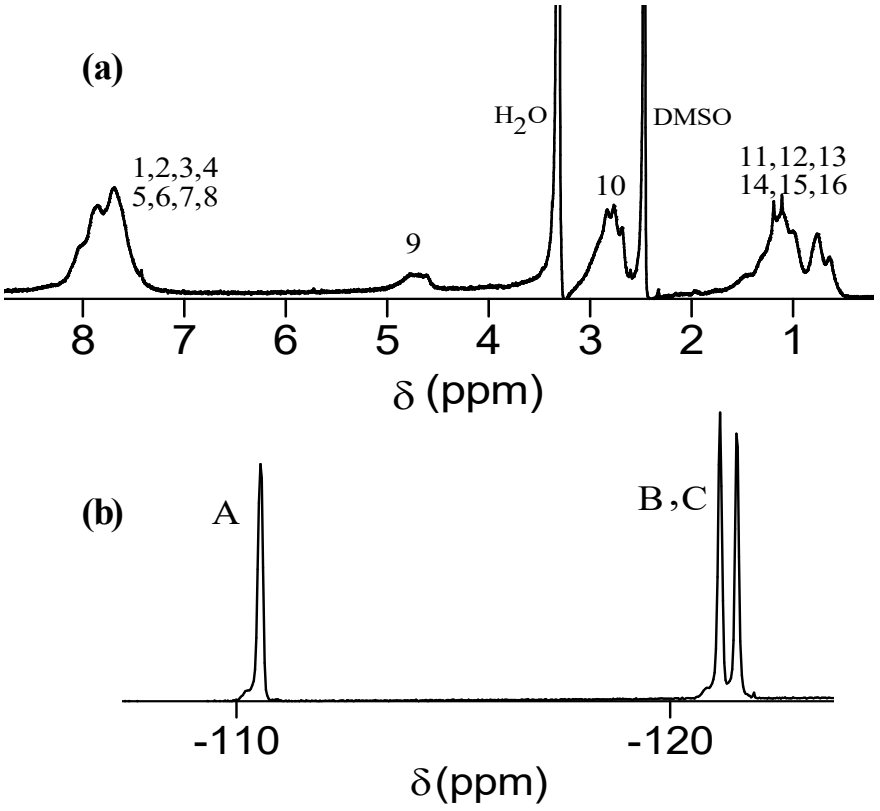

Figure 3-4. (a) ^{1}H and (b) ^{19}F NMR spectra of QPAF-DMHA in DMSO-d_6 at r.t.

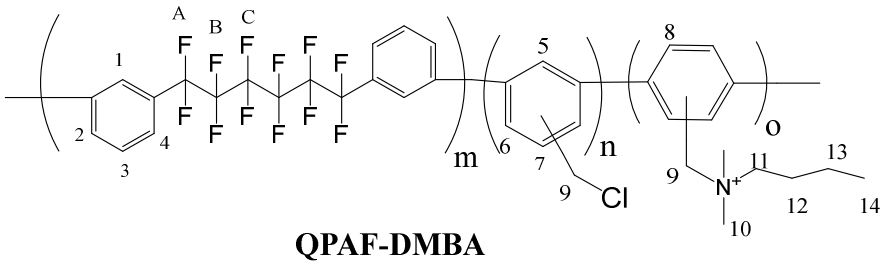

QPAF-DMBA

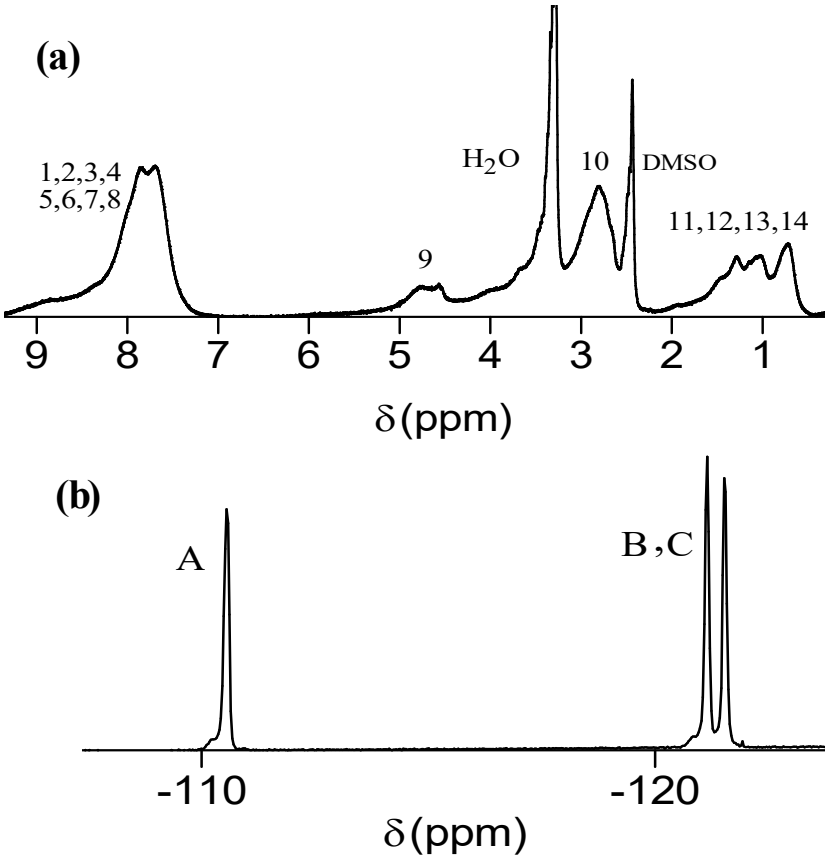

Figure 3-5. (a) ^{1}H and (b) ^{19}F NMR spectra of QPAF-DMBA in DMSO-d_6 at r.t.

Table 3-2. Effect of the Quaternization Conditions on the Properties of QPAF Membranes.

QPAF-	m:n:o	in methanol at 60 ºC		in DMSO at 60 ºC		neat at 40 ºC	
		IEC[a] (meq g^{-1})	DQ[b] (%)	IEC[a] (meq g^{-1})	DQ[b] (%)	IEC[a] (meq g^{-1})	DQ[b] (%)
DMBA	0.79:0.48:0.62	1.00	63	na[c]	-	1.00	63
DMHA	1.0:0.48:0.62	1.22	100	0.68	56	1.03	84
	0.79:0.48:0.62	1.10	75	na[c]	-	1.00	68
DMIm	1.0:0.67:0	0.67	65	0.50	48	na[c]	-
	0.79:0.48:0.62	1.02	82	0.80	64	na[c]	-

[a] Estimated from Mohr titration method. [b] Degree of quaternization per chloromethylated phenylene unit in the oligophenylene moieties. [c] Self-standing membrane was not obtained.

QPAFs were soluble in polar organic solvents and casting from NMP solutions at 60 ºC provided transparent and flexible membranes. The membranes did not show any distinct differences in brown color and flexibility among QPAFs with three different ammonium groups. In most cases, the titrated IEC values (IEC_{tit}) of the resulting membranes were in fair agreement with IEC_{theor} and IEC_{NMR}. However, in some cases, the titrated IECs were slightly lower than the theoretical values possibly because of aforementioned cross-linked groups, unreacted chloromethyl groups, and/or minor errors in titration. Regarding the unreacted chloromethyl groups which would affect the properties of the membranes, they should have been hydrolyzed in alkaline solution (during the ion exchange reactions) to the corresponding benzylic alkoxide and thus have minor impact on the alkaline stability and fuel cell performance.

3.3.2 Morphology of QPAF Membranes.

One of the most important issues for developing AEMs is to balance ion conductivity and water uptake by controlling phased-separated morphology based on the hydrophilic/hydrophobic differences in the copolymer component. TEM observations were performed for the selected QPAF-DMBA, -DMHA and -DMIm membranes stained with tetrachloroplatinate ions (Figure 3-6). In the images, the dark areas represent the stained ionic clusters while the bright areas represent the hydrophobic domains. QPAF-DMBA (1.33 meq g^{-1}) and QPAF-DMHA (1.17 meq g^{-1}) membranes showed nanoscale phase separated morphology with well-connected ionic channels. The hydrophilic domains were ca. 2-6 nm for QPAF-DMBA and 2-8 nm for QPAF-DMHA in diameter, which were somewhat larger than that for QPAF-TMA (1.26 meq g^{-1}) (ca. 1-2 nm).[1] QPAF-DMBA with lower IEC (1.16 meq g^{-1}) also showed phase separated morphology with hydrophilic domains 2-5 nm in diameter as shown in Figure 3-7. The larger ionic clusters would be attributed to the pendant butyl and hexyl groups attached to the ammonium groups to promote the self-aggregation of the ammonium groups. QPAF-DMIm (1.24 meq g^{-1}) membrane exhibited similar morphology with smaller hydrophilic domains (1-2 nm in diameter) than those of QPAF-DMBA and -DMHA. The smaller domain size must be related with compact and planar imidazolium rings. Similar results were obtained for our previous AEM copolymers (QPE-bl-9) containing DMIm groups.[9]

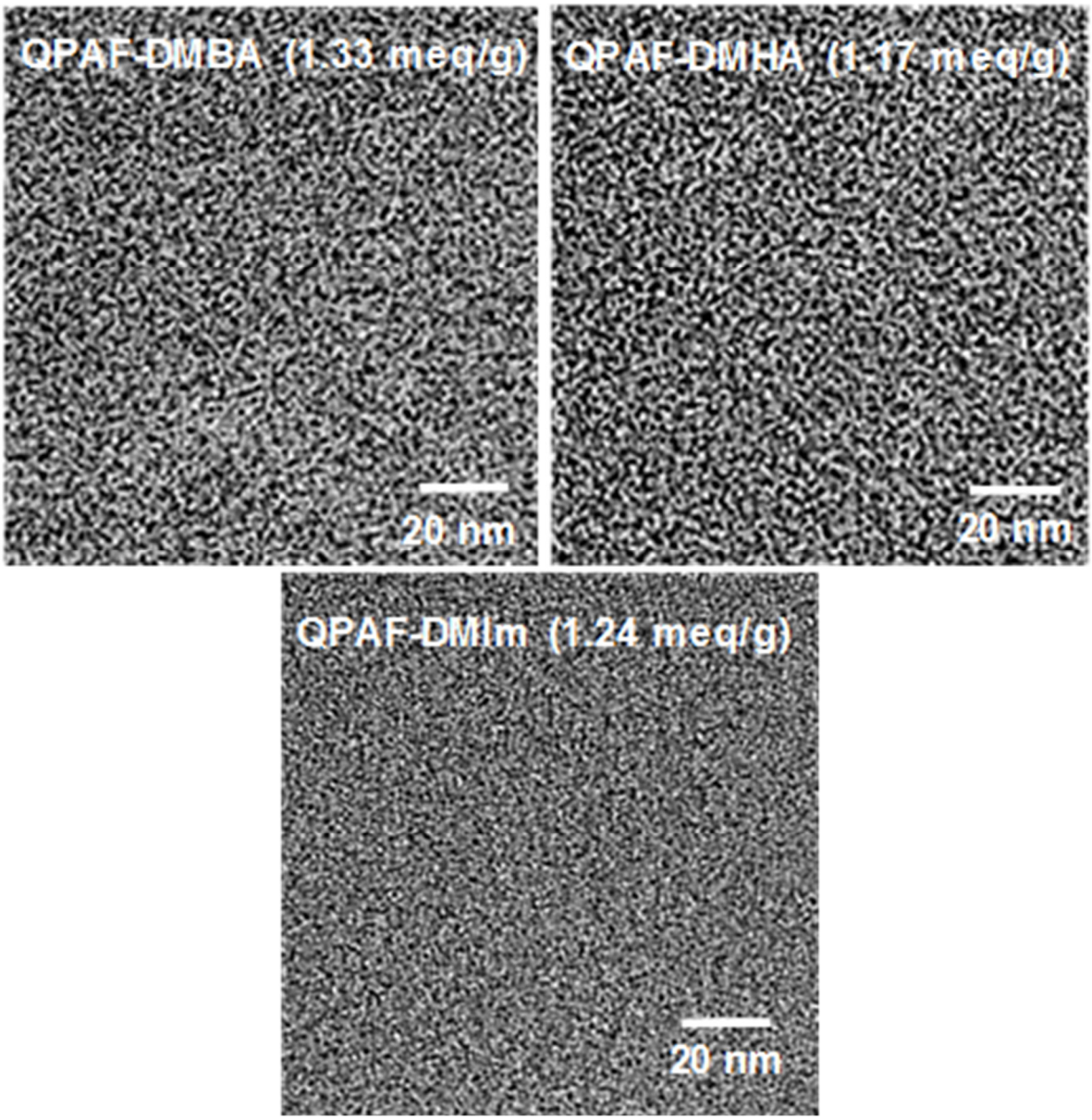

Figure 3-6. TEM images of QPAF membranes stained with tetrachloroplatinate ions.

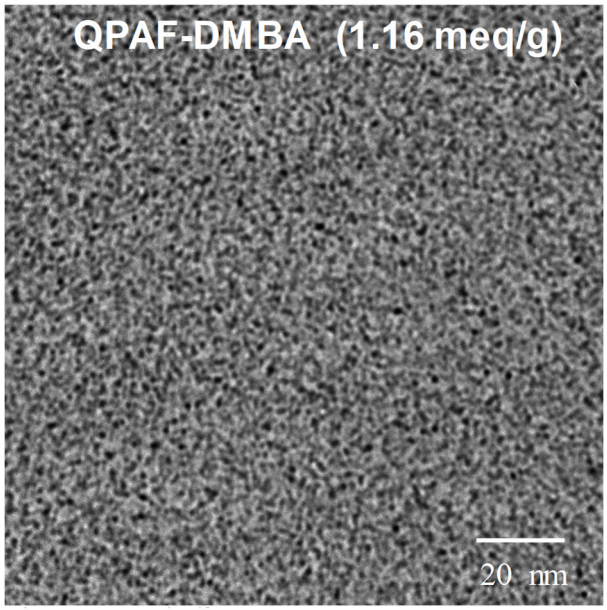

Figure 3-7. TEM image of QPAF-DMBA with IEC = 1.16 meq g^{-1}.

3.3.3 Water Uptake of QPAF Membranes.

Water uptake plays an essential role in AEMs in facilitating ionic conduction through developed ionic channels. In this regard, water uptake of QPAF membranes with various ammonium groups in hydroxide ion form was measured at room temperature in water and plotted as a function of their IEC values (Figure 3-8a). QPAF with aliphatic ammonium groups exhibited comparable water uptake to that of QPAF-TMA; QPAF-DMBA (1.16 meq g^{-1}), QPAF-DMHA (1.17 meq g^{-1}), and QPAF-TMA (1.26 meq g^{-1}) exhibited 43%, 45%, and 45% of the water uptake, respectively. The results suggest no or minor dependence of the water uptake on the morphology but on the IEC. QPAF-DMIm exhibited a large jump in the water uptake at IEC = 1.24 meq g^{-1} probably because of the strong hydrophilicity of the imidazolium rings. Compared to our previous AEMs sharing the same hydrophilic component (QPE-bl-9),[8] QPAF membranes exhibited higher water uptake despite the strong hydrophobic nature of the perfluoroalkyl groups. Smaller content of rigid aromatic groups in the hydrophobic component might weaken interpolymer interactions and eventually cause larger water absorption.

3.3.4 Ion Conductivity.

In Figure 3-8b, hydroxide ion conductivity of QPAF membranes in water at 30 ºC is plotted as a function of IEC. Similar to the water uptake, the ion conductivity increased as increasing IEC values. Among the tested membranes with different ammonium groups, QPAF-DMBA exhibited strong dependence of the conductivity on the IEC values, and QPAF-DMBA (IEC = 1.33 meq g^{-1}) achieved the highest conductivity (87 mS cm^{-1}) which was one of the highest hydroxide ion conductivity for AEMs under the same conditions. It was 1.8 times higher than that of QPAF-TMA (1.26 meq g^{-1}, 50 mS cm^{-1}) and even higher than those of our previous AEMs such as QPE-bl-9 with comparable IEC.[8,9] QPAF-DMHA exhibited comparable to or slightly higher conductivity than that of QPAF-TMA. Taking their volumetric IEC into account (1.31 meq cm^{-3} for QPAF-DMHA with 1.17 meq g^{-1} and 1.78 meq cm^{-3} for QPAF-TMA with 1.26 meq g^{-1}), DMHA groups seemed more effective for ion conduction than TMA groups. For their relatively high water uptake, QPAF-DMIm membranes showed moderate ion conductivity probably because of their minute ionic channels caused by rigid planar imidazolium groups as discussed above. As whole, long alkyl substituents on the ammonium groups contributed to improving the ion conductivity of QPAF membranes mostly because of more developed phase separated morphology.

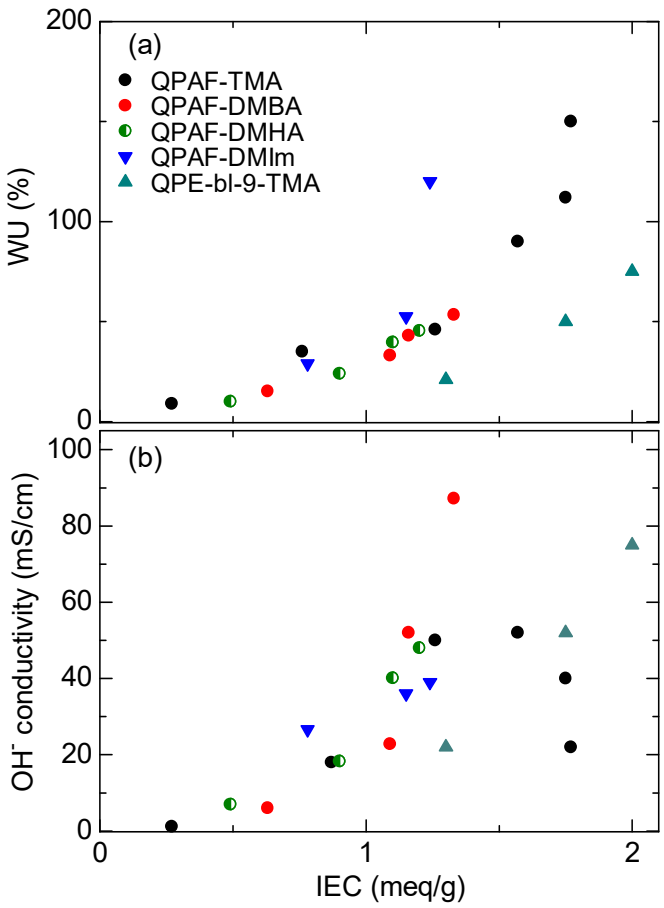

Figure 3-8. (a) Water uptake (room temperature) and (b) hydroxide ion conductivity of QPAF and QPE-bl-9 membranes at 30 ºC in water as a function of IEC.

To evaluate the balance between the ion conductivity and water uptake of QPAF membranes, hydroxide ion conductivity was replotted as a function of water uptake in Figure 3-9. QPAF-DMBA and QPE-bl-9-TMA membranes exhibited high hydroxide ion conductivity for their water uptake values compared to the other membranes, implying that these two membranes effectively utilize water molecules for ion conduction. Among them, QPAF-DMBA with IEC = 1.33 meq g^{-1} exhibited the best balanced properties.

Some membranes with high IEC values such as QPAF-DMIm (1.24 meq g^{-1}) and QPAF-TMA (1.75 meq g^{-1}) swelled excessively with the water uptake higher than 100% and showed plateau or decrease in the conductivity because of the dilution of the ion groups.

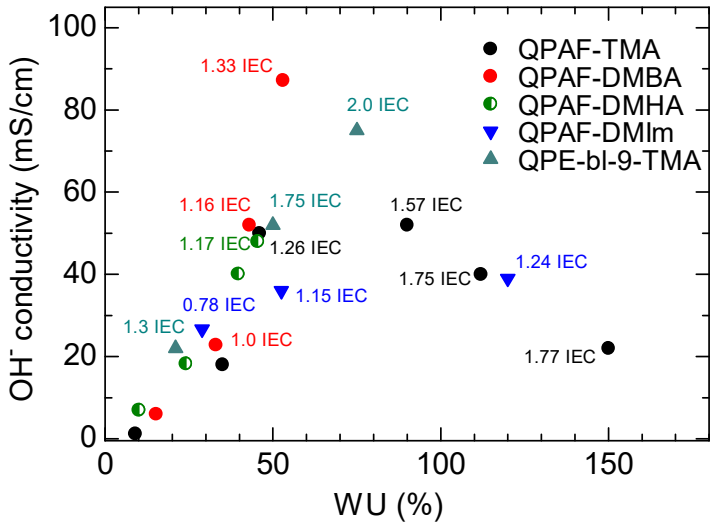

Figure 3-9. Hydroxide ion conductivity of QPAF and QPE-bl-9 membranes at 30 ºC in water as a function of water uptake.

Another effective parameter to compare the ion conduction in swollen AEMs is the ratio between diffusion coefficient of a membrane in hydroxide ion form (D) and its maximum diffusivity of hydroxide ion in water (D_0) known as normalized diffusion coefficient (D/D_0).[10, 11] Thus, D/D_0 ratios of QPAF membranes were calculated and plotted as a function of λ (hydration number per ammonium group) in Figure 3-10. D/D_0 ratio increased as increasing the hydration number. QPAF membranes with long aliphatic ammonium groups achieved higher D/D_0 values at similar hydration numbers. QPAF-DMBA exhibited the highest D/D_0 ratio, 0.41 at λ = 22.0, followed by QPAF-DMHA (D/D_0 = 0.31 at λ = 21.6), significantly higher than that of QPAF-TMA (D/D_0 = 0.23 at λ = 20.2). The high D/D_0 ratio reflects faster mobility of the hydrated hydroxide ions through the ionic channels based on the phase-separated morphology, resulting in high

conductivity. In the literature, there have been a few reports on normalized diffusion coefficient (D/D_0) of AEMs in hydroxide ion forms. It was reported that poly(2,6-dimethyl-phenylene oxide) (PPO) (IEC = 2.47 meq g^{-1}) with multi-side chains exhibited high $D/D_0 = 0.41$ at $\lambda = 25$.[10] Both of their and present results support the idea that the pendant alkyl chains on ammonium groups are effective in developing ionic channels and improving the ion conductivity.

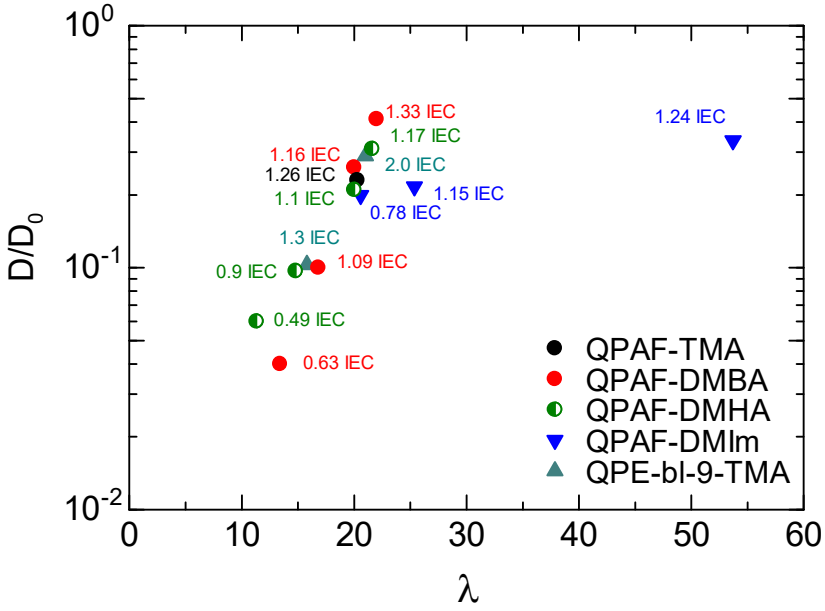

Figure 3-10. Ratio of the effective diffusion coefficient (D) to the dilute solution diffusivity (D_0) of QPAF and QPE-bl-9 membranes as a function of hydration number (λ).

Figure 3-11 shows the temperature dependence of hydroxide ion conductivity in water of QPAF membranes with comparable IEC values. An approximate Arrhenius-type temperature dependence of the conductivity was observed for these selected membranes at the temperature range of 30 – 80 ºC. QPAF-DMBA (1.33 meq g^{-1}) exhibited the highest conductivity (152 mS cm^{-1} at 80 ºC), which was 1.6 times higher than that of QPAF-TMA (1.26 meq g^{-1}, 96 mS cm^{-1}) and 3.4 times higher than that of QPE-bl-9 (1.3 meq g^{-1}, 44 mS cm^{-1}). QPAF-DMHA (1.17 meq g^{-1}) also exhibited high conductivity of 101 mS cm^{-1}

at 80 ºC. QPAF-DMIm (1.24 meq g^{-1}) showed lower conductivity than the aliphatic amine based QPAF-DMBA and -DMHA membranes, but higher than that of QPE-bl-9 (1.3 meq g^{-1}). The apparent activation energies (E_a) were calculated from the slopes to be 10.0 kJ mol^{-1} for QPAF-DMBA, 13.3 kJ mol^{-1} for -DMHA and 9.2 kJ mol^{-1} for -DMIm. The E_a values were comparable to those of QPAF-TMA (9.2-12.1 kJ mol^{-1}) and our previous AEMs containing aromatic arylene ether groups as hydrophobic segments (11-14 kJ mol^{-1}), suggesting that varying ammonium structure had minor effect on the ion conduction mechanism.[1-3, 8, 9]

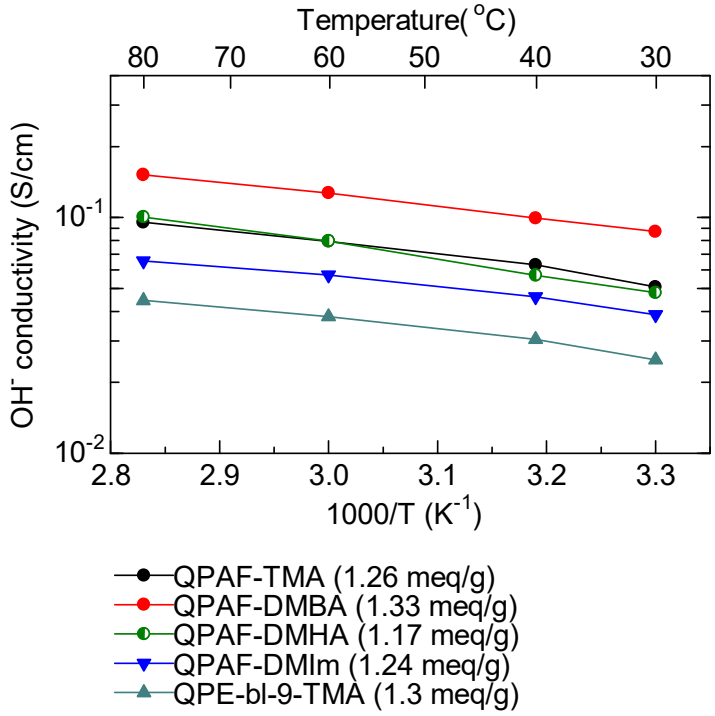

Figure 3-11. Temperature dependence of the hydroxide ion conductivity of QPAF and QPE-bl-9 membranes in water.

3.3.5. Alkaline Stability.

Alkaline stability of QPAF membranes was evaluated in 1 M KOH at 60 ºC. The conductivity at 40 ºC and retention of the conductivity are plotted as a function of testing time up to 1000 h in Figures 3-12 and 3-13. The membranes in chloride ion forms were used in order to avoid the effect of ion exchange treatment prior to the testing. Therefore, the conductivity increased initially by the ion exchange reaction from chloride to hydroxide anions. Among the tested membranes, QPAF-DMBA (1.33 meq g^{-1}) was the most stable with 44 mS cm^{-1} of the hydroxide ion conductivity after 1000 h and the retention was 58% of its maximum conductivity, compared to 22 mS cm^{-1} and 50% for QPAF-DMHA and 1.0 mS cm^{-1} and 1% for both of QPAF-TMA and QPAF–DMIm, respectively.[1] The higher stability of pendant aliphatic ammonium groups was in accordance with the previous studies by Li et al.[12] The steric shielding caused by flexible alkyl chains around the ammonium centers is likely to mitigate the attack by hydroxide ions.[13] Hickner et al. recently claimed that trimethylbenzyl ammonium compounds degraded much faster than dimethylhexylbenzyl ammonium groups in alkaline media.[14]

We reported previously that QPE-bl-9-TMA was more stable than QPE-bl-9-DMHA in the same alkaline conditions.[9] The differences in the stability of TMA and DMHA between QPAF and QPE-bl-9 owe partly to the differences in the water uptake; QPE-bl-9-DMHA absorbed more water and thus swelled more than QPE-bl-9-TMA. More swollen membranes are more likely to be attacked by hydroxide ions.

The balance between retention of the conductivity after the stability test and the remaining conductivity is crucial for practical applications. As shown in Figure 3-14, QPAF-DMBA achieved the best balanced properties followed by QPAF-DMHA.

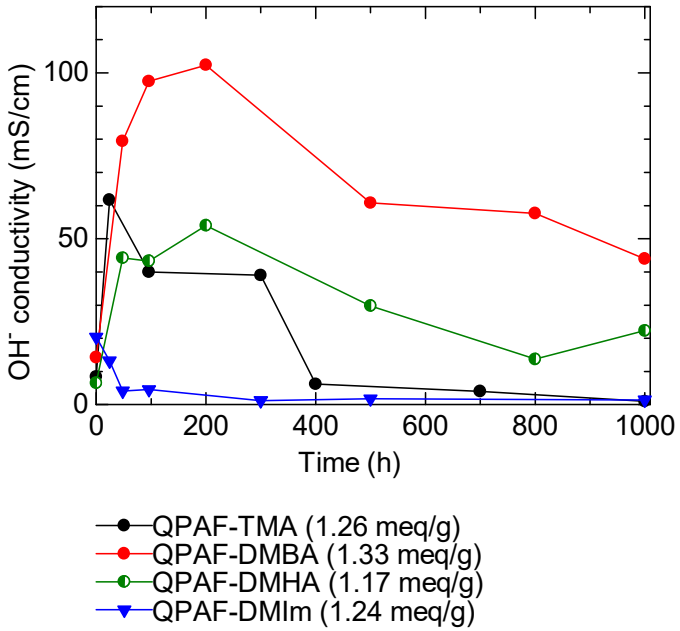

Figure 3-12. Alkaline stability of QPAF membranes in 1 M KOH at 60 ºC (the conductivity at 40 ºC in water is plotted as a function of testing time).

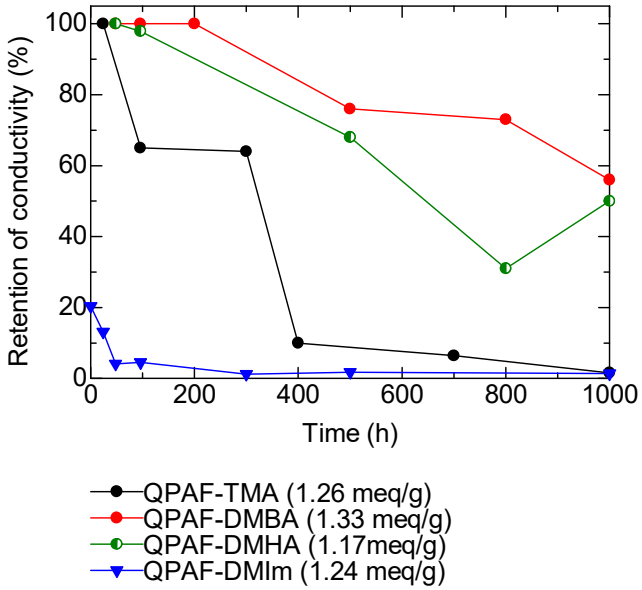

Figure 3-13. Normalized hydroxide ion conductivity as a function of alkaline stability testing time (the maximum conductivity was defined as 100%).

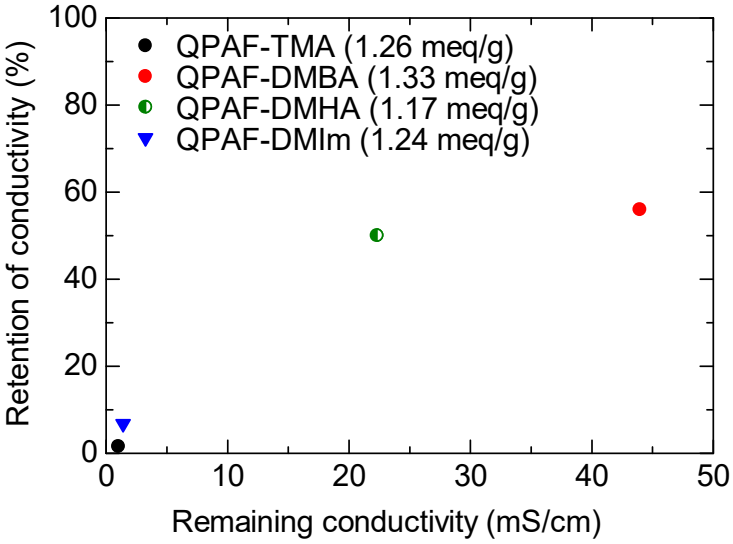

Figure 3-14. Retention of ion conductivity as a function of the remaining conductivity after 1000 h alkaline stability test at 60 ºC for QPAF membranes.

The post-test membranes were insoluble in organic solvents and thus NMR analyses were unavailable. The insolubility of the post-test membranes may imply some structural changes in the polymer main chain presumably involving cross-linking. IR spectra were measured and compared between the pristine and post-test membranes in Figure 3-15. In Figure 3-15a and b, the peak at 891 cm^{-1} assignable to stretching vibration of $C\text{-}N^{+}$ remained unchanged suggesting the stability of the ammonium groups in QPAF-DMBA and QPAF-DMHA compared to QPAF-TMA (Figure 3-16) in which the same peak was smaller after the alkaline stability test.[1] The differences in the degradation of the ammonium groups between QPAF-DMBA and -DMHA could be discussed with the enlarged spectra in the wavenumber range between 2400-3600 cm^{-1} (Figure 3-17a and b). The peaks at 2854-2956 cm^{-1} assignable to the aliphatic C-H stretching vibration became smaller for DMHA than for DMBA after the stability test. Loss in the peak intensity suggests the degradation of the ammonium groups via Hofmann elimination and/or

nucleophilic substitution reactions. The degradation of the ammonium groups is accountable for the decrease in the hydroxide ion conductivity as discussed above. Minor degradation was also confirmed by the appearance of new peaks at 1572 cm^{-1} and 1580 cm^{-1} for QPAF-DMBA and –DMHA, respectively. The peaks were assignable to C=C stretching vibration of aromatic rings, suggesting some structural changes in the polymer main chain similar to that for QPAF-TMA.[1]

QPAF-DMIm membrane (Figure 3-15c) showed major degradation of imidazolium groups as suggested by the lowered intensities of the peaks at 1589, 1545, and 1440 cm^{-1}, assignable to in-plane asymmetric stretching vibration of imidazole ring, C=C and C-N stretching vibrations, respectively. The results suggest some degradation in the polymer main chain as well as the imidazolium groups similar to QPE-bl-9-DMIm.[9] Moreover, the appearance of new peaks at 2855 cm^{-1} and 2918 cm^{-1} assignable to aliphatic C-H stretching vibration (Figure 3-17c) illustrates the major degradation of the imidazolium cation presumably via ring opening reaction.[14, 16] The peak at 3000-3500 cm^{-1} assignable to OH stretching vibration became smaller after the stability test, in particular for QPAF-DMIm membrane, suggesting the loss of water absorbability (hydrophilicity). Then, the water uptake of the post-test membranes was measured (Figure 3-18). The pos-test water uptakes (and the retention of water uptakes) were 28% (53%), 13% (28%), and 4% (3%) for QPAF-DMBA, -DMHA, and DMIm membranes respectively. The remaining water uptake was in the same order to that of the remaining hydroxide ion conductivity.

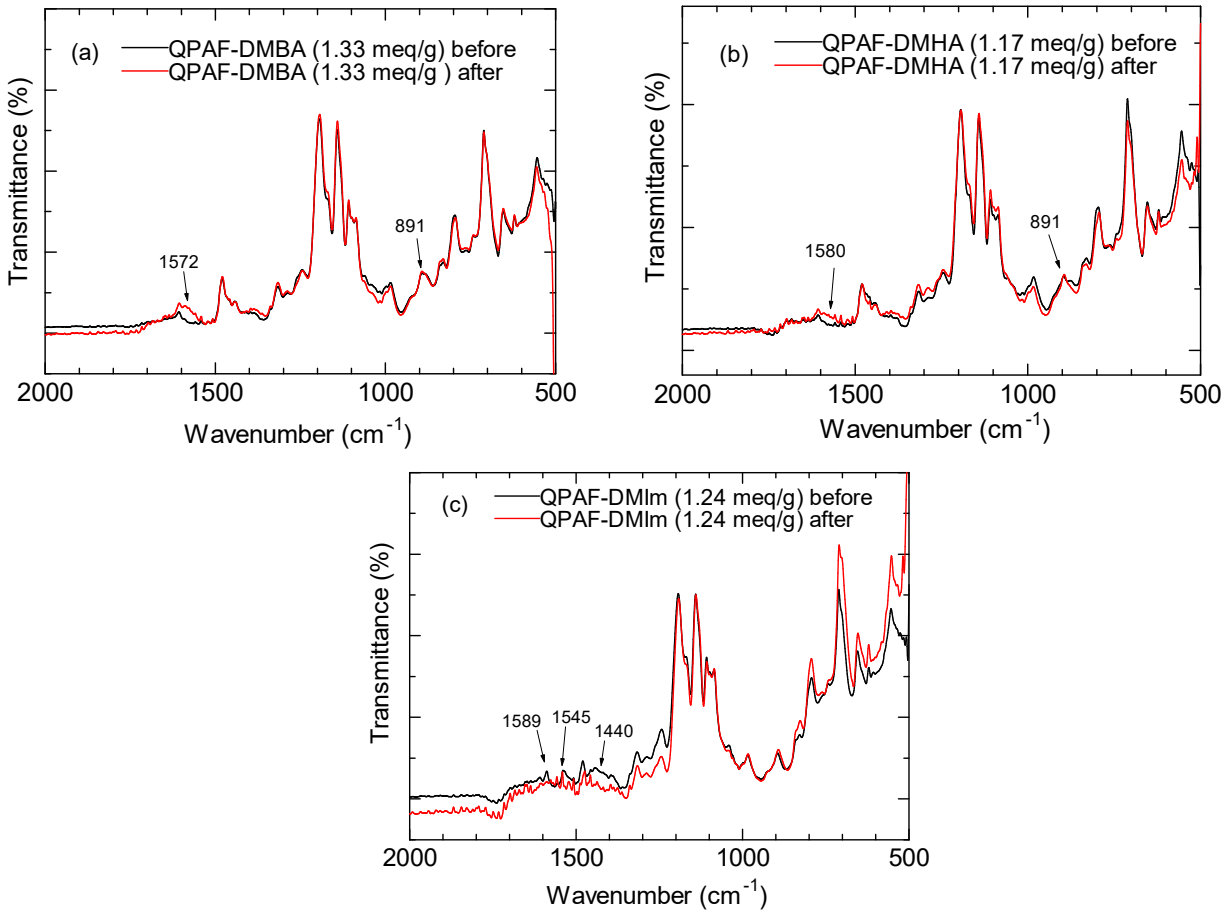

Figure 3-15. FT-IR spectra of QPAF membranes before and after 1000 h alkaline stability test at 60 ºC. (a) QPAF-DMBA, (b) QPAF-DMHA, and (c) DMIm.

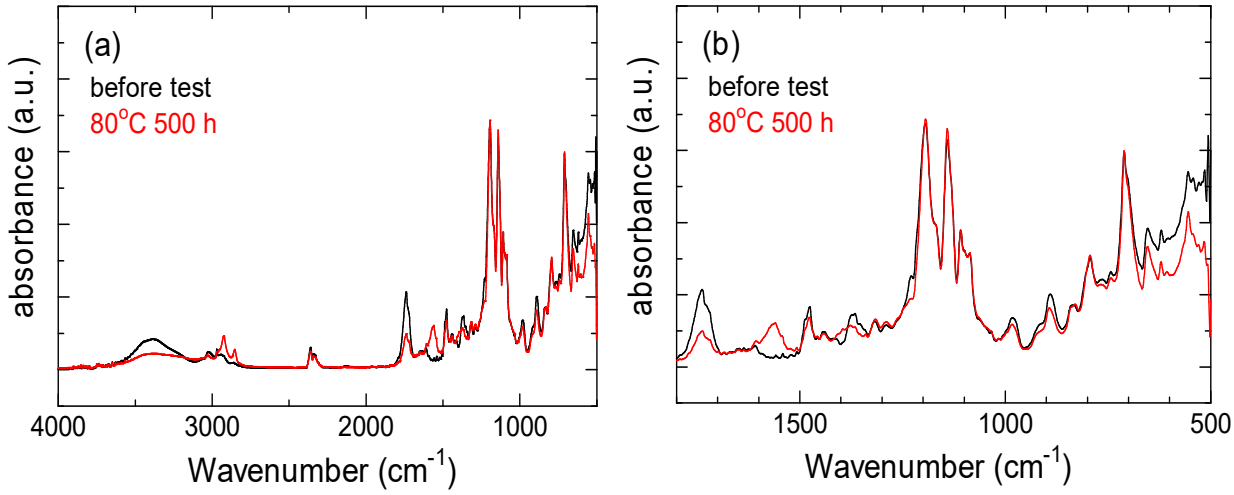

Figure 3-16. FT-IR spectra of QPAF-TMA membrane (IEC = 1.26 meq g-1) before and after 500 h alkaline stability test at 80 ºC (Ono, H.; Miyake, J.; Shimada, S.; Uchida, M.; Miyatake, K. Anion exchange membrane composed of perfluoroalkylene chains and ammonium-Functionalized oligophenylenes. *J. Mater. Chem. A* **2015**, *3*, 21779-21788.).

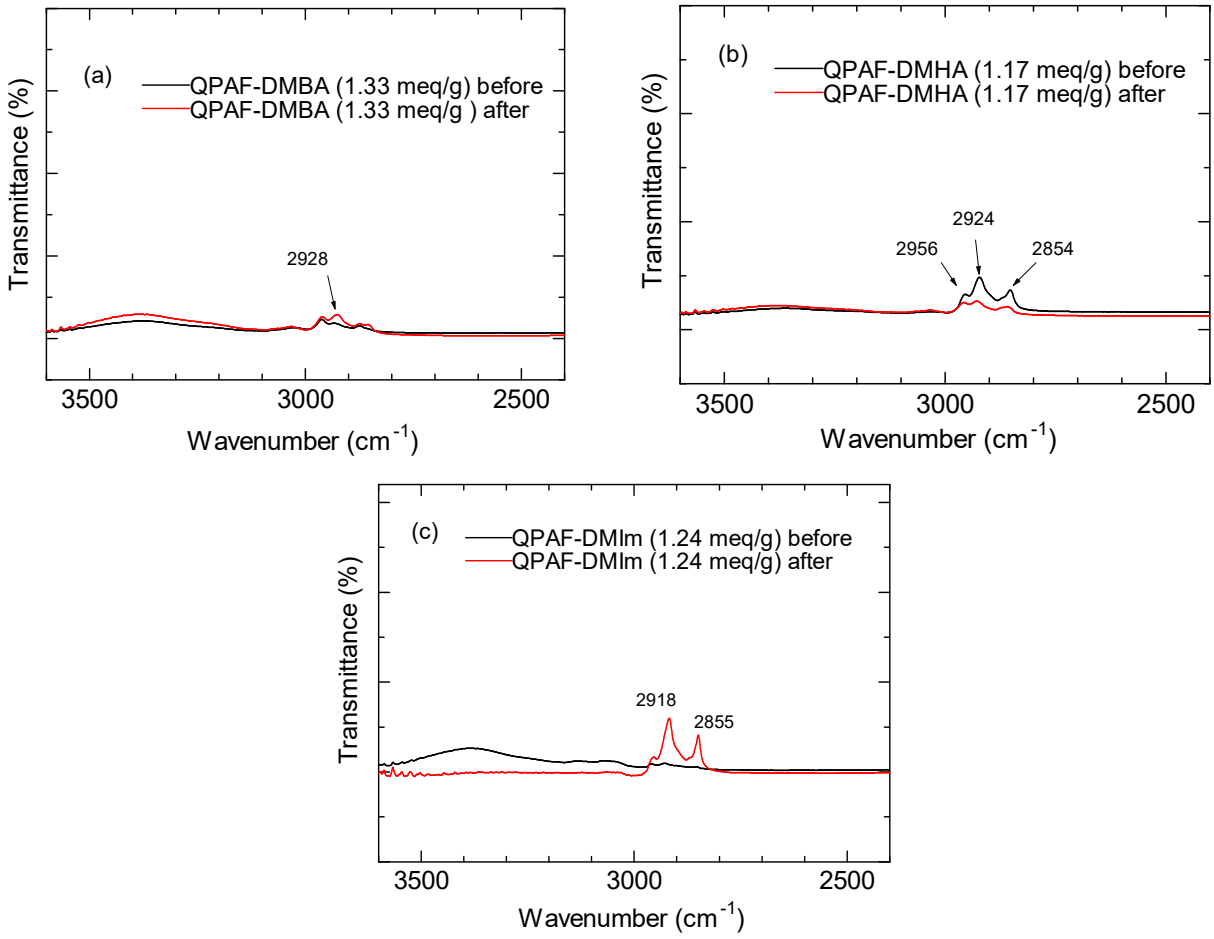

Figure 3-17. FT-IR spectra of (a) QPAF-DMBA, (b) QPAF-DMHA, and (c) QPAF-DMIm membranes before and after the alkaline stability test in 1 M KOH at 60 ºC.

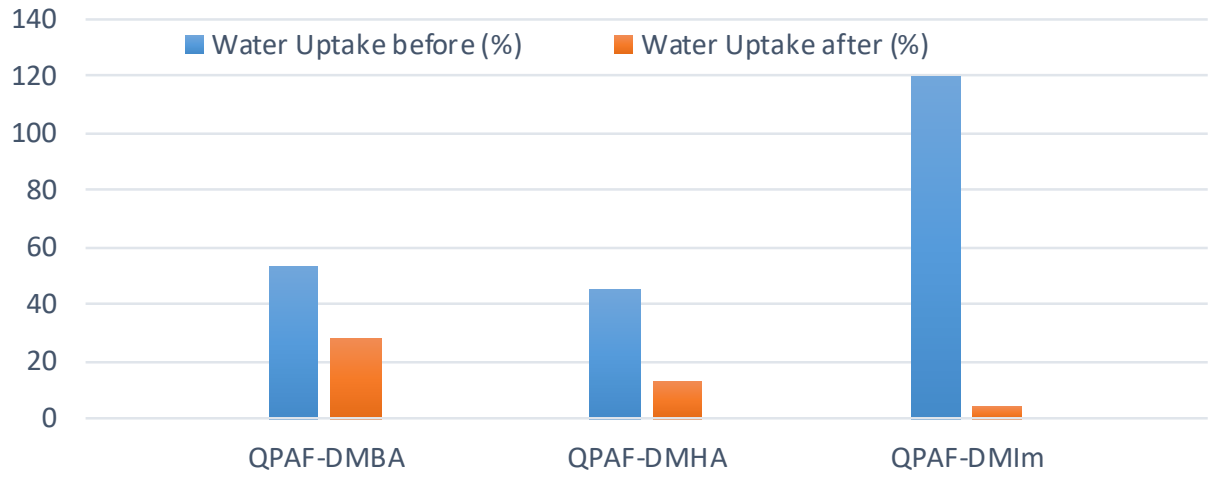

Figure 3-18. Water uptake of QPAF membranes before and after the alkaline stability test in 1 M KOH at 60 ºC.

The alkaline stability test was then performed under severer conditions at 80 ºC for QPAF-DMBA and QPAF-DMHA membranes with similar IEC = ca. 1.10 meq g^{-1} as shown in Figure 3-19. (Please note that higher IEC membranes used in Figure 3-12 were not applied because of their excess swelling at 80 ºC for long period of time making the conductivity measurement very difficult and unreliable.) QPAF-DMIm was not included in the test due to its instability even at 60 ºC. Similar to the results at 60 ºC, QPAF-DMBA exhibited better stability with no practical loss in conductivity after 500 h (22 mS cm^{-1} with 100% remaining). QPAF-DMHA was also stable up to 400 h, and then exhibited a drop of the conductivity to 16 mS cm^{-1} with 58% remaining. Both QPAF membranes with aliphatic pendant groups were more stable than our reported QPAF-TMA at 80 ºC which lost conductivity much faster under the same conditions.[26] QPAF-DMBA seemed more stable than those containing pendant alkyl ammonium groups recently reported in the literature.[12, 14] To make sure the effect of initial counter anions on the stability of the QPAF membranes, membranes in hydroxide ion forms were also tested under the same conditions (Figure 3-20). The results clearly suggested that the initial counter anions did

not affect the stability and that the conductivity values during the stability test were reproducible.

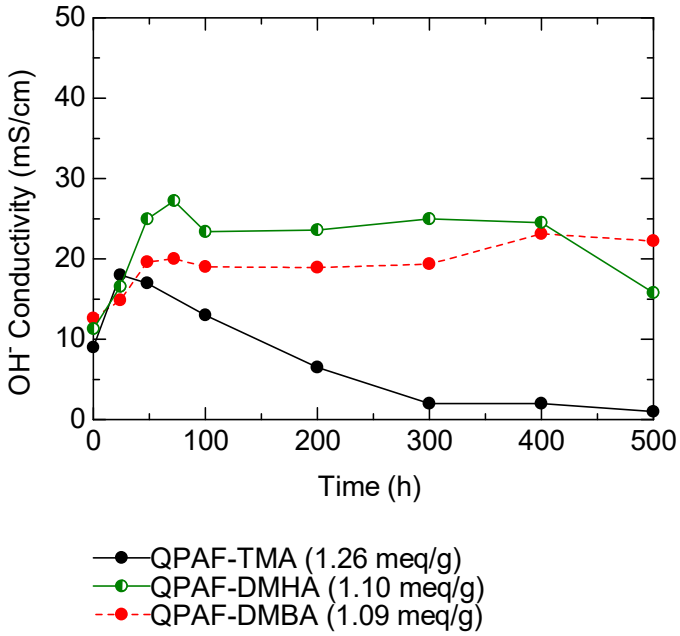

Figure 3-19. Alkaline stability of QPAF membranes in 1 M KOH at 80 ºC (the conductivity at 40 ºC in water is plotted as a function of testing time).

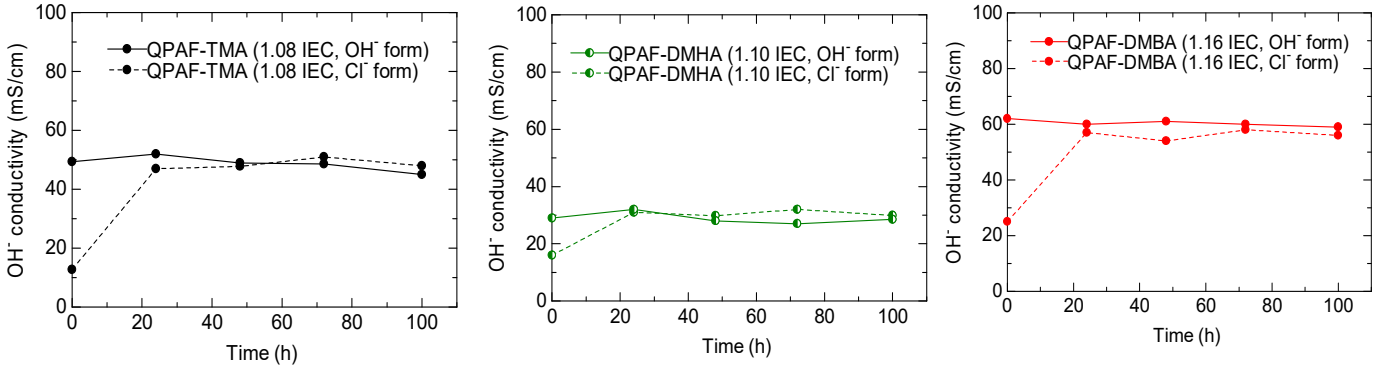

Figure 3-20. Alklaine stability of QPAF membranes starting with chloride and hydroxide ion forms in 1 M KOH at 80ºC as a function of time (the conductivity at 40 ºC in water is plotted as a function of testing time).

3.3.6 Mechanical Properties.

In addition to the chemical stability, mechanical properties are also crucial for fuel cell membranes. In this regard, dynamic mechanical analysis (DMA) of QPAF membranes in chloride ion forms was carried out at 60% RH (relative humidity) from room temperature to 95 ºC (Figure 3-21). QPAF-TMA and -DMBA showed small temperature dependence of storage modulus (E') and loss modulus (E''). In contrast, QPAF-DMHA and -DMIm exhibited decrease in E' and E'' as increasing the temperature. The latter two membranes showed broad peaks at ca. 80 ºC, presumably associated with α relaxation of the membranes or glass transition of the polymer chains. These results indicate that the viscoelastic properties of QPAF membranes are adjustable by the ammonium structure, and differ from our poly(arylene ether)-based AEMs (QPE-bl-9) whose DMA properties were insensitive to the ammonium structure.[9]

The mechanical properties of the post-alkaline stability test QPAF membranes were also measured under the same conditions as shown in Figure 3-22. While the post-test QPAF membranes retained their bendability and flexibility after 1000 h stability test, their E' and E'' moduli were lower than those of the pristine membranes suggesting the degradation (or the structural changes) of the polymer main chains. Taking the conductivity, alkaline stability and mechanical properties into account, it is concluded that QPAF-DMBA membranes exhibited the most balanced properties among the QPAF membranes investigated in this study.

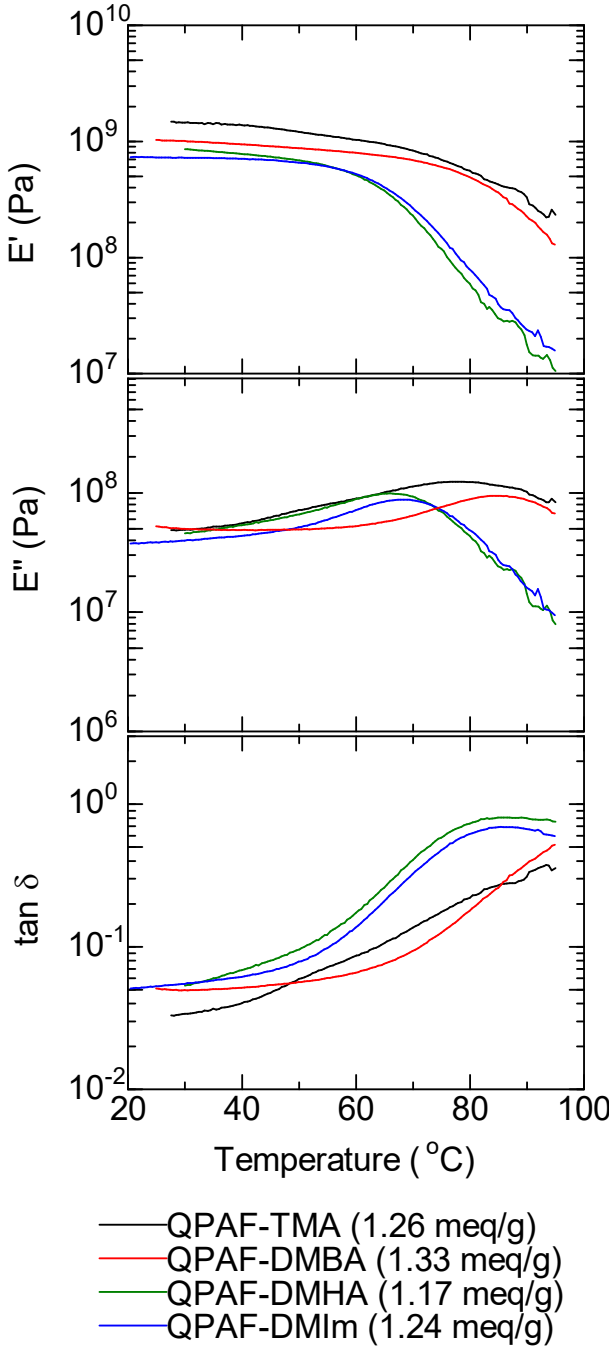

Figure 3-21. DMA curves of QPAF membranes at 60% RH.

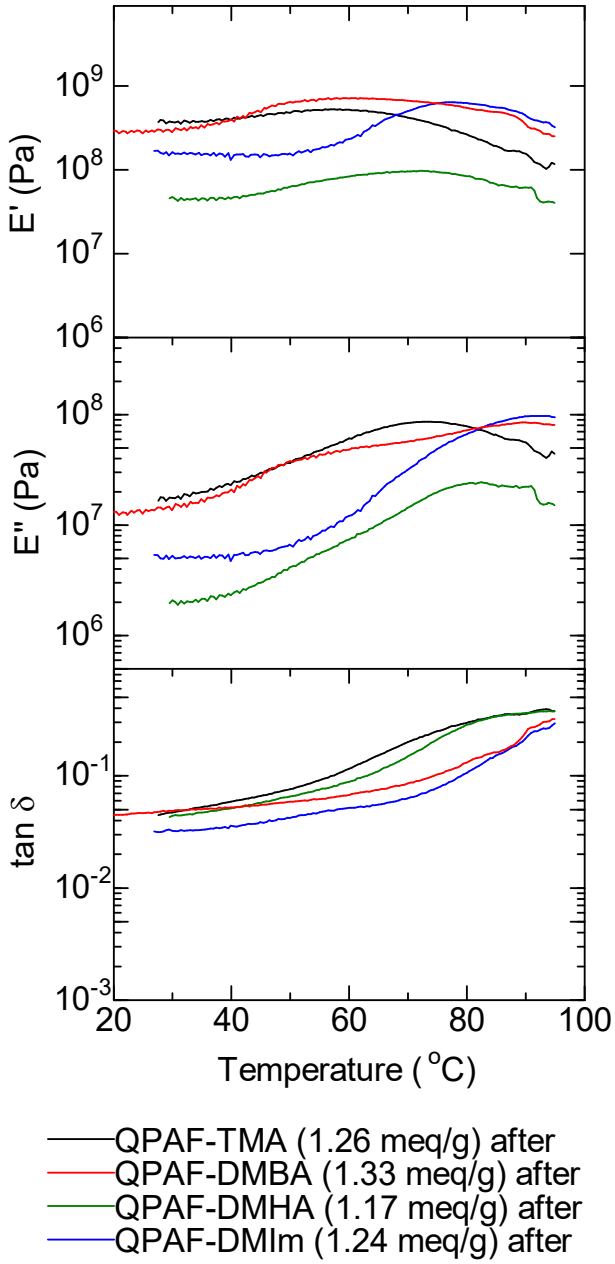

Figure 3-22. DMA curves of QPAF membranes at 60% RH after 1000 h alkaline stability test.

3.3.7 Fuel Cell Performance.

Since QPAF-DMBA exhibited high hydroxide ion conductivity and good alkaline stability as discussed above, a catalyst coated membrane was prepared with QPAF-DMBA membrane (1.33 meq g^{-1}, 45 μm thick), Pt/C both for the anode and cathode catalysts, and QPAF-TMA (1.16 meq g^{-1}) as electrode binder. The fuel cell was operated under the same conditions (40 ºC, 100% RH for both gases) as reported for QPAF-TMA membrane with comparable thickness.[1] The open circuit voltage (OCV) of QPAF-DMBA cell was as high as 1.03 V (Figure 3-23a) comparable to that of QPAF-TMA (1.01 V),[1] suggesting low gas permeability of QPAF-DMBA and QPAF-TMA membranes. The ohmic resistance of the QPAF-DMBA cell was nearly constant at 0.2 Ω cm^2 (Figure 3-23b), which was higher than that (0.05 Ω cm^2) calculated from its hydroxide ion conductivity in water at 40 ºC (99 mS cm^{-1}, in Figure 3-11) and thickness, probably because of the differences in the conductivity between in water and in humidified gas. The interfacial contact resistance between the membrane and the catalyst layers might also be responsible. The ohmic resistance of the QPAF-DMBA cell was lower than that of QPAF-TMA cell (0.3 Ω cm^2),[26] reflecting the former's higher ion conductivity. The QPAF-DMBA achieved high power density (167 mW cm^{-2}) at the current density of 0.42 A cm^{-2}, higher than that of QPAF-TMA cell (138 mW cm^{-2} at the same current density). The fuel cell performance did not degrade for several tens of hours during the performance evaluation testing. Replacing the TMA groups with DMBA groups as ion exchange groups for QPAF membranes contributed to the better membrane and alkaline fuel cell performance.

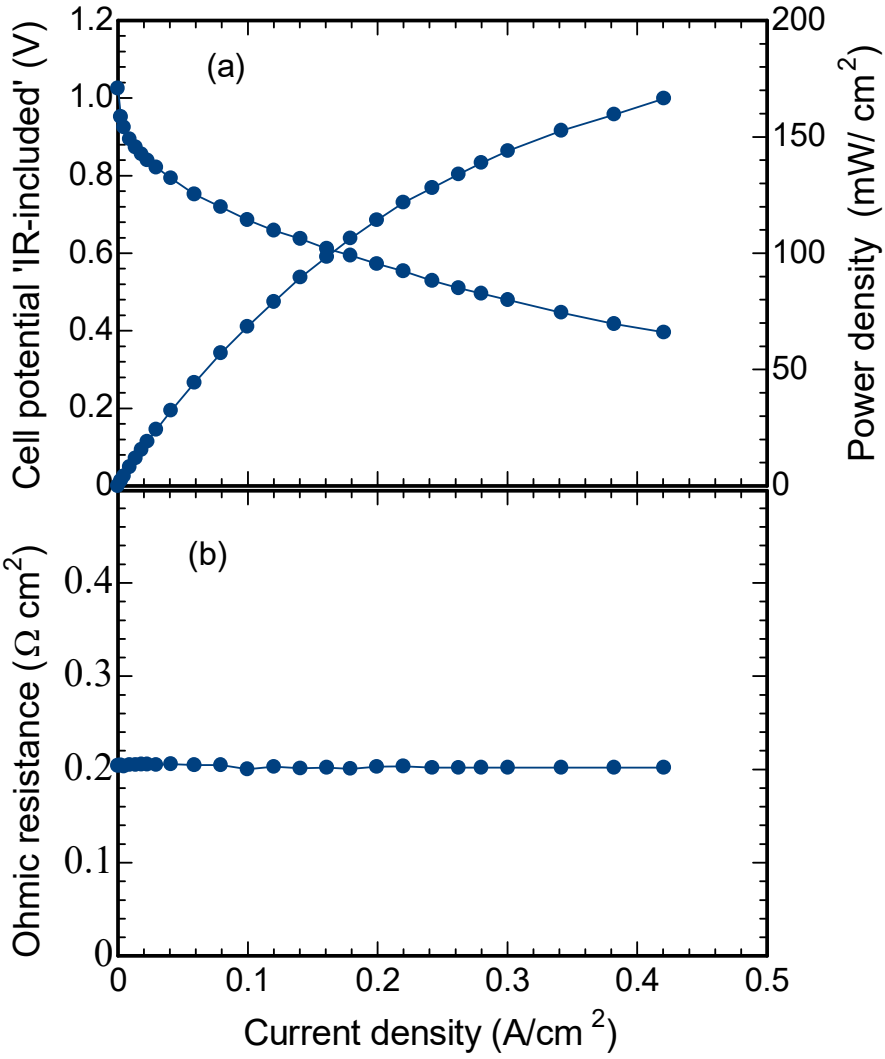

Figure 3-23. (a) Cell potential and power density (b) ohmic resistance as a function of current density for an H_2/O_2 fuel cell with QPAF-DMBA membrane (IEC = 1.33 meq g^{-1}, 45 μm thick) at 40 ºC and 100% RH.

3.3.8 Conclusion

The effect of ammonium groups on the properties of our original quaternaized aromatic/perfluoroalkylene copolymer (QPAF) membranes was investigated. Different types of ammonium groups, trimethylammonium (TMA), dimethylbutylammonium (DMBA), dimethylhexylammonium (DMHA), and 1,2-dimethylimidazolium (DMIm), were nearly quantitatively substituted onto the copolymers. While all these QPAF membranes formed nanometer-scale phase-separated morphology based on the hydrophilic/hydrophobic differences in the copolymer components, aliphatic ammonium groups with pendant chain (DMBA and DMHA) exhibited slightly larger and well connected ionic domains than those of TMA and DMIm based QPAF membranes. QPAF-DMBA and QPAF-TMA utilized water molecules more efficiently for the hydroxide ion conduction than the other membranes. Accordingly, QPAF-DMBA with IEC = 1.33 meq g^{-1} exhibited the highest hydroxide ion conductivity. The high ion conductivity of QPAF-DMBA membrane was supported by its high ion diffusion coefficient (D/D_0) compared to those of the other membranes. From the temperature dependence of the conductivity, QPAF membranes with different ammonium groups seemed to share the similar ion conduction mechanism involving the hydrated hydroxide ions. Beside their high ion conductivity, QPAF with aliphatic amines showed good alkaline stability under the accelerated conditions. The QPAF-DMBA (IEC = 1.09 meq g^{-1}) showed no change in the ion conductivity at 80 ºC for 500 h, while QPAF-DMHA with the similar IEC maintained 58% of its conductivity. QPAF-TMA and QPAF-DMIm membranes were much unstable than these two membranes. The post-test FT-IR analyses revealed that DMBA and DMHA groups degraded to much less extent than DMIm groups. Since main chain degradations were not significant, the QPAF membranes retained flexibility and mechanical properties after the stability test. QPAF-DMBA as the best balanced QPAF membrane was tested for fuel cell experiments and achieved a maximum power density of 167 mW cm^{-2} at the current density of 0.42 A cm^{-2} which was higher than that of

QPAF-TMA membrane under the same operating conditions. The results indicate that aliphatic ammonium groups with pendant chain (DMBA, DMHA) were suitable for QPAF as anion exchange membranes.

3.4 References

(1) Ono, H.; Miyake, J.; Shimada, S.; Uchida, M.; Miyatake, K. Anion exchange membrane composed of perfluoroalkylene chains and ammonium-functionalized oligophenylenes. *J. Mater. Chem. A* **2015**, *3*, 21779-21788.

(2) Ono, H.; Miyake, J.; Miyatake, K. Partially Fluorinated and Ammonium-Functionalized Terpolymers: Effect of Aliphatic Groups on the Properties of Anion Conductive Membranes. *J. Polym. Sci., A: Polym. Chem.* **2017***, 55,* 1442-1450.

(3) Akiyama, R.; Yokota, N.; Nishino, E.; Asazawa, K.; Miyatake, K. Anion Conductive Aromatic Copolymers from Dimethylaminomethylated Monomers: Synthesis, Properties, and Applications in Alkaline Fuel Cells. *Macromolecules* **2016**, *49*, 4480-4489.

(4) Walls, H. J.; Fedkiw, P. S.; Zawodzinski, T. A.; Khan, S. A. Ion Transport in Silica Nanocomposite Electrolytes. *J. Electrochem. Soc.* **2003**, *150*, E165−E174.

(5) Kim, Y.; Einsla, B.; Sankir, M.; Harrison, W.; Pivovar, B. Structure–property–performance relationships of sulfonated poly(arylene ether sulfone)s as a polymer electrolyte for fuel cell applications. *Polymer* **2006**, *47*, 4026−4035.

(6) Muthukumar, M.; Rice, S. A. Polyelectrolyte Dynamics. *Adv. Chem. Phys.* **2005**,

131, 1-60.

(7) Hara, M.; Kimura, T.; Nakamura, T.; Shimada M.; Ono, H.; Shimada, S.; Miyatake, K.; Uchida, M.; Inukai, J.; Watanabe, M. Effect of Surface Ion Conductivity of Anion Exchange Membranes on Fuel Cell Performance. *Langmuir* **2016**, *32*, 9557-9565.

(8) Yokota, N.; Shimada, M.; Ono, H.; Akiyama, R.; Nishino, E.; Asazawa, K.; Miyake, J.; Watanabe, M.; Miyatake, K. Aromatic Copolymers Containing Ammonium-Functionalized Oligophenylene Moieties as Highly Conductive Membranes. *Macromolecules* **2014**, *47*, 8238-8246.

(9) Mahmoud, A. M. A.; Elsaghier, A. M. M.; Miyatake, K. Effect of ammonium groups on the properties of anion conductive membranes based on partially fluorinated aromatic polymers. *RSC Adv.* **2016**, *6*, 27862-27870.

(10) Zhu, L.; Pan, J.; Wang, Y.; Han, J.; Zhuang, L.; Hickner, M. A. Multication Side Chain Anion Exchange Membranes. *Macromolecules* **2016**, *49*, 8150-824.

(11) Pan, J.; Zhu, L.; Han, J.; Hickner, M. A. Mechanically Tough and Chemically Stable Anion Exchange Membranes from Rigid-Flexible Semi-Interpenetrating Networks. *Chem. Mater.* **2015**, *27*, 6689-6698.

(12) Li, N.; Yan, T.; Li, Z.; Albrecht, T. T.; Binder, W. H. Comb-shaped polymers to enhance hydroxide transport in anion exchange membranes. *Energy Environ. Sci.* **2012**, *5*, 7888-7892.

(13) Kreuer, K.-D. Ion Conducting Membranes for Fuel Cells and other Electrochemical Devices. *Chem. Mater.* **2014**, *26*, 361-380.

(14) Li, N.; Leng, Y.; Hickner, M. A.; Wang, C. Y. Highly Stable, Anion Conductive, Comb-Shaped Copolymers for Alkaline Fuel Cells. *J. Am. Chem. Soc.* **2013**, *135*, 10124-10133.

(15) Ye, Y.; Elabd, Y. A. Relative Chemical Stability of Imidazolium-Based Alkaline Anion Exchange Polymerized Ionic Liquids. *Macromolecules* **2011**, *44*, 8494-8503.

(16) Wang, Z.; Parrondo, J.; Ramani, V. Alkaline Stability of Poly(Phenylene Oxide) Based Anion Exchange Membranes Containing Imidazolium Cations. *J. Electrochem. Soc.* **2016**, *163*, F824-F831.

Chapter 4

4.1 Conclusion

In the last decades, anion exchange membranes (AEM) gained more attention due to their various applications and specially for alkaline fuel cell that turned to be the promising alternative resource for clean energy. However, AEMs meet many challenges as described in chapter 1. The most critical challenge was the alkaline stability under harsh alkaline conditions (high temperature > 80 ºC for long period). In the literature, many strategies have been applied on the polymer backbones and the tethered cations to enhance the stability of AEMs. Ammonium cation was found to play crucial effect on the membrane properties as concluded in chapter 1. In our group QPAF and QPE-bl-9 membranes were developed and the both membranes exhibited high conductivity and good mechanical stability, however they degraded after short time in harsh alkaline conditions. The objective of this study was to investigate the effect of ammonium groups on the properties and mainly the alkaline stability of QPE-bl-9 and QPAF membranes.

In chapter 2, various ammonium groups were investigated to functionalize the block copolymer poly(arylene ether) based AEM (QPE-bl-9), looking for the highest conductive and the most stable cation. The ammonium structure showed significant impact on the conductivity, water absorbability and alkaline stability, while the mechanical strength was not affected. However, all the ammonium groups under investigation were less stable and lower conductive than the common benzyltrimethylammonium (BTMA). Notably, BTMA was the smallest in volume among the tested groups, suggesting that the rigid aromatic structure of QPE-bl-9 is likely to hinder the facile interaction between polymer main chain and bulky ammonium groups leading to either low degree of qauternization (at low IECs) and/or low conductivity (even at high IECs). The alkaline stability of QPE-bl-9 membranes was tested in 1M KOH at 60 ºC, in which QPE-bl-9-TMA was more stable than the pendant alkyl, bulky and

heterocyclic groups contrary to some recent literatures. The relative stability of BTMA was attributed to the low hydration levels that mitigate the free access of OH^- ion to quaternary ammonium. Moreover, the effect of β-hydrogen in the pendant alkyl, bulky and heterocyclic groups that is likely to accelerate the degradation of benzylic carbon-nitrogen bond (C_{Bn}-N^+). The results and their comparison with the literature suggested that the optimum ammonium groups might depend on the polymer main chain structure since the rigidity and free volume are closely related with the polymer main chain.

In chapter 3, replacing rigid aromatic block copolymer of QPE-bl-9 with flexible perfluoroalkylene in random copolymer QPAF membranes lead to higher water uptakes and higher conductivities, facilitated the complete quaternization at different IECs. I selected the aliphatic ammonium groups with pendant alkyl chains (DMBA and DMHA) that were more promising than bulky groups in the chapter 1, and investigated their effect on the stability and other properties of QPAF membranes. The results were compared with TMA and heterocyclic 1,2-dimethylimidazole (DMIm). In contrast to QPE-bl-9 described in chapter 2, QPAF functionalized by DMBA and DMHA possessed higher conductivity and excellent alkaline stability than the BTMA and heterocyclic DMIm. QAF-DMBA exhibited 152 mS/cm at 80 ºC that was 1.6 times higher than the reported QPAF-TMA and considered as one of the highest conductivities for state-of-the-art AEMs. In terms of alkaline stability, QPAF-DMBA retained 100% of its high conductivity (22 mS/cm) even after 500 h in 1M KOH at 80 ºC, while QPAF-DMHA retained 58% of is conductivity (16 mS/cm) and QPAF-TMA degraded completely at the same conditions. The high conductivity of QPAF-DMBA was attributed to the faster mobility of hydroxide ions that was confirmed through the good phase separation and higher values of normalized diffusion coefficient (D/D_0). The high alkaline stability of QPAF-DMBA was referred to the pendant alkyl chain of DMBA that provided effective steric shielding around the ammonium cation and hindered OH^- attack. QPAF-DMHA, was degraded faster than QPAF-DMBA as supported by spectroscopic analysis, conductivity and post-

test water uptake measurements. Since the phase separation may not always lead to enhanced stability, it seems that the wider hydrophilic hydrophobic phase separation of DMHA (2-8 nm), provides facile access of OH^- to attack quaternary ammonium, specifically at high temperatures (i.e. less effective shielding around ammonium cation). Using pendant aliphatic and heterocyclic groups decreased the mechanical strength of QPAF membranes to some extent. A fuel cell has been operated using QPAF-DMBA as the highest conductive and most stable membrane and as expected it achieved higher power density (167 mW/cm^2) than that of the QPAF-TMA (138 mW/cm^2).

In conclusion, the optimum ammonium structure differed from chapter 2 to 3 by varying the polymer main chain structure, suggesting that the affinity between polymer main chain and the suitable ammonium structure is crucial for membrane morphology, conductivity, stability and mechanical strength.

Based on the results in chapters 2 and 3, the hydration levels, morphology and steric shielding on ammonium cation, seem the dominant factors affecting membrane properties. The critical point is how to control these factors to develop better-performing AEM. The hydration levels mainly can be controlled by varying the aromatic content in the polymer backbone and by using bulky or hydrophobic ammonium structures (For example using lower aromatic content in QPAF lead to higher hydration levels compared to that of aromatic QPE-bl-9 membranes). While the phase separated morphology can be achieved by constructing flexible and hydrophobic polymer backbones and/or by increasing the pendability of ammonium structures (such as long alkyl chain QAs) (For example, the flexible perfluoroalkyl and bendable DMHA in QPAF-DMHA membrane lead to much better phase separation and higher conductivity than those of the bulky QPE-bl-9-DMHA membrane). On the other hand, the steric shielding on the ammonium cation is introduced by providing bulky and sterically hindered ammonium structures tethered to the suitable polymer backbone (For example using long alkyl ammonium groups such as DMBA and

DMHA).

Taking this into account, using flexible polymer backbone and pendant alkyl ammonium groups may result in lower mechanical strength. The mechanical strength can be further improved through a crosslinking strategy by introducing crosslinker in the polymer main chain.

A combination of the aforementioned factors suggests that a durable AEM is achievable by combining flexible aromatic polymer backbone (free of ether or sulfone linkages) and tethered to sterically hindered QA, preferably long alkyl ammonium either as terminal or interstitial between QA and polymer chains.

4.2 Comparison with state-of-the-art AEMs

In order to know the status our AEMs among the recently reported AEMs and propose the future prospects, I compare the highest conductive and the most stable membranes developed in this study (QPE-bl-9-TMA and QPAF-DMBA) with the recently reported state-of-the-art AEMs **(AEM-1-17)**.[1-17] To make a good comparison, two parameters were selected to compare the AEM properties. First the efficiency of the membranes for ionic conduction by comparing the hydroxide ion conductivity at different hydration numbers (high conductivity at minimum hydration numbers required for AEMs to maintain is high performance at low hydration levels in practical fuel cell). Second parameter, is the stability in harsh alkaline conditions such as 1M KOH or NaOH at 80 ^{o}C. (Alkaline stability is crucial for the membrane durability in fuel cell).

(i) Efficiency for ionic conduction

The efficiency of AEM for ionic conduction was investigated through the relation between hydroxide ion conductivity at 30 ^{o}C and λ (hydration number or number of

absorbed water molecules per ammonium group) as shown in Figure 4-1. Interestingly, **QPAF-DMBA** and **QPE-bl-9-TMA** were more efficient for ionic conduction than the reported state-of-the-art AEMs, since the two membranes exhibited the highest conductivity at low hydration numbers. **AEM-10** (poly(phenylene oxide) (PPO) grafted by poly(quaternary 4-vinylbenzyl chloride) showed comparable conductivity to that of **QPE-bl-9-TMA** but at higher hydration number. On the other hand, some of the reported AEMs were also efficient for ionic conduction such as **AEM-7** (PPO containing imidazolium cations), **AEM-11**(poly (biphenylalkylene)), **AEM-12** (fluorene based with interstitial alkyl spacer) and **AEM-17** (poly(arylene ether sulfone) containing spirocyclic ammonium in the main chain) but these AEMs exhibited lower conductivity than **QPAF-DMBA** and **QPE-bl-9-TMA** at all hydration numbers**.**

(ii) Alkaline stability

In terms of alkaline stability, most AEMs showed good stability at 60 ^{o}C but in particular, increasing the alkaline testing temperature to 80 ^{o}C or higher is necessary for reliable stability of AEM materials. In the literature, using different temperatures and alkali concentrations for stability testing makes it difficult to compare the stability of AEMs with various functionalities. Therefore, I tried to compare the stability of our developed membranes with those in the literature tested under the same conditions (1M alkaline solution at 80^{o}C). Taking into account that stability of QPE-bl-9 membranes were not tested at 80 ^{o}C in this work, due to their insufficient stability at milder conditions (60 ^{o}C), so that I cited here the stability of **QPE-bl-9-TMA** (1.3 meq/g) at 80 ^{o}C that was reported by Ono *et. al.*.[23] As shown in Figure 4-2, **QPAF-DMBA** was the most stable among AEMs in the literature, since it retained 100% of its high conductivity for 500 h similar to those of **AEM-5, AEM-11** and **AEM-12.** Interestingly, the chemical structures of **QPAF-DMBA**, **AEM-11** and **AEM-12** were mainly free of ether bonds and contain pendant or interstitial alkyl spacing in the main chains. While **AEM-5** (alkali-doped

polybenzimidazole), however it possesses excellent stability, it suffers from some drawbacks such as alkali release during long periods and low solubility in organic solvents that hinder facile fabrication as ionomer in fuel cell.

In spite of its high conductivity, **QPE-bl-9-TMA** was less stable than the recent AEMs. Some recent AEMs showed good alkaline stability but for shorter time than that of **QPAF-DMBA**. Notably, most of the less stable AEMs contain either ether or (ether sulfone) bonds that are more susceptible to alkaline degradation.

Chemical structures of state-of-the-art AEMs are shown in Figures 4-3 and 4-4.

(iii) Fuel cell performance

The cell performance of QPAF-DMBA as the most stable membrane in this work, was compared to state-of-the-art AEMs taking the power density and Pt-loading into account. Compared to the power densities in the literature, in spite of the low catalyst loading (0.2 mg Pt/cm^2) of QPAF-DMBA, was superior to that of poly(phenylene oxide) based AEM containing pendant hexyl groups (105.8 mW/cm^2, 0.4 mg Pt/cm^2),[18] polysulfone based AEM (70 mW/cm^2, 0.4 mg Pt/cm^2),[19] Poly(arylene ether sulfone) based AEM (56.8 m/cm^2, 1.0 mg Pt/cm^2)[20] and to that of Tokuyama A201 (148 mW/cm^2, 1.0 mg Pt/cm^2).[21] On the other hand, at high Pt-Loading, polyphenylene based AEM achieved 577 mW/cm^2 at 3.0 mg Pt/cm^2.[22] Figure 4-5 shows the normalized power density (mW/mg Pt) of QPAF-DMBA in comparison to state-of-the-art AEMs, in which QPAF-DMBA was superior to those in the literature. However, further investigations required to optimized the operating conditions of QPAF-DMBA for better performance.

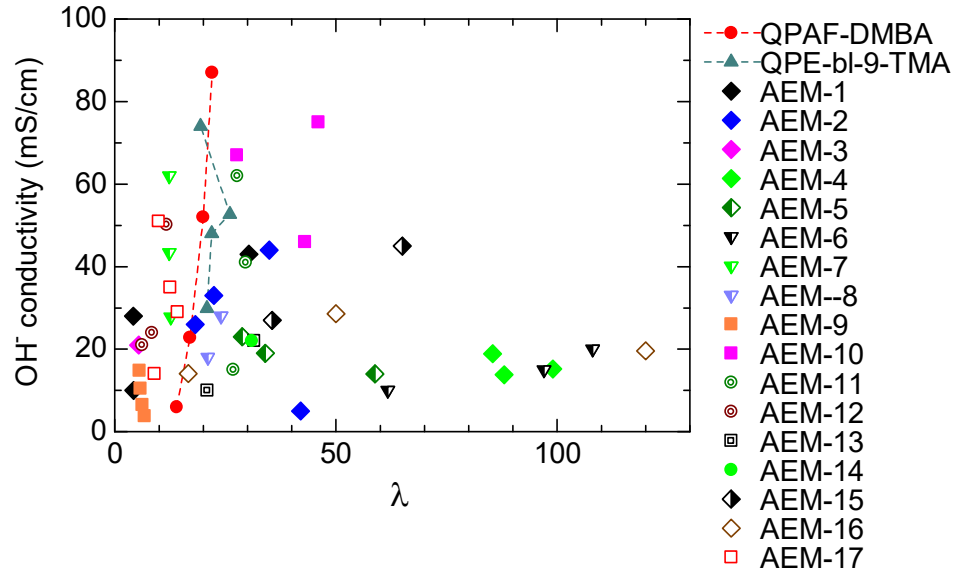

Figure 4-1. Hydroxide ion conductivity at 30°C of state-of-the-art AEMs as a function of λ.

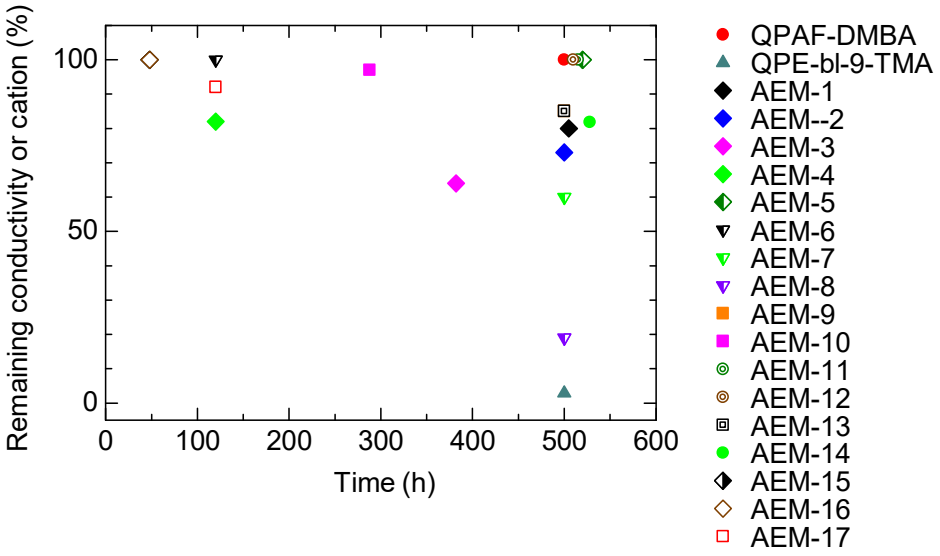

Figure 4-2. Alkaline stability of state-f-the-art AEMs in 1M KOH at 80 °C.

(Note: (1) **AEM-3** was tested in 0.5 M KOH. (2) Post-test conductivity of **AEM-11** and **AEM-12** were unavailable, so that, we considered NMR data as sign for remaining cation).

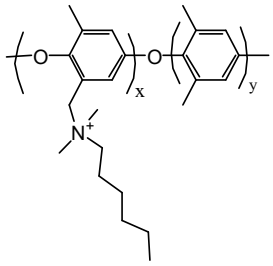

AEM-1 [6]

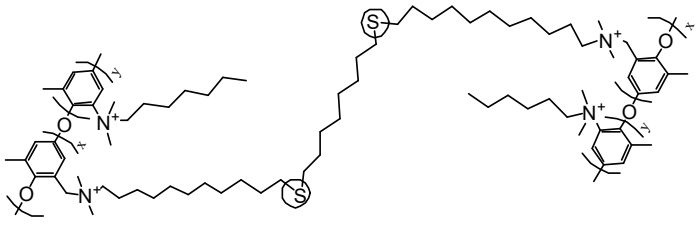

AEM-2 [7]

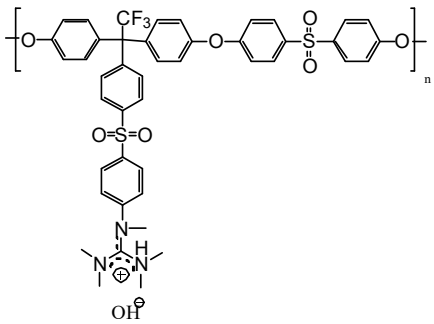

AEM-3 [8]

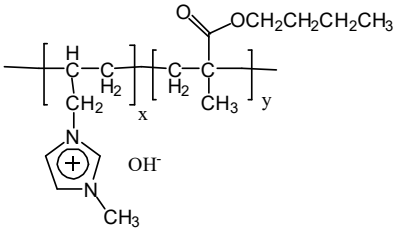

AEM-4 [9]

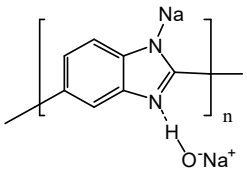

AEM-5 [10]

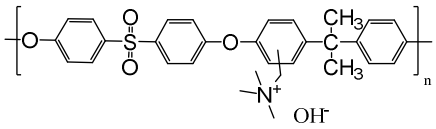

AEM-6 [11]

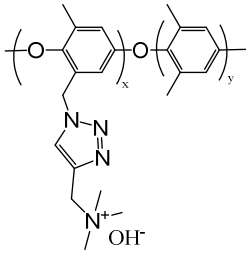

AEM-7 [12]

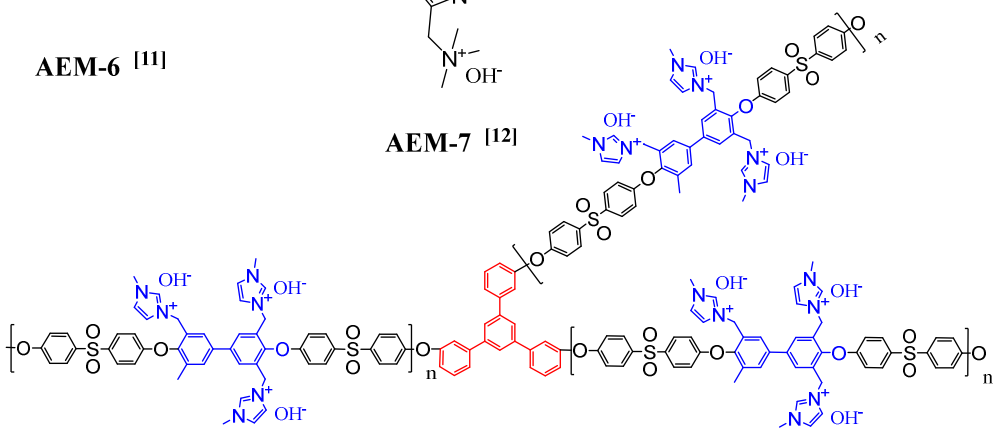

AEM-8 [13]

Figure 4-3. Chemical structures of state-of-the-art AEMs.

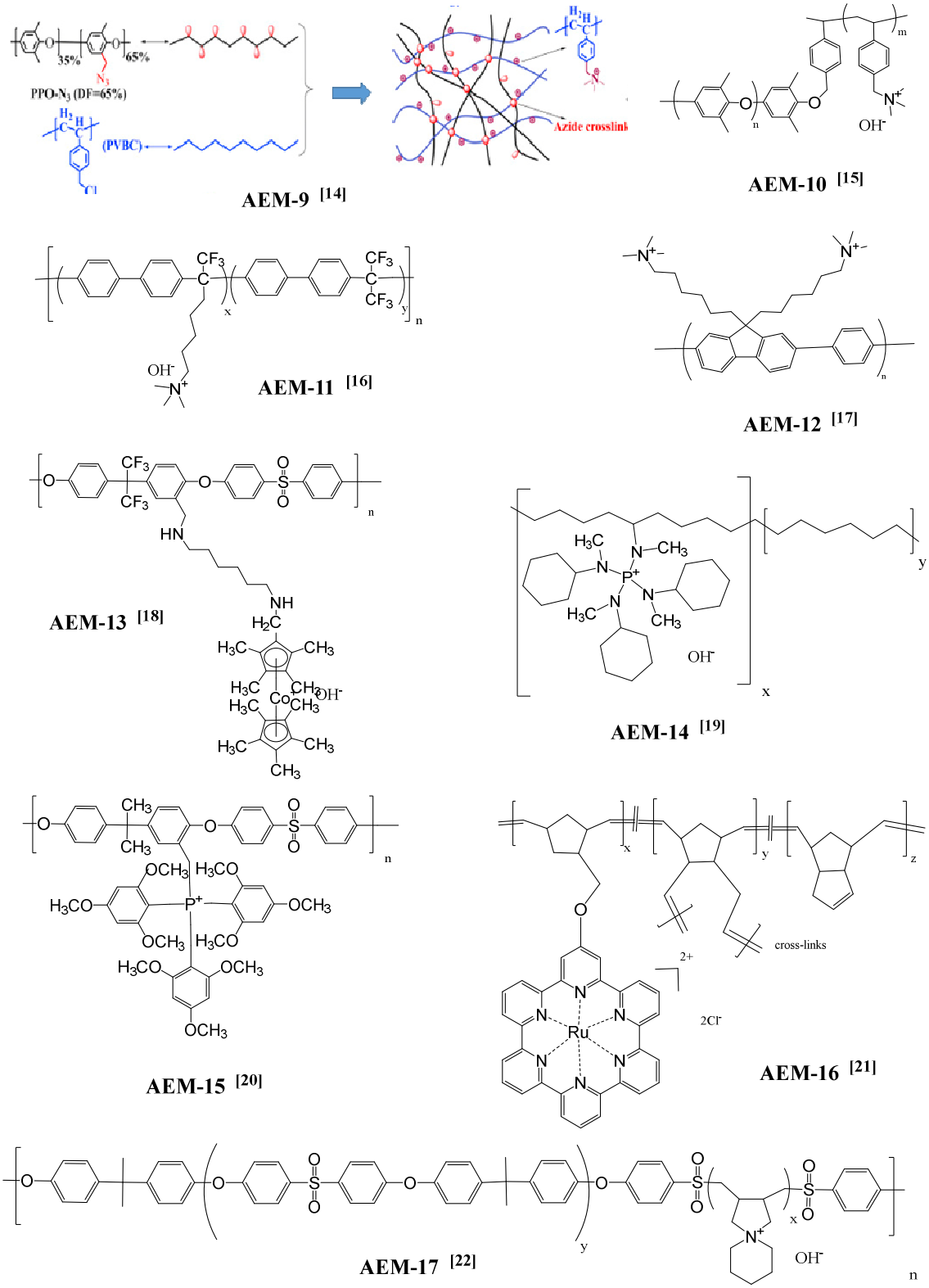

Figure 4-4. Chemical structures of state-of-the-art AEMs.

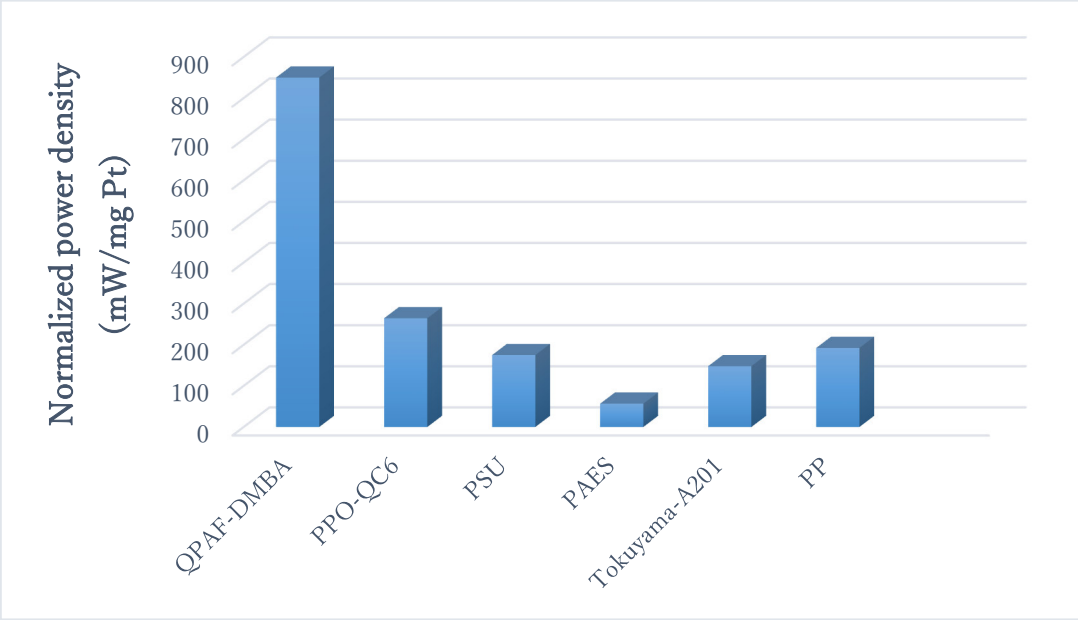

Figure 4-5. Normalized Power density (mW/mg Pt) of QPAF-DMBA membrane in comparison to State-of-the-art AEMs.

4.3 Challenges and Future Perspectives

The mains objective of the research on AEMs is to achieve high power output in practical alkaline fuel cell. Thus, the membrane should be highly conductive specially at low hydration levels. Also the membrane should possess excellent alkaline stability at 80 ºC or higher, besides the mechanical strength and low gas permeability.

In chapter 2, QPE-bl-9-TMA (as the best among the investigated ammonium groups) maintained its high conductivity at low hydration levels and exhibited good mechanical properties besides it high power density (512 mW/cm^2). But unfortunately it degraded at mild alkaline conditions (60 ºC), the main future approach for that membrane is using different chemistries to enhance its resistance to alkli. Main future objective is to avoid the benzylic positions since it more susceptible to degradation, by introducing interstitial alkyl chains between polymer backbone and ammonium cation and/or combination between interstitial and pendant alkyl groups on ammonium cation (Figure 4-6), that is expected to achieve higher resistance to alkaline attack and improve the flexibility and mechanical strength of the membrane. Moreover, this strategy is expected to improve the phase separation leading to more effective water management and gas permeability.

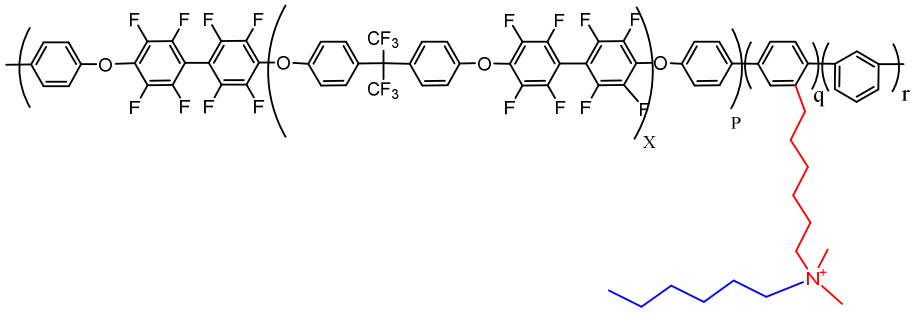

Figure 4-6. Chemical structure of prospective QPE-bl-9 membranes.

In Chapter 3, I have achieved a promising AEMs (QPAF-DMBA) with high hydroxide conductivity and excellent alkaline stability. However, power density of that membrane (167 mW/cm^2) was lower than the state-of-the-art recently reported in the literature (500-

900 mW/cm^2). The future objective of QPAF-DMBA is to optimized the best fuel cell operating conditions such as temperature, catalyst loading and gas rate flow to reach a comparable or higher power density to those in the literature. The next Plan is introducing interstitial alkyl chains between polymer backbone and ammonium cation and/or combination between interstitial and pendant alkyl groups. Now I'm working on this strategy and initial results revealed that propyl spaces are the most promising (Figure 4-7) since it maintained its high conductivity without change up to 1000 h in 1M or 4M KOH at 80 ^{o}C. However, alkyl spacer resulted in decrease in mechanical strength compared to QPAF-TMA and -DMBA. So that, the future prospective is the crosslinking of that membrane with propyl interstitial chains, to control and improve the mechanical strength, gas permeability and power density. In practically operating fuel cells, the membranes experience large pressure between the electrodes. There are gradients in potential, water, fuels, and oxidant between the anode and cathode. These are also affecting the properties and durability of AEMs, which should be looked at in details in the future.

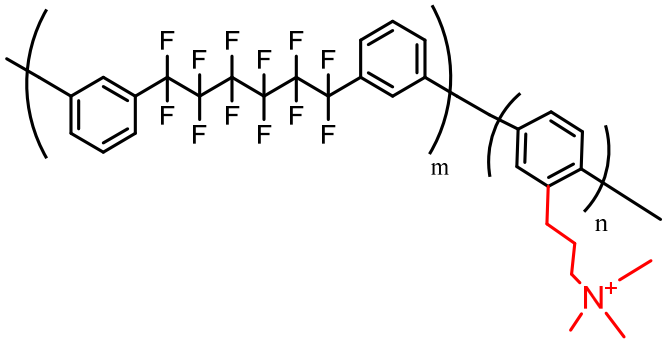

Figure 4-7. Chemical structure of QPAF with interstitial alkyl spacer.

4.4 References

1- Li, N. W., Leng, Y. J., Hickner, M. A. & Wang, C. Y. *J. Am. Chem. Soc.* **2013**, *135*, 10124–10133.

2- Zhu, L.; Zimudzi, T.; Li, N.; Pan, J.; Lin, B.; Hickner, M. A. *Polym. Chem.* **2016**, *7*, 2464-2475.

3- Kim, D. S., Labouriau, A., Guiver, M. D. & Kim, Y. S. Chem. Mater. **2011**, *23*, 3795–3797.

4- Guo, M.; Fang, J.; Xu, H.; Li, W.; LU, X.; Lan, C.; Li, K. *J Membr. Sci.* **2010**, *362*, 97–104.

5- Luo, H.; Vaivars, G.; Agboola, B.; Mu, S.; Mathe, M. *Solid State Ionics* **2012**, *208*, 52–55.

6- Pan, J.; Lu, S.; Li, Y.; Huang, A.; Zhuang, L.; Lu, J. *Adv. Funct. Mater.* **2010**, *20*, 312–319.

7- Li, N.; Guiver, Michael D., Wolfgang H. Binder, *ChemSusChem,* 2013*, 6,* 1376-1383.

8- *Lee, K. H.; Cho, D. H.; Kim, Y. M.; Moon, S. J.; Seong, J. G.; Shin, D. W.; Sohn, J. Y.; Kim J. F .and Lee, Y. M. Energy Environ. Sci.,* **2017***, 10,* 275-285

9- Xue, J.; Liu, L.; Liao, J.; Shen, Y.; Li, N. *J. Memb. Sci.* **2017***, 535,* 322-330.

10- Pandey, T. P.; Seifert, S.; Yang, Y.; Yang, Y.; Knauss, D. M.; Liberatore, M. W.; Herring, A. M. *Electrochim. Acta.* **2016**, *222*, 1545-1554.

11- Lee, W. H.; Kim, Y. S.; and Bae, C. *ACS Macro Lett.* **2015**, *4*, 814-818.

12- Lee, W.-H.; Mohanty, A. D.; Bae,C. *ACS Macro Lett.*, **2015**, 4, 453–457.

13- Gu, S.; Wang, J.; Kasper, R. B.; Fang, Q.; Zhang, B.; Coughlin, E. B.;Yan, Y. *Sci.*

Reprt. **2015**, *5*, 11668.

14- Noonan, K. J. T.; Hugar, K. M.; Kostalik, H. A.; Lobkovsky, E. B.; Abrunna, H. D.; Coates, G. W. *J. Am. Chem. Soc.* **2012**, *134*, 18161-18164.

15- Gu, S.; Cai. R.; Luo, T.; Chen, Z.; Sun, M; Liu, Y.; He, G.; Yan, Y. *Angew. Chem. Int. Ed.* **2009**, *48*, 6499-6502.

16- Zha, Y.; Miller, M. L. D.; Johnson, Z. D.; Hickner, M. A.; Tew, G. N. *J Am Chem Soc* **2012**, 134, 4493–4496.

17- Strasser, D. J.; Graziano, B. J.; Knauss, D. M. *J. Mater. Chem. A* **2017**, **5**, 9627-9640.

18- Zhu, L.; Pan, J.; Wang, Y.; Han, J.; Zhuang, L.; Hickner, M. A. *Macromolecules*, 2016, 49 (3), pp 815–824.

19- C. X. Lin, Y. Z. Zhuo, A. N. Lai, Q. G. Zhang, A. M. Zhu, M. L. Ye and Q. L. Liu, J. Member. Sci., 2016, 513, 206-216.

20- D. Tang, J. Pan, S. Lu, L. Zhuang and J. Lu, Sci. China: Chem., 2010, 53, 357

21- Ren, X.; Price, S. C.; Jackson, A. C.; Pomerantz, N.; Beyer, F. L. ACS Appl. Mater. Interfaces 2014, 6, 13330−13333.

22- Kim, Y. S. US DOE Hydrogen and fuel cells program and vehicle technologies program annual merit review, 2011,

http://www.hydrogen.energy.gov/pdfs/review11/fc043_kim_2011_o.pdf

List of publications

1- High Hydroxide Conductivity with Enhanced Alkaline Stability of Partially Fluorinated and Quaternized Aromatic Copolymers as Anion Exchange Membranes

Ahmed Mohamed Ahmed Mahmoud, Ahmed Mohamed Mohamed Elsaghier, Kanji Otsuji and Kenji Miyatake

Macromolecules, 2017, 50, 4256-4266.

2- Effect of ammonium groups on the properties of anion conductive membranes based on partially fluorinated aromatic polymers.

Ahmed Mohamed Ahmed Mahmoud, Ahmed Mohamed Mohamed Elsaghier, Kenji Miyatake

RSC. Adv. 2016, 6, 27862-27870.

Meeting abstracts

1- Partially fluorinated aromatic copolymers functionalized with pendant alkyl ammonium groups as highly conductive and alkaline stable anion exchange membranes, *66th SPSJ Symposium on Macromolecules*, 2017, Ahmed Mohamed Ahmed Mahmoud, Ahmed Mohamed Mohamed Elsaghier and Kenji Miyatake.

2- Stability of aromatic copolymer anion exchange membranes for fuel cell applications: Impact of varying ammonium structure, *65th SPSJ Symposium on Macromolecules*, 2016, Ahmed Mohamed Ahmed Mahmoud, Ahmed Mohamed Mohamed Elsaghier and Kenji Miyatake.

3- Stability of perfluoroalkylene based anion exchange membrane for alkaline fuel cell applications: Impact of varying ammonium structure, *The 5th International Seminar on Green Energy Conversion*, 2016, Ahmed Mohamed Ahmed Mahmoud, Ahmed Mohamed Mohamed Elsaghier and Kenji Miyatake.

4- Anion conductivity and alkaline syability of partially fluorinated oligophenylene based anion exchange membranes: Effect of ammonium structure, *The 7th International fuel cell workshop*, 2015, Ahmed Mohamed Ahmed Mahmoud, Ahmed Mohamed Mohamed Elsaghier and Kenji Miyatake.

Acknowledgement

The current work is the summary of research at Clean Energy Research Center, Fuel Cell Nanomaterials center and Interdisciplinary Graduate School of Medicine and Engineering in University of Yamanashi, during 2014-2017.

I would like to express my deepest gratitude to my supervisor Professor Kenji Miyatake of University of Yamanashi for providing me such invaluable opportunity to join his group, as a joint supervision fellow at first then giving me the precious chance to be student in Yamanashi University under his supervision. Not only did I learn knowledge from him, I also learned scientific attitude, critical thinking, and the ability to continually be evaluating and solving problems. I could not do this work without his valuable Psycho- and scientific support.

I would like to express my gratitude to Professor Ahmed Mohamed Mohamed ELsaghier, for his valuable advice and encouragement during three years of my master in Egypt and throughout my work in PhD in Yammanashi Univerity.

I would like to express my sincere gratitude to professor Hiroyuki Uchida, Professor Masahiro Watanabe and professor Akihiro Iiyama of University of Yamanashi for giving me the such chance to start my scientific career.

I would like to express my gratitude to Professor Donald Alexandor Tryk, Professor Makoto Uchida, Professor Junji Inukai, Professor Masaharu Komiyama, Professor Katsuyoshi Kakinuma, Professor Manuel Brito, Associate Professor Shinji Nohara, Assistant Professor Junpei Miyake and Assistant Professor Toshihiro Miyao for their beneficial instructions and help.

A deep appreciation is expressed to my senior Researchers; Dr. Naoki Yokota, Dr. Hideaki

Ono, Dr. Ryo Akiyama and Dr. Manai Shimada for their technical support, valuable advice, constructive discussion and continuous help. They were the best helpful lab mates for me.

I would like to thank, Dr. Yuji Chino, Dr. Iwataki Toshio, Mr. Yaojian Zhang, Ms. Natsumi Yoshimura, Mr. Taro Kimura, Mr Ryo Shimizu, Ms. Jinju Ahn, Mr. Febrina Tri Hartani, Mr. Ryunosuke Taki, Mr. Ibuki Hosaka and Ms. Mizuki Ozawas for all the kind help.

I am grateful to Ms. Toshiko Gomyo for technical support and help in TEM measurements in Chapters 2,3. and Mr. Kanji Otsuji for his help in fuel cell performance measurement in Chapter 3.

Sincere gratitude is expressed to Ms. Kaori Ichinose, Ms. Makie Endo and all the staffs of Clean Energy Research Center and Fuel Cell Nanomaterials Center for their kind help.

A special appreciation and sincere gratitude to my parents, uncle Aboasem, my elder brother Eng. Hossam, younger brother Mahmoud, sisters, grandmothers, aunts and all my family in Egypt who have always encouraged, motivated and supported me unconditionally in all my endeavors.

I cannot forget my dear naughty sons, Omar and Marawan, the gift of my god, their smile always push me forward.

Finally, My beloved wife, Walaa Ziedan was constantly giving me strength and courage to get this far. She stayed long time in home raising my two kids to support me. I am grateful for her wisdom, positive attitude, and that I have her in my life.

June 2017

Ahmed Mahmoud